國家太空計畫室委託計畫

期末報告

中文計畫名稱：稀薄噴流流場量測及模擬技術研究

英文計畫名稱：Experimental and Numerical Investigation of Low-density Jet Plume

申請機構：交通大學

執行單位：機械工程學系

主 持 人：吳宗信

計畫編號：NSC91-NSPO(A)-PC-FA06-01

日期：中華民國 92 年 5 月 15 日

Abstract

In this study, experimental and numerical investigation is performed and compared for the flow of nitrogen in a nozzle used in reaction control system on satellite and in the near field of plume. Total pressure is measured, using a traversable and rotatable pitot tube, at the exit plane of the nozzle and in the near field of the plume. A stochastic particle approach, direct simulation Monte Carlo method, is used to solve the flow field inside the nozzle and in the near field of the plume, which the inflow conditions at throat are provided by using the simulation results from a CFD solver. Comparison of the experimental data and numerical results at nozzle exit shows that the parallel DSMC method using dynamic domain decomposition and variable time-step scheme can provide an accurate description of the expanding flow under rarefied condition.

Keywords: reaction control system, nozzle, direct simulation Monte Carlo method, parallel

中文摘要

本研究中，以實驗量測和數值模擬兩種方式，來觀察以氮氣氣源之衛星控制系統中的噴嘴噴流流場。在噴嘴出口和噴嘴附近的噴流，以一個可以移動及旋轉的皮托管來量則其全壓值。另以統計為基礎的直接模擬蒙地卡羅法用來模擬噴嘴內及噴嘴附近的噴流流場，而且入口條件則以計算流體力學模擬的方式取得。比較實驗量測和數值模擬的在噴嘴出口的結果，吾人發現使用動態區域切割及變時步法的平行化直接模擬蒙地卡羅法可以準確預測在稀薄狀態下的噴流擴張流場。因此使用動態區域切割及變時步法之平行化直接模擬蒙地卡羅法，將有效率地模擬噴流對衛星污染及衛星姿態控制影響。

關鍵詞：衛星控制系統、噴嘴、直接模擬蒙地卡羅法、平行化

TABLE OF CONTENTS

LIST OF FIGURES AND TABLES

NOMENCLATURE

A	area of cell
D_e	diameter of nozzle exit
D_t	diameter of nozzle throat
k	Boltzmann constant, $k = 1.380658\times10^{-23}$
Kn	Knudsen number
L	characteristic length
M_x	Mach number before shock
N_i	number of the simulated particle in cell i
n	number density
n_0	inlet flow density
P_0	inlet flow pressure
P_{0y}	pressure behind the shock
P_{om}	pressure measured by pitot tube
P_e	pressure of outlet boundaries
P_s	stagnation pressure
P_x	pressure before the shock
R	radius distance
Re	Reynolds number
T_0	inlet flow temperature
U	axial velocity
U_0	thermal velocity
U_m	velocity of Mach number = 1
U_{max}	maximum velocity
V_c	cell volume
W_i	particle weight in cell i
Z	axial distance from nozzle-exis plane
λ	mean free path
γ	specific heat ratio
Φ's	conserved flux quantity
Δt_i	time step in cell i
ΔX	$V_c^{1/3}$, characteristic length of the cell

Chapter 1 Introduction

1.1 Background

For the control of spacecraft in orbit, low-density nozzles are often used. Thrust level of the nozzle is generally small, and it was considered previously that they posed few problems of integration with the spacecraft. However, Dettleff [1] has pointed out that such small rockets may cause some problems for the reducing the lifetime of spacecraft operation. Although the firing period of these nozzles is usually only a few seconds, it must be remembered that they are fired repeatedly for a number of years. This may cause some problem such as the contamination on the spacecraft (e.g., solar array). In addition, the plume can cause the heating and electrical charging of the spacecraft, which can alter the thermal balance and damage scientific instruments. Thrust loss and disturbance torques are also unwanted effects, which can result from the repeated firing of the small rockets (nozzles). The magnitude of the influence is very much dependent on both the thruster design and the satellite configuration.

Understanding of the interaction between the plume and the spacecraft requires an accurate description of the plume flow field. Normally the analysis strongly depends upon the simulation tool such as direct simulation Monte Carlo method [6] due to the difficulties of real-scale experiments on the ground. Hence, the verification of the simulation tool becomes a critical step in using them as the assessment of design of the reaction control system on spacecraft.

However, accurate measurements in rarefied gas dynamics are relatively difficult as compared with those in continuum gas dynamics. In the past, Pitot tube has been used to measure the total pressure distribution within rarefied plume [3]. Electron beam technique has been used to measure the number density and rotational temperature in a rarefied supersonic nozzle [4]. In addition, spontaneous Raman scattering technique was employed to measure the total number density, rotational temperature and the number density of the first level [5].

A crucial underlying assumption of Navier-Stokes equations is that fluid may be treated as a continuum, rather than as a collection of discrete particles, as is assumed and more difficult to solve, in the Boltzmann Equation [6]. Unfortunately continuum assumption begins to break down when the mean free path (λ, average distance travelled by molecules before collision) becomes comparable to flow characteristic length (L). Hence, the N-S based computational fluid dynamics (CFD) techniques are often inappropriate for higher-Kn flows. DSMC, first introduced by Bird [6], has been recognized as the standard method for studying rarefied gas dynamics. It has been applied very successfully to the analysis of hypersonic flows and high vacuum technology, to name a few [see Ref. 6 and the references cited therein]. Most importantly, DSMC is the only tool available to deal with gas flows in the transitional regime, without resort to more difficult Boltzmann Equation, which requires modeling of the integro-differential (collision) term. For the analysis of rarefied gas dynamics, DSMC has been proved to be a very powerful tool.

The DSMC method requires the introduction of computational cells (meshes) similar to those in CFD, while the cells are mainly used for selecting collision partner, sampling and averaging the macroscopic flow properties. Many physical problems involve very complicated geometry of objects; thus, unstructured mesh has been recommended to take advantage of the flexibility of handling this situation [20-22]. In addition, using unstructured mesh has the flexibility of applying graph-partitioning technique for parallel implementation of the DSMC method [16,24].

In our laboratory, Wu and Tseng [22] had developed a two dimension DSMC method using unstructured mesh, and was used to analyze micro-scale gas flow with pressure boundaries. Wu et al. [29] developed two important treatments of boundaries for micro-scale flow (ex: micromechanical devices). There are specific pressure and flux. The DSMC method is used to predict the rarefied flow in space, such as the space shuttle re-entry problem. It is mainly to deal with external flow not internal flow. Hence, to deal with internal flow boundaries is a challenge. Wu et al. [30] developed the DSMC method using unstructured adaptive mesh, it is used to simulated the hypersonic flow. This adaptive mesh model can adjust the mesh grid size, and makes it suitable for flow conditions, the model does will with the flow of large density gradient. Wu et al. [25] and Wu et al. [31] successful made a parallelization of the two dimension DSMC method as above mention with static domain decomposition, and discussed the efficiency and speed up of parallelization. Figure 1 illustrates the speed up performance, in this figure, the speed up performance is obey the Amdahl's assumption [32]. When the CPU number increasing, the speed up performance curve becomes more smooth. Lian and Wu [2] completed the three dimension parallel DSMC method using unstructured mesh, applied in external flow simulations, and compared with published experimental data. It still used the static domain decomposition. Wu and Tseng [24] used the graph-partitioning technique to develop the dynamic decomposition domain model, applied in two and three dimension DSMC code, it has a better efficiency. Figure 2 illustrates speed up performance of parallel DSMC computation for a high-speed driven cavity flow with dynamic domain decomposition on IBM SP2 at NCHC. This figure shows that using dynamic decomposition domain model to distribute computation domain makes a more efficient usage of computational resource. Wu and Tseng [33] used the base of Wu and Tseng [24], and combined the variable time step scheme and unstructured adaptive mesh, it makes a precision and efficient predictions.

1.2 Objectives

The objectives of current project can be summarized as follows:

(1) To complete the total pressure measurements using pitot tube in the near-nozzle region of a convergent-divergent nozzle which is used for ROCSAF-1 satellite;

(2) To simulate the flow field in the near-nozzle region of the same nozzle as above using DSMC method;

(3) To compare the experimental data with DSMC simulation data.

Chapter 2 Numerical Method

Generally, there are two methods to simulate the gas flow. One is the continuum method and the other is particle method. In the current study, we use a commercial Navier-Stokes equations solver, UNIC [18], for simulating the flow field within the C-D nozzle to provide the throat conditions for DSMC method. The information is skipped. For details, refer to its manual [18]. The direct simulation Monte Carlo (DSMC) method, which is a particle-based method, is then used to simulate the flow field of jet plume under rarefied conditions.

2.1 The Conventional DSMC Method

The basic idea of the DSMC method is to calculate practical gas flows through the use of no more than the collision mechanics. The molecules move in the computational domain so that the physical time is a parameter in the simulation and all flows are computed as unsteady flows. An important feature of DSMC is that the molecular motion and the intermolecular collisions are uncoupled over the time intervals that are much smaller than the mean collision time. Both the collision between molecules and the interaction between molecules and solid boundaries are computed on a probabilistic basis and, hence, this method makes extensive use of random numbers. In most practical applications, the number of simulated molecules is extremely small compared with the number of real molecules. In current study, Variable Hard Sphere (VHS) model [6] and No Time Counter (NTC) [6] are used to simulate the molecular collision mechanism. The details of the procedures, the consequences of the computational approximations can be found in Bird (1994); thus, it is only briefly described here for brevity. In brief summary, general procedure of the DSMC method consists of four major steps: moving, indexing, collision and sampling, as shown in figure 3.

2.2 Parallel DSMC Method

The DSMC algorithm is readily parallelized through physical domain decomposition. The cells of the computational grid are distributed among the processors. Each processor executes the DSMC algorithm in serial for all particles and cells in its domain. Data communication occurs when particles cross the domain (processor) boundaries and are then transferred between processors. Figure 4 illustrates a simplified flow chart of the 3-D parallel DSMC method used in the current study. Procedures can be found in Lian's MS thesis [2] and are not repeated here in detail. First, we construct an unstructured tetrahedral using a commercial meshing tool. The output grid data are then processed using a conversion program to transform them into a *globally sequential but locally unstructured mesh* data [2] conforming the partitioning information, as schematically shown in figure 5. In addition, a processor neighbor-identifying array is created for each processor, which is used to identify the surrounding processors due to the unstructured format of the processor distribution in the domain. From previous practical experience [2], the maximum numbers of processor neighbor are on the order of ten; therefore, the increase of memory cost is negligible. The resulting *globally sequential but locally unstructured* mesh data is then imported into the parallel DSMC code.

After reading the mesh data on a master processor (cpu0), the mesh data are then distributed to all other processors according to the predetermined domain decomposition. All the particles on each processor then start to move as in sequential algorithm. The particle data are sent to a buffer and is numbered sequentially when hitting the inter-processor boundary (IPB) during its journey within a simulation time step. After all the particles on a processor are moved, the destination processor for each particle in the buffer is identified via a simple arithmetic computation, owing to the approach adopted for the cell numbering, and are then packed into arrays. Considering communication efficiency the packed arrays are then sent as a whole to its surrounding processors in turn based on the tagged numbers. Once a processor sends out all the packed arrays, it waits to receive the packed arrays from its surrounding processors in turn. This “send” and “receive” operation serves practically as a synchronization step during each simulation time step. Received particle data are then unpacked and each particle continues to finish its journey for the remaining time step. The above procedures are repeated twice since there might be some particles cross the IPB twice during a simulation time step.

After all particles on each processors have come to their final locations at the end of a time step, the program then carries out the indexing of all particles and the collisions of particles in each computational cell on each processor as usual in a sequential DSMC code. The particles in each cell are then sampled at the preset appropriate time.

Higher parallel efficiency can only be achieved if communication is minimized and the computational load is evenly distributed among processors. To minimize communication for between processors, the spatial domain decomposition should adapt according to the workload distribution as simulation continues, which requires dynamic domain decomposition. For the DSMC algorithm, the workload (or equivalently particle numbers) on each processor changes frequently, especially during the transient period of a simulation, while the workload attains a roughly constant value during steady-state sampling.

Although DSMC possesses nearly 100% parallelism (except for initialization and final output), both the values of speedup and efficiency are expected to be lower than the ideal values due to the load unbalancing and communication as mentioned previously. It is needed to make the load balanced.

2.3 Dynamic Load Balancing (DLB)

In the current study, we have incorporated a multi-level graph-partitioning technique [23] to dynamically re-decompose the computational domain. Figure 6 shows the flow chart of the parallel DSMC method using dynamic domain decomposition. Details can be found in Wu and Tseng [19,24]; it is only briefly described here. The current DSMC method is implemented on an unstructured mesh using particle ray-tracing technique by defining a cell neighbor-identifying array [2,19,21,24,25], which takes the advantages of the cell connectivity information. Number of particles is taken as the vertex (cell center in the DSMC mesh) weight and unitary weight is used for edge cut under the framework of graph theory. Stop at Rise (SAR) [9] scheme is used to determine when to repartition the computational domain by defining a degradation function, which represents the average idle time for each processor including the cost of repartition. Communication of particle data between processors only occurs when particle hits the inter-processor boundary, while communication of cell data only occurs when repartitioning the domain takes effect. Data for communication are sent and received as a whole to reduce the communicational time between processors. From previous studies [19,24], the current parallel DSMC method using dynamic domain decomposition in general runs 50-100% faster than that using static domain decomposition up to 64 processors on IBM-SP2 parallel Machine.

The current parallel code, in SPMD (Single Program Multiple Data) paradigm, is implemented on the PC-cluster system (distributed memory system) using message passing interface (MPI) to communicate information among processors. In addition, it is essentially no code modification required to adapt to other parallel Machines (e.g., IBM-SP2 and IBM-SMP) if similar distributed memory system is used and employs the same MPI libraries for data communication.

2.4 Variable Time Step Scheme (VTS)

In DSMC, particle distribution per cell has been shown to be linearly proportional to the inverse of number density for two-dimensional flow if the constant weight for each particle is used and cell size scales exactly with local mean free path; that is, the number of simulation particles is lower in higher-density regions, while low-density regions are over resolved [26]. More computational time is indeed wasted in calculating the low-density regions than is needed. This situation is even more obvious in three-dimensional flows, where the number of particles per cell is squarely proportional to the inverse of gas density. To obtain a more uniform distribution of simulated particles per cell throughout the computational domain without detrimental effects caused by particle cloning, a variable time-step method for DSMC is then proposed on the unstructured mesh system as follows. Advantages of implementing the variable time-step scheme are to reduce both the simulated particle numbers and the number of iterations of transient period towards steady state, when the sampling normally starts in DSMC.

Figure 7 shows the sketch of variable time-step concept for a simulated particle moves across the cell interface. Fluxes (mass, momentum and kinetic energy) conservation should be enforced when a simulated particle crosses the cell interface. Thus,

$$\frac{W_1\Phi_1}{A\Delta t_1}=\frac{W_2N_2\Phi_2}{A\Delta t_2} \tag{1}$$

where W's, Φ's (=m, mv, $mv^2/2$ or other internal energy) and Δt's are the particle weight, conserved flux quantity and time step, respectively, and the number at subscripts represents cell numbers. Note that A represents the area of cell interface between cell 1 and 2. N_2 is number of the simulated particle in cell 2, which originated from cell 1. There are several choices of the corresponding parameters to satisfy Eq. (1), with which we can play. The best choice is to set N_2=1 (without particle cloning) and to keep $\Phi_1 = \Phi_2$ without changing the velocity across the cell interface, such that $\frac{W_1}{\Delta t_1} = \frac{W_2}{\Delta t_2}$ holds. In other words, $\frac{W_i}{\Delta t_i}$ will be the same for all cells throughout the computational domain. Using this approach, resulting number of simulated particles per cell for the three-dimensional flow scales with Δx ($\sim\sqrt[3]{V_c}$, V_c is the cell volume) [26] if cell size is proportional to the local mean free path, which otherwise scales with $(\Delta x)^2$. In doing so, the simulated particle will only have to adapt its weight that is proportional to the size of time step, which is approximately commensurable to the local mean free path if solution-based adaptive mesh is used. Of course, the remaining time for a simulated particle, when crossing cell interface, should be rescaled according to the ratio of time steps in original and destination cells. In the DSMC code, a reference time step is first computed by selecting a reference cell volume (often the minimum cell volume). Then, time steps in other cells are scaled using the fact $\frac{W_i}{\Delta t_i}$=constant.

Consequences of using VTRS in the DSMC method are to, first, reduce the number of simulation particles, and, secondly, to decrease the number of iteration required for transient period. It is thus expected to reduce greatly the computational time. It has been shown it can be reduced to an order of magnitude in computational time [Wu and Tseng, 28].

Chapter 3 Experimental Method

3.1 Experimental Apparatus

A small vacuum chamber test facility at Gas Dynamics & Kinetics Laboratory (GDKL) along with other test arrangements (as illustrated in figure 8) will be used to provide the high vacuum environment for the experiment of jet plume.

It consists of a high-pressure gas source, plenum chamber (as illustrated in figure 9), a convergent-divergent (C-D) nozzle with area ratio 100 (as illustrated in figure 10) and a small vacuum chamber at GDKL (as illustrated in figure 11). Both Pitot tube and nozzle assembly, which is movable and rotatable, is installed in the main chamber for total pressure measurements.

Nozzle for producing the flowfield that simulated a thruster as shown schematically in figure 12, which is the same design with ROCSAF-1 satellite except the size is 1.41 times larger.

3.2 Experimental Instruments

Gas pressure at plenum chamber was measured with a capacitance-manometer transducer having range of 0-1000 torr (MKS 627B 1000torr) having accuracy of 0.12% reading. Gas temperature at plenum chamber and vacuum chamber were measured with K-type thermocouples.

A pitot tube that was shown in figure 13 which is traversable and rotatable in the chamber, was used to measure total pressures in the nozzle plume. The pitot tube was attached directly to a capacitance-manometer having range of 0-100 torr (MKS 627B 100torr) having accuracy of 0.12% reading.

3.3 Test Procedure and Test conditions

Test gas source is nitrogen gas. Nozzle flow conditions are listed at Table 1. Chamber pressures are maintained at the level of 0.16 (condition 1) and 0.09 (condition 2) torr to simulate the environment in orbit. Pressure ratios of plenum to main chamber are about 94 and 111. The test section containing the pitot tube was first evacuated without gas flow to establish zero settings for the capacitance-manometers. The vacuum pressure without flow is under 10^{-3} torr which serves as the zero-reference pressure. After the instruments were zeroed, gas source is turned only by adjusting a valve attached at gas source.

After the system reaches steady state, pressure scans were made by moving the pitot probe and plenum chamber to defined location of measurement and the probe is rotated to determine the direction of maximum pressure. The flow is symmetric and then all reported pressure scans were made in the line through the nozzle center point

(R/De=0) and extending outward radially.

Chapter 4 Results and Discussions

4.1 Calculation of Total Pressure

To compare the numerical solutions with experimental data, pitot pressure were first calculated from numerical results using the computed state variables. The calculated pitot pressure can be viewed as the pressure would be measured if a pitot tube were insert into the stream. Because the flow contains supersonic and subsonic regions, we converted the numerical data with two different formulas.

(1) If the flow state at computed point is supersonic (Mach number > 1), the pressure ratio across normal shock was calculated with Rayleigh pitot equation (Ref. 7, p. 154) represented by the functional relation:

$$\frac{p_{0y}}{p_x}=\left(\frac{\gamma+1}{2}M_x^2\right)^{\frac{\gamma}{\gamma-1}}\bigg/\left(\frac{2\gamma}{\gamma+1}M_x^2-\frac{\gamma-1}{\gamma+1}\right)^{\frac{1}{\gamma-1}} \tag{2}$$

where γ is the ratio of specific heats which for nitrogen is 1.4

(2) If the flow state at computed point is subsonic (Mach number < 1), the stagnation pressure was calculated as isentropic flow of perfect gas with equation as follow (Ref. 7, p. 83):

$$\frac{p_s}{p_x}=\left(1+\frac{\gamma-1}{2}M_x^2\right)^{\frac{\gamma}{\gamma-1}} \tag{3}$$

4.2 DSMC Simulation

4.2.1 Verification of parallel DSMC code

We have verified our parallel DSMC code with previously published experimental data by Boyd [17], under similar conditions of the current study. Related flow conditions of Boyd [17] are listed in Table 2 Boyd [17] has used the continuum computation (Navier-Stokes equations solver, VNAP2) to obtain the inflow conditions at the throat. Similarly, we use a commercial CFD solver, UNIC [18], to obtain the inlet condition for the flows. Figure 12 is the normalized radial distribution of streamwise velocities near inflow location (nozzle throat). In this figure, the nearly uniform velocity region is in the range of $R/D_t = 0$ to 0.2 and gradually reach to the peak velocity about $R/D_t = 0.45$. Appreciable boundary is observed due to the low Reynolds number of the nozzle flow (Re=311.2). Thus, viscous effects can not be neglected in the flow, as can be seen later. We used the information as inflow conditions for DSMC simulation.

Figure 15-18 illustrated the total pressure distributions of experimental data and simulated data at Z=0, Z=12, Z=24 and Z=36, repetitively. Considering experimental uncertainties, simulation data using current parallel DSMC code show reasonable agreement with Bird's experimental data [17]. Thus, as a first step, we are confident that current parallel DSMC code is capable of predicting flow field in the near plume correctly.

4.1.2 DSMC simulation conditions for ROCAT-1 thruster

Nitrogen gas flows are simulated at the conditions of Knudsen numbers of 0.0022 (condition 1) and 0.0034 (condition 2), based on throat conditions. Knudsen number is defined as the ratio of mean free path in the plenum chamber to the nozzle throat diameter. Current flow conditions represent near-continuum rarefied flows, which is otherwise impossible. All other flow conditions are listed in Table 1.

In the upstream, the flow is near-continuum flow. A commercial CFD solver, UNIC [18], is used to simulate the flow within the nozzle, and the boundaries conditions of UNIC [18] simulation domain are the nozzle as figure 19 show. The inlet boundaries are fixed pressure condition, and outlet boundaries are extrapolated condition.

Simulated flow properties by UNIC [18] at nozzle throat are used as the inlet conditions for DSMC simulation. Figure 20 and figure 21 are the normalized axial velocity profiles of condition 1 and condition 2, they are normalized by the calculated speed that assuming the nozzle flow is isotropic flow. Because the viscosity effect, the boundary layer is very obvious.

Figure 22 and figure 23 show the normalized temperature profiles of condition 1 and condition 2, they are normalized by the stagnation temperature T_0. Temperature is higher within the boundary layer than outside, because of the viscosity effect.

Figure 24 and figure 25 show the normalized density profiles of condition 1 and condition 2, they are normalized by the stagnation density n_0. Density is lower near the wall than away, because there is the higher temperature near the nozzle wall.

These simulated properties can provide more reasonable inlet conditions rather than assuming that Mach number of unity is reached at the throat of the nozzle. The viscous effects can be taken into consideration.

The DSMC simulation domain for a single nozzle jet as well as the boundary conditions is illustrated in figure 26. The nozzle wall temperature is set as outlet temperature. And the other outlet boundaries employed the same setting with experimental conditions. Figure 27 is the mesh for DSMC simulation. Because the nozzle flow is axis-symmetric, we use the 1/16 domain and symmetric boundaries to reduce the computation domain.

We have used this parallel three-dimensional DSMC code to simulate the flow field. Approximately 380,000 tetrahedral cells and approximately 2,220,000(condition 1) and 3,200,000(condition 2) particles are used for the DSMC simulation, and 8 PCs were used.

4.3 Experimental and Simulated Results

4.3.1 Results of conditions 1

The pitot pressure profiles in nozzle exit plane (Z=0) are shown in Figure 28 (pitot pressure, P_{om}, has been normalized by the stagnation pressure P_o). Two separate profiles are shown: the experimental data, the DSMC solution. We can see the experimental data is higher the DSMC solution, it is because that the probe is inserted into the plume. It could be an obstacle, and interfered the flow. But we still can see the trend of pitot pressure dropping is very fast, about to radial distance R/D_e=0.6 the pitot pressure is dropped to outlet boundary pressure.

In figure 29- 33, the pitot pressure profiles at a constant axial distance of Z = 5, Z=10, Z=20, Z=30, Z=40 mm from nozzle exit plane. The simulated pressure are still higher than experimental pressure, it shows that the effect of nozzle's exist is still on. The pitot pressure dropping is fast, and all about the radial distance R/D_e=0.6 the pressure dropped to outlet boundary pressure.

Pitot pressures on the central line (R=0, Z=constant) are shown in figure 34, pitot pressure of simulated and experimental data are closely, and experimental data are slight higher than simulated data.

Figure 35 is the normalized Density contour of simulated data. It shows that the pressure ratio (P_o/P_e) is not high enough to make the nozzle plume continuously expand. The lowest density is nearly the nozzle wall about Z=-10 to 0, not at outlet boundaries.

Figure 36 illustrates the streamlines profiles. Because outlet boundaries are not vacuum conditions, it means that there are particles entering to the flow field form outlet boundaries. The particles are dragged to the downstream wise, so there are regions of vortexes nearly the up and down outlet boundaries.

Figure 37 and figure 38 are the temperature and Mach number contours of nozzle plume. Generally, the temperature are decreasing with increasing (flow speed up) Mach number, and increasing with decreasing (flow slow down) Mach number. There are some regions nearly nozzle wall, the flow temperature are higher than inlet flow condition, it causes by the viscosity effect.

Figure 39 is the normalized pressure contour, it was calculated by simulated data from the equation: P=nkT and normalized by stagnation pressure. The n is number density, k is Boltzmann constant and T is total temperature. The lowest pressure region is located about Z=-4.

Figure 40 is velocity profile at Z = -1. It shows that the viscosity effect is very obviously in the nozzle, the axis-direction velocity gradient in radial-direction near the wall is very large. There are slip conditions near the wall.

Over all, the nozzle flow is low Reynolds number and high speed flow, because of low density and small geometry.

The pressure profile of an isentropic supersonic C-D nozzle flow can be calculated with eq (3). If P_x is higher than eq (3) predicted, the flow field will be a shock. Figure 39 shows that the pressure first drops below the P_e and then rises to P_e in the region of Z=-10 to Z=0, it seems there be a shock. But in Figure 38, the Mach number profiles do not show any shock structure, it may because the exist of boundary layer.

4.3.3 Results of conditions 2 and comparison with condition 1

Figure 41 to figure 52 are the results for condition 2. All data from simulation and experiment of condition 2 have the same trend of flow with condition 1, but different flow conditions.

Compare figure 28 and figure 41, the nozzle exit plane normalized pitot pressure, condition 1 are higher than condition 2 about 50%.

Figure 38 and figure 50 are the Mach number contours. Form eq (3), higher P_o/P_e ratio can make the flow reach a higher Mach number. But in the figures, the local Mach numbers in condition 1 are higher than condition 2. It is because the eq (3) that is for inviscid flow. The viscosity effect must be considered. Lower Reynolds number means the viscosity effect is more important than the other. Condition 2 has higher

P_o/P_e ratio and lower Reynolds number, so the normalized pitot pressure are much lower condition 2.

Figure 35 and figure 47 are the normalized density contours. Figure 36 and figure 48 are the normalized pressure contours. Condition 2 has higher P_o/P_e ratio, so its normalized density dropping more quickly, and the lowest pressure region is more closely to the downstream wise than condition 1.

Figure 40 and figure 52 are the normalized axial direction velocity profiles. Slip conditions are more obviously in condition 2.

Chapter 5 Conclusions

In the current research, numerical and experimental studies for a small nozzle, which is a scaled-up of ROCSAT-1 thruster, are conducted. The flow regimes of the nozzle flow are varied form continuum to rarefied flows. A CFD solver, UNIC [18] simulated continuum region, it provides a reasonable inlet conditions for the DSMC simulation. The DSMC method simulated the nearly continuum to rarefied regimes.

By comparing simulated and measured data of condition 1 and condition 2. The DSMC method using Variable Time Step scheme (VTS) and Dynamic Load Balancing (DLB) technique can provide an accurate and efficient predition of a low-density flow in the nozzle. The viscosity effect and slip boundary condition in this study are important, because of low Reynolds number and rarefied flow condition. Current DSMC method makes the investigation of low-density flow easier and more efficient, which can be applied to the analysis of plume impingement in the future.

Because the pumping power is not enough, chamber pressure is relatively high as compared with that in space. There is still much room in low-density nozzle flow studies, the different pressure ratio make the different expanding flow conditions. Using pitot tube measures the flow total pressure is a kind of interfering measurement, the size of pitot tube design is very important. Improper design leads to the error of measurement. In the future, we should use a smaller pitot tube design.

Reference

1. Dettleff, G., "Plume flow and plume impingement in space technology, " Progress in Aerospace Science, Vol. 28, 1991, pp. 1-77.
2. J.-S. Wu and Y.-Y. Lian, "Parallel Three-Dimensional Direct Simulation Monte Carlo Method and Its Applications, " Computers & Fluids Volume 32, Issue 8 , Pages 1133-1160, September 2003.
3. Penko, P.F., Boyd, I.D, Meissner, D.L. and DeWitt, K.J., "Measurement and Analysis of a Small Nozzle Plume in Vacuum, " J. Propulsion, Vol. 9, 1993, pp. 646-648.
4. Rothe, D.E., "Electron Beam Studies of Viscous Flow in Supersonic Nozzles, " AIAA Journal, Vol. 9, 1971, pp. 804-811.
5. Boyd, I.D., Beattie, D.R. and Cappelli, M.A., "Numerical and Experimental Investigations of Low-Density Supersonic Jets of Hydrogen, " J. Fluid Mechanics, Vol. 280, 1994, pp. 41-67.
6. Bird, G.A.,"Molecular Gas Dynamics and the Direct Simulation of Gas Flows," Oxford University Press, New York, 1994.
7. Shapiro, A.H., "The Dynamics and Thermodynamics of Compressible Fluid Flow, " Ronald Press, New York, 1953.
8. Walshaw, C., Cross, M., Everett M.G., Johnson, S, and McManus, K.,

"Partitioning and Mapping of Unstructured Meshes to Parallel Machine Topologies, " in A.Ferreira and J.Rolim (Eds) .Proc Irregular 95: "Parallel Algorithms for Irregularly Structured Problems, " Volume 980 of LNCS. pp 121-126. Springer, 1995

9. Nicol, D. M., and Saltz, J. H., "Dynamic Remapping of Parallel Computations with Varying Resource Demands," IEEE Transactions of Computers, Vol. 39, No. 9, 1988, pp. 1073-1087.
10. R. P. Nance, D. B. Hash, and H. A. Hassan, "Role of boundary conditions in Monte Carlo simulation of microelectromechanical systems, " J. Thermophys. Heat Transfer 12, Techniqueal Notes: 447 (1998).
11. R. P. Nance, R. G. Wilmoth, B. Moon, H. A. Hassan, and J. H. Saltz, "Parallel Solution Monte Carlo Simulation of Three Dimensional Flow Over a Flat Plate, "J. Thermophys. Heat Transfer, 9(3), 471 (1995).
12. C. Walshaw, "Parallel Jostle Library Interface: Version 1.2.1, " School of Computation & Mathematical Sciences, University of Greenwich, London, SE10 9LS, UK, 2000.
13. C. Walshaw, "The jostle user manual: Version 2.1, " School of Computation & Mathematical Sciences, University of Greenwich, London, SE10 9LS, UK, (1999).

14. C. D. Robinson and J. K. Harvey, "A Parallel DSMC Implementation on Unstructured Meshes with Adaptive Domain Decomposition, " In Proc. of 20th Intern. Symposium on RGD, 1996, p. 227.
15. C. D. Robinson and J. K. Harvey, "Adaptive Domain Decomposition for Unstructured Meshes Applied to the Direct Simulation Monte Carlo Method, " Parallel Comput. Fluid Dynam., pp. 469-476, 1997.
16. C. D. Robinson, "Particle Simulation on Parallel Computers with Dynamic Load Balancing, " PhD thesis, Imperial College of Science, Technology and Medicine, U.K, 1998.
17. Boyd, I.D., Penko, P.F., Meissner, D.L. and DeWitt, K.J., "Experimental and Numerical Investigations of Low-Density Nozzle and Plume Flows of Nitrogen," AIAA Journal, Vol. 30 (10), 1992, pp. 2453-2461.
18. UNIC-CFD: "User's Manual," Engineering Sciences, Inc., Huntsville, AL 35802, USA.
19. J.-S. Wu, and K.-C. Tseng, "Concurrent DSMC Method Using Dynamic Domain Decomposition," Journal of Computational Physics, 2003 (submitted).
20. Bird, G. A., "Molecular Gas Dynamics, " Clarendon Press, Oxford, UK, 1976.

21. Piekos, E. S., and Breuer, K. S., "Numerical modeling of micromechanical devices using the direct simulation Monte Carlo method, " Transaction of the ASME: Journal of Fluids Engineering, Vol. 118, 1996, pp. 464-469.

22. Wu, J.-S. and Tseng, K.-C., "Analysis of micro-scale gas flows with pressure boundaries using the direct simulation Monte Carlo method," Computers & Fluids, Vol. 30, pp. 711-735, 2001.

23. Walshaw, C., Cross, M., and Everett, M., "Parallel Dynamic Graph Partitioning for Adaptive Unstructured Meshes," Journal of Parallel and Distributed Computing, Vol. 47, No. 2, 1997, pp. 102-108.

24. Wu, J. S., and Tseng, K. C., "Concurrent DSMC Method Using Dynamic Domain Decomposition," 23rd International Symposium on Rarefied Gas Dynamics, Whistler Conference Centre Whistler, British Columbia July 20-25, 2002.

25. Wu, J. S., Tseng, K. C., and Yang, T. J., "Parallel Implementation of the Direct Simulation Monte Carlo Method Using Unstructured Mesh and Its Application, " International Journal of Computational Fluid Dynamics, 2003. (in press)

26. Kannenberg, K., and Boyd, I. D., "Strategies for Efficient Particle Resolution in the Direct Simulation Monte Carlo Method, " Journal of

Computational Physics, Vol. 157, 2000, pp. 727-745.

27. S.J. Kline, "The Purpose of Uncertainty Analysis," Journal of Heat Transfer-Transactions of the ASME, vol. 117, pp.153-160 ,1985.
28. J.-S. Wu, K.-C. Tseng and F.-Y. Wu, "Three-Dimensional Direct Simulation Monte Carlo Method Using Mesh Refinement and Variable Time-Step," AIAA Journal, 2003. (submitted)
29. Wu, J.-S., Lee, Fred and Wong, S.-C., "Pressure boundary treatment in micromechanical devices using the direct simulation Monte Carlo method," JSME International Journal, Series B, Vol. 44, No.3, pp.439-450, 2001.
30. Wu, J.-S., Tseng, K.-C. and Kuo, C.-H., "The direct simulation Monte Carlo method using unstructured adaptive mesh and its application," International Journal of Numerical Methods in Fluids, Volume 38, Issue 4, pp, 351-375, 2002.
31. Wu, J.-S and Tseng, K.-C., "Parallel Particle Simulation of the near-continuum hypersonic flows over compression ramps," Journal of Fluids Engineering Transactions of ASME, Vol. 125, No. 1, pp. 181-188, 2003.
32. Vipin, K., Ananth, G., Anshul, G. and George, K., Introduction to Parallel

Computing – Design and Analysis of Algorithms, The Benjamin/Cummings Publishing Company, Inc., 1994.

33. Wu, J.-S. and Tseng, K.-C., "Concurrent DSMC Method Combining Variable Time-Step and Unstructured Adaptive Mesh," Parallel CFD 2003 Conference, Moscow, Russia, May 11-13, 2003. (accepted)

Table. 1 Current study experimental and simulation conditions

	Condition 1	Condition 2
Stagnation Pressure P_o	15 torr	10 torr
Stagnation Temperature T_o	30 ℃	31 ℃
Outlet Pressure P_e	0.16 torr	0.09 torr
Outlet Temperature T_e	29 ℃	30 ℃
Reynolds number Re	311.2	207.1
Knudsen number Kn	0.0022	0.0034
Pressure ratio P_o/P_e	94	111

*The Reynolds number is defined by nozzle throat diameter, assuming the flow speed reach to Mach number=1 at throat, and flow parameters as table 1 listed.

*The Knudsen number is defined by nozzle throat diameter and gas mean free path at stagnation pressure P_o and temperature T_o.

Table. 2 Simulation and flow conditions of Boyd [17]

Stagnation Pressure P_o	6400 Pa
Stagnation Temperature T_o	699 K
Outlet Pressure P_e	10^{-4} Pa (served as vacuum)
Outlet Temperature T_e	NA
Reynolds number Re	850
Knudsen number Kn	0.0006

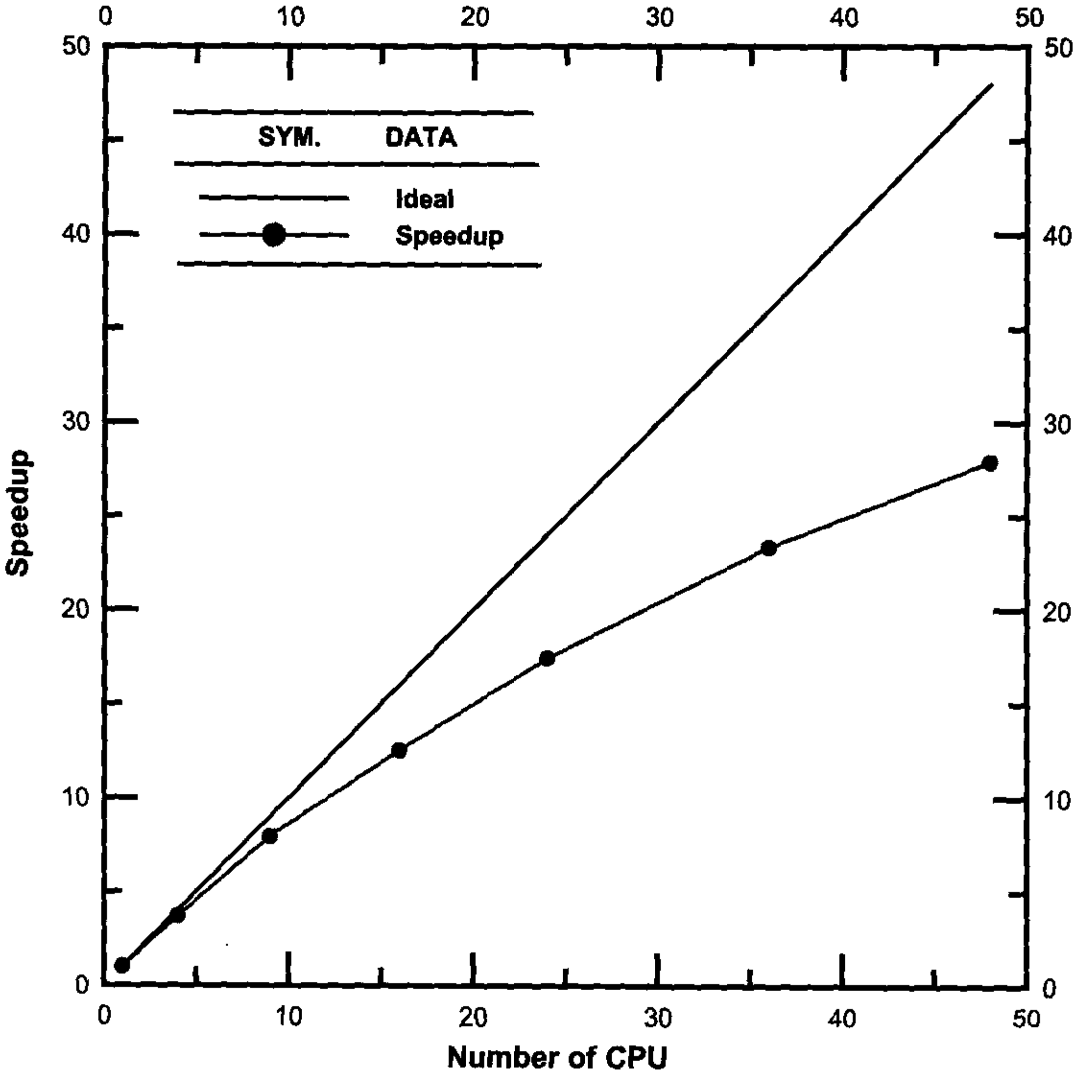

Fig. 1. Speedup of parallel DSMC computation for a high-speed driven cavity flow.

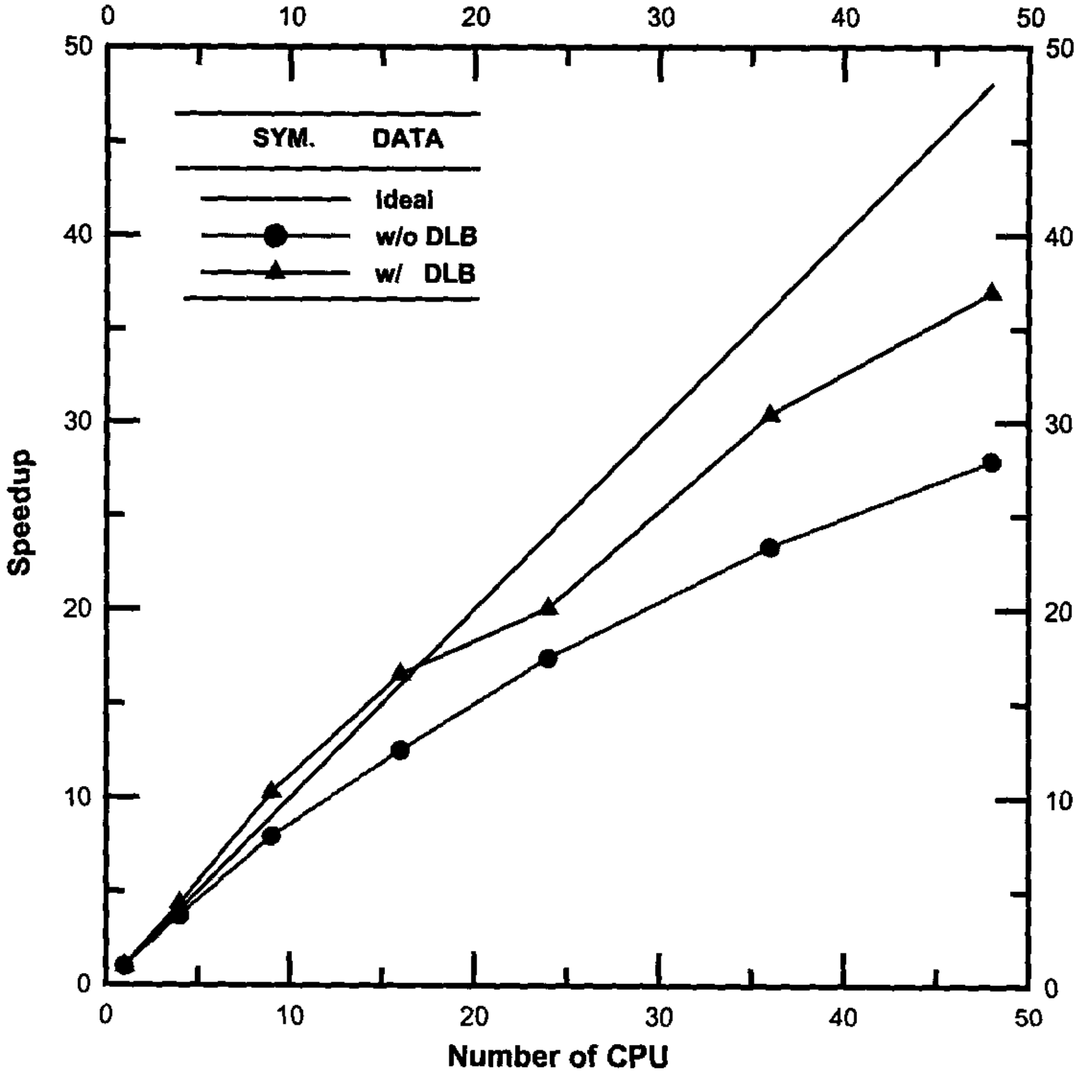

Fig. 2. Speedup of parallel DSMC computation for a high-speed driven cavity flow with dynamic domain decomposition on IBM SP2 at NCHC. (small problem size)

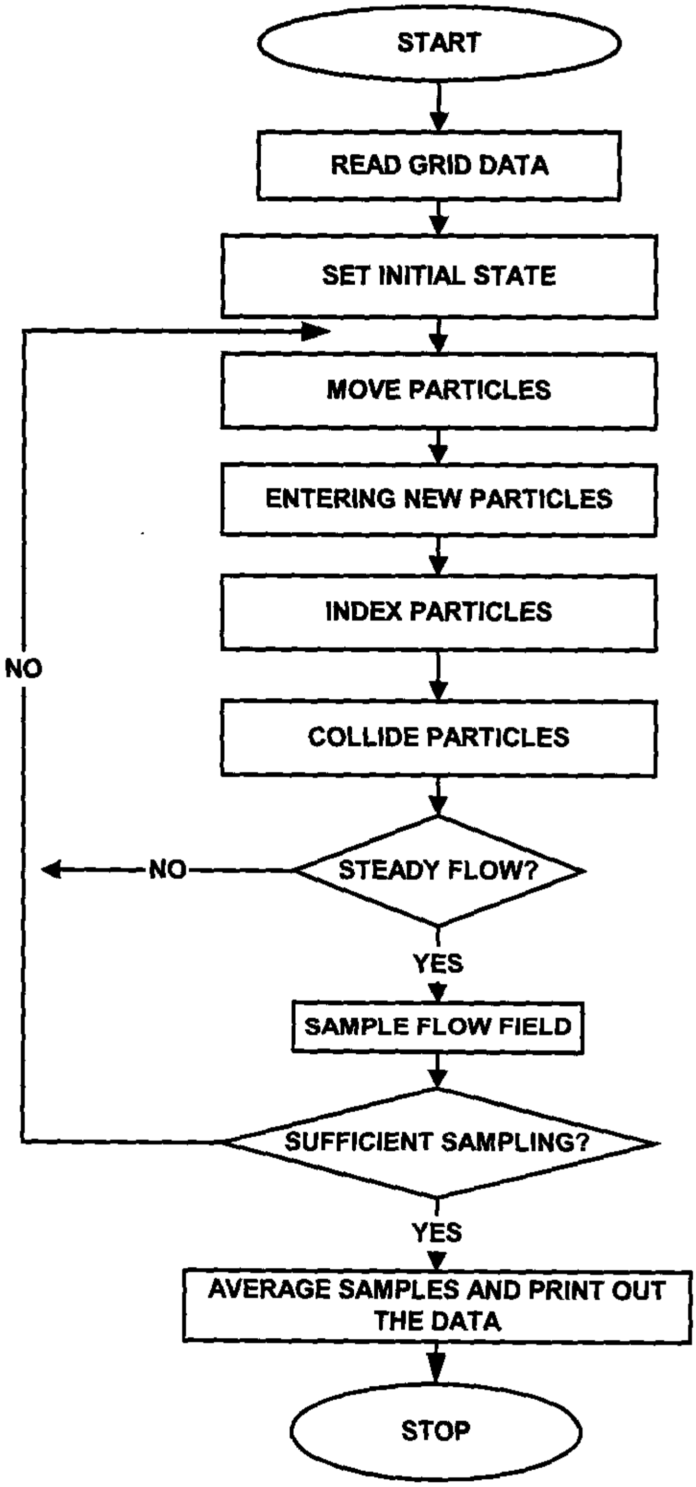

Fig. 3. Conventional DSMC flow chart

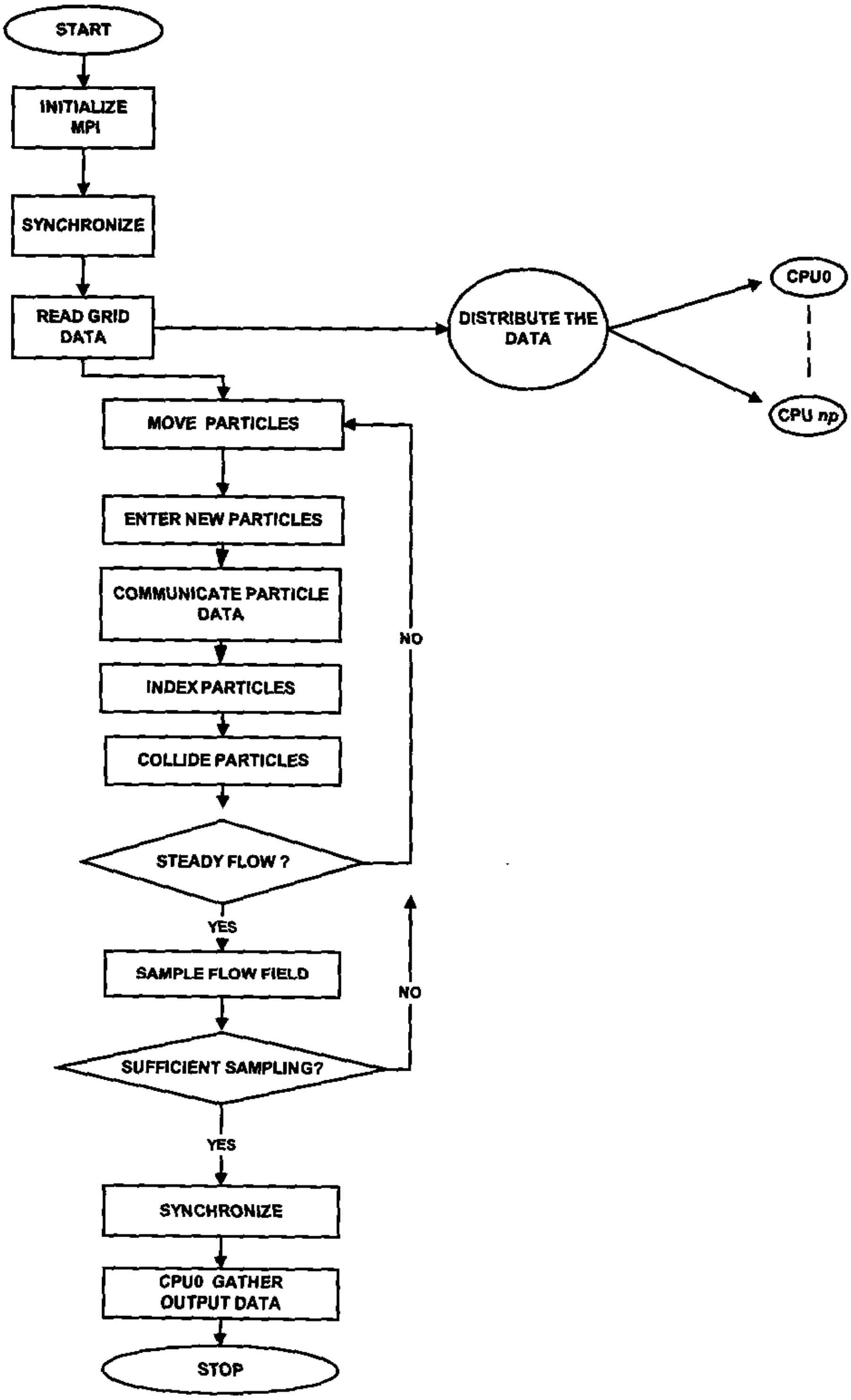

Fig 4. Simplified flow chart of the parallel DSMC method for np processors

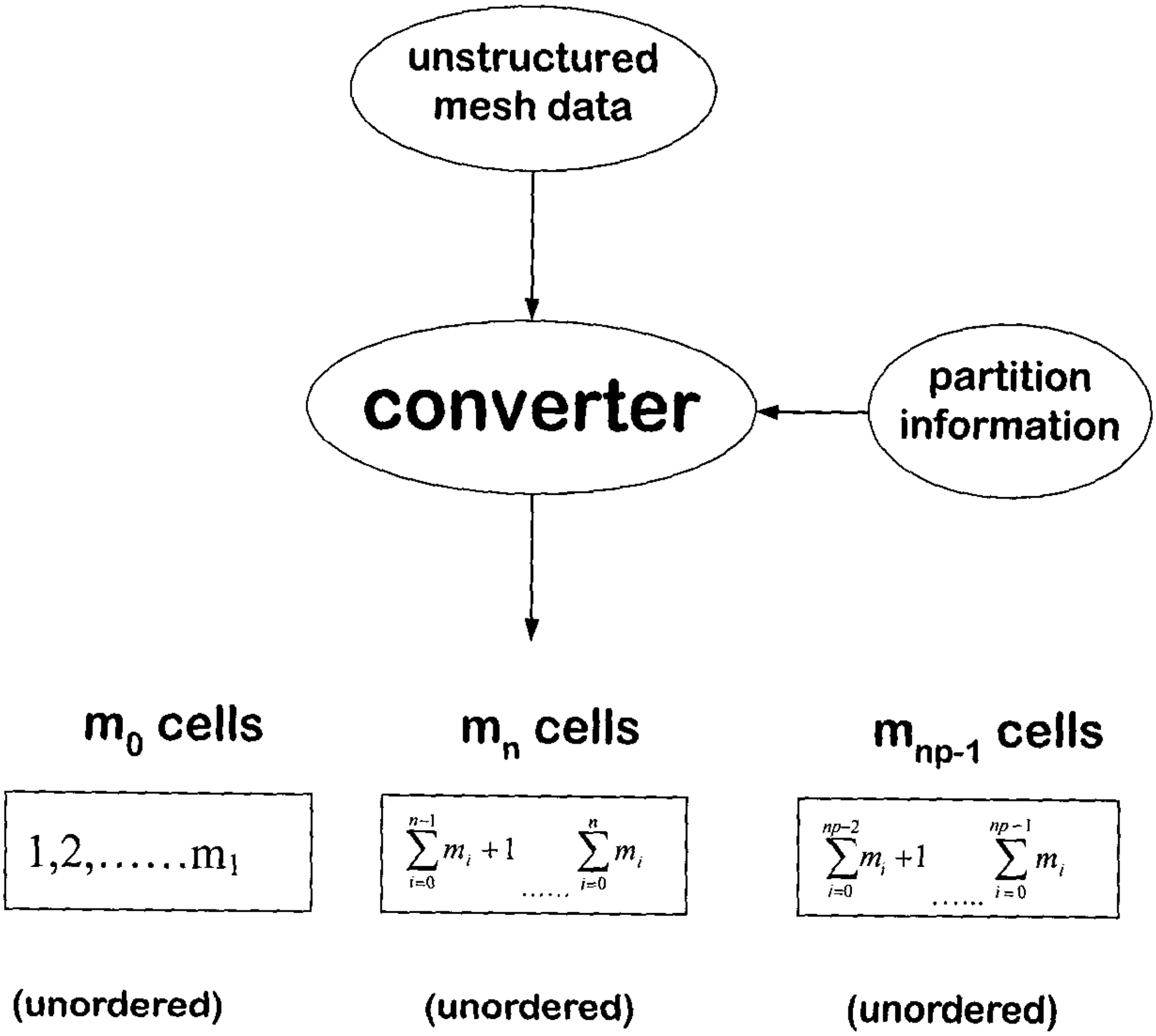

Fig 5. The sketch of the concept of conversion program

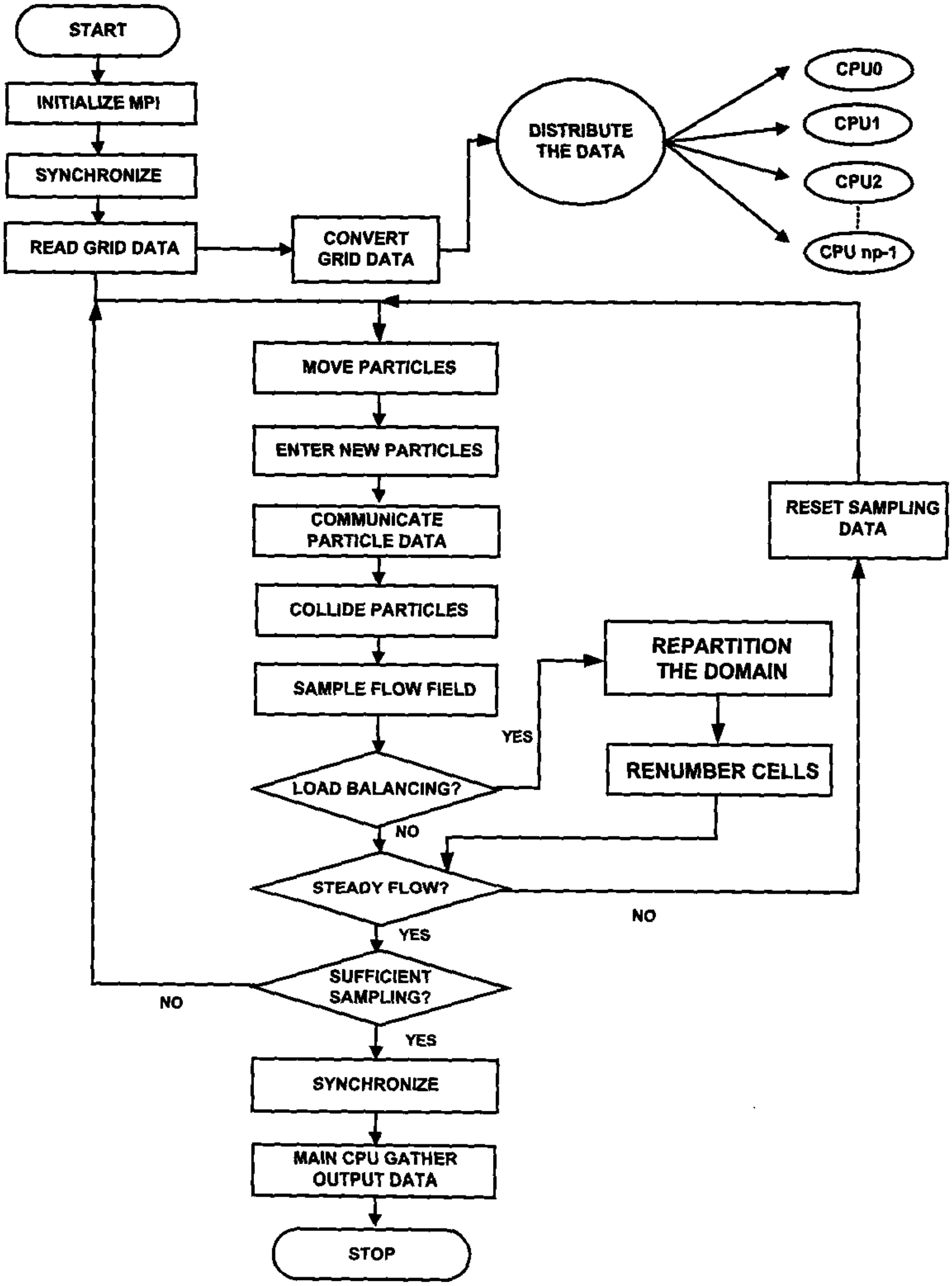

Fig 6. Simplified flow chart of the parallel DSMC method with Dynamic Load Balancing technique

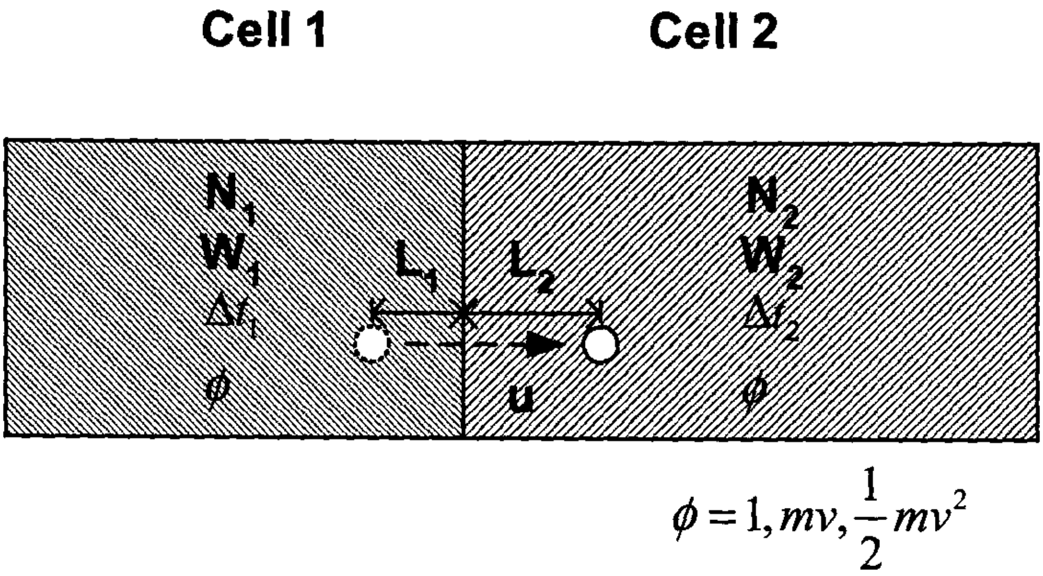

Fig 7. The sketch of the concept of variable time step scheme

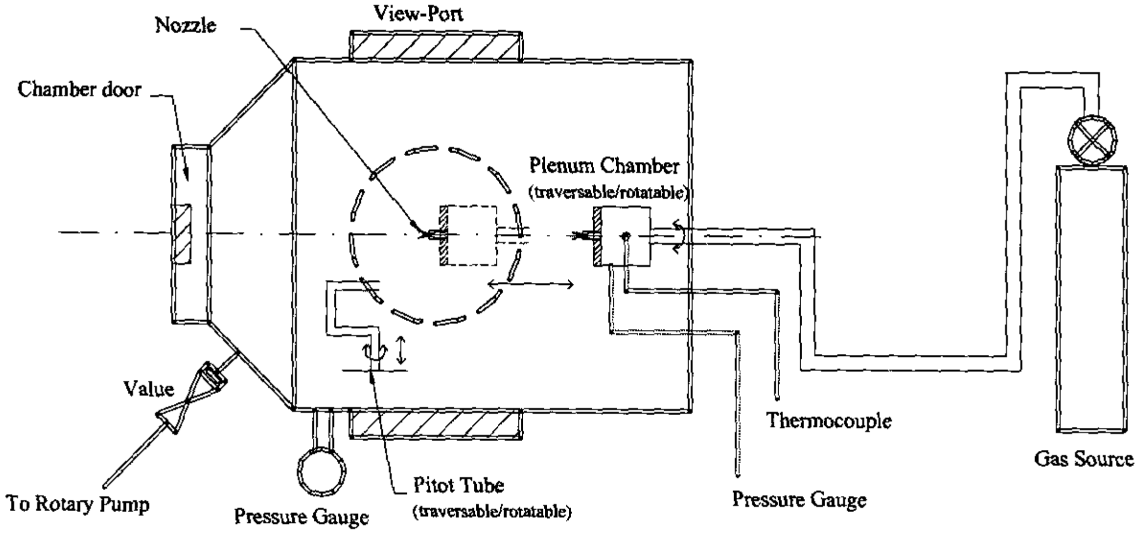

Fig. 8. Small vacuum chamber test facility at GDKL along with other test arrangements.

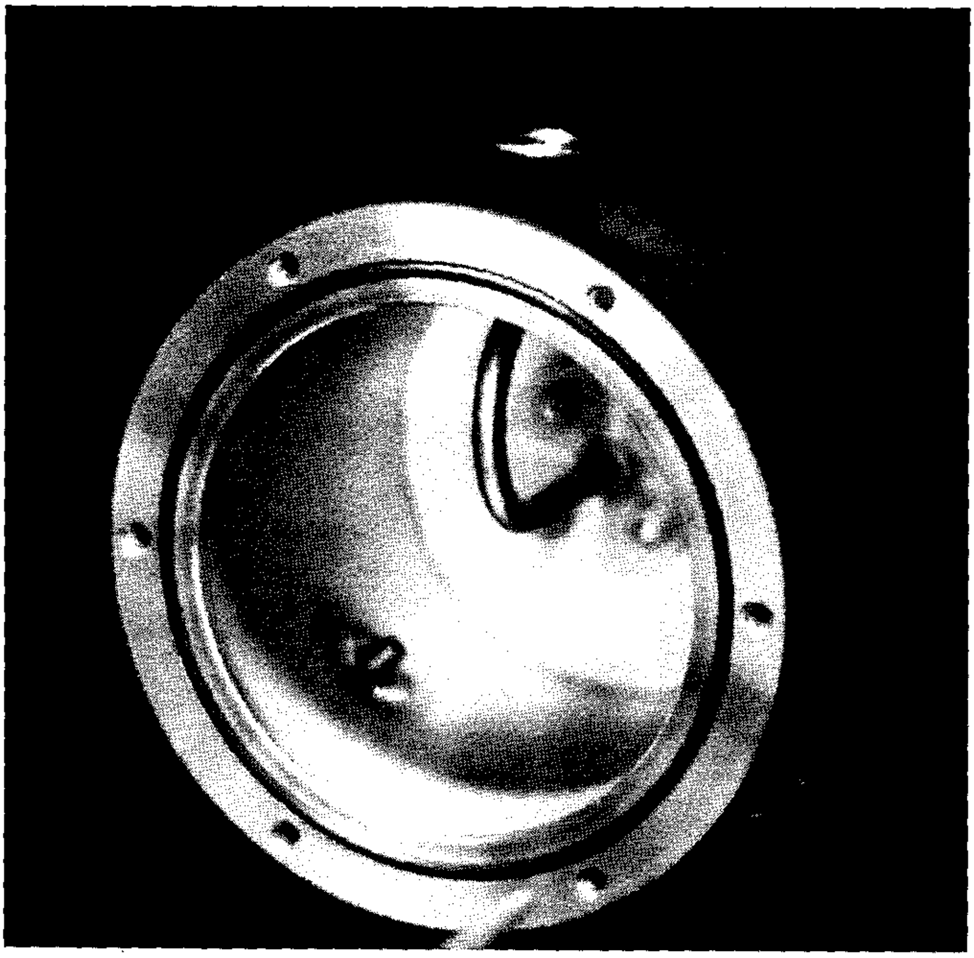

Fig. 9. Picture of plenum chamber with the end cap removed.

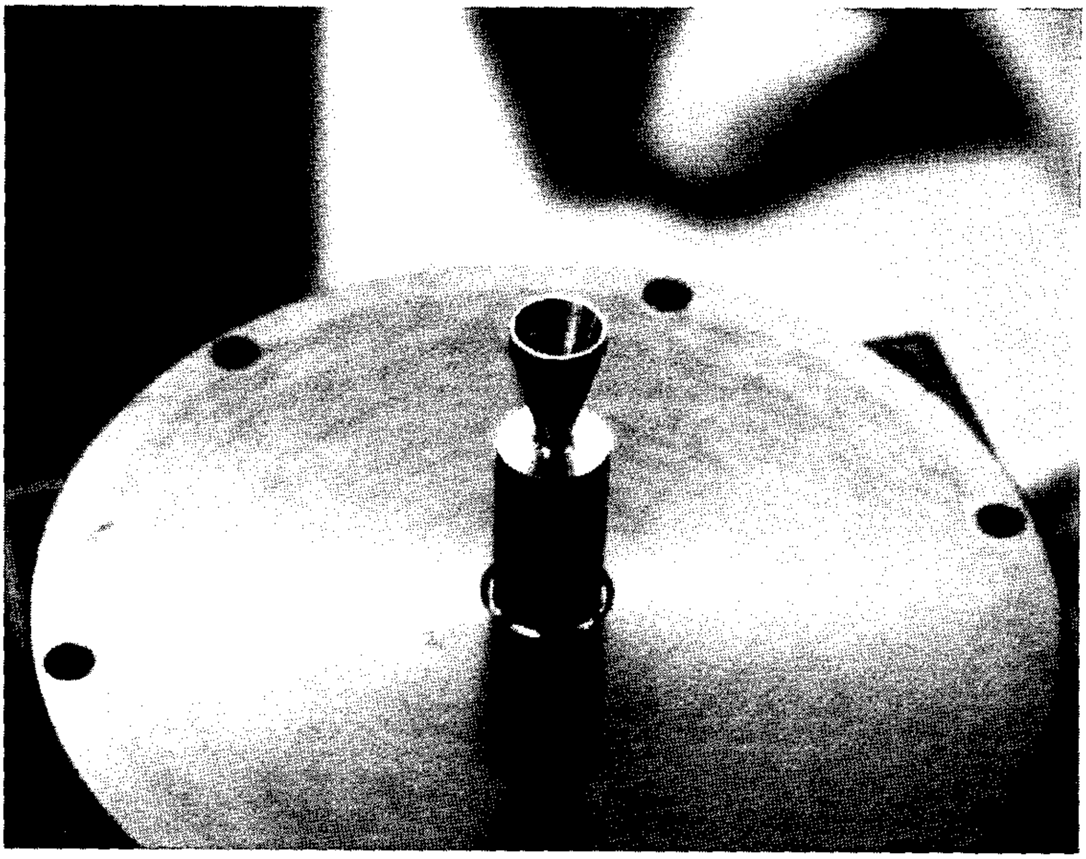

Fig. 10. Pictured of C-D nozzle and it's support fixture

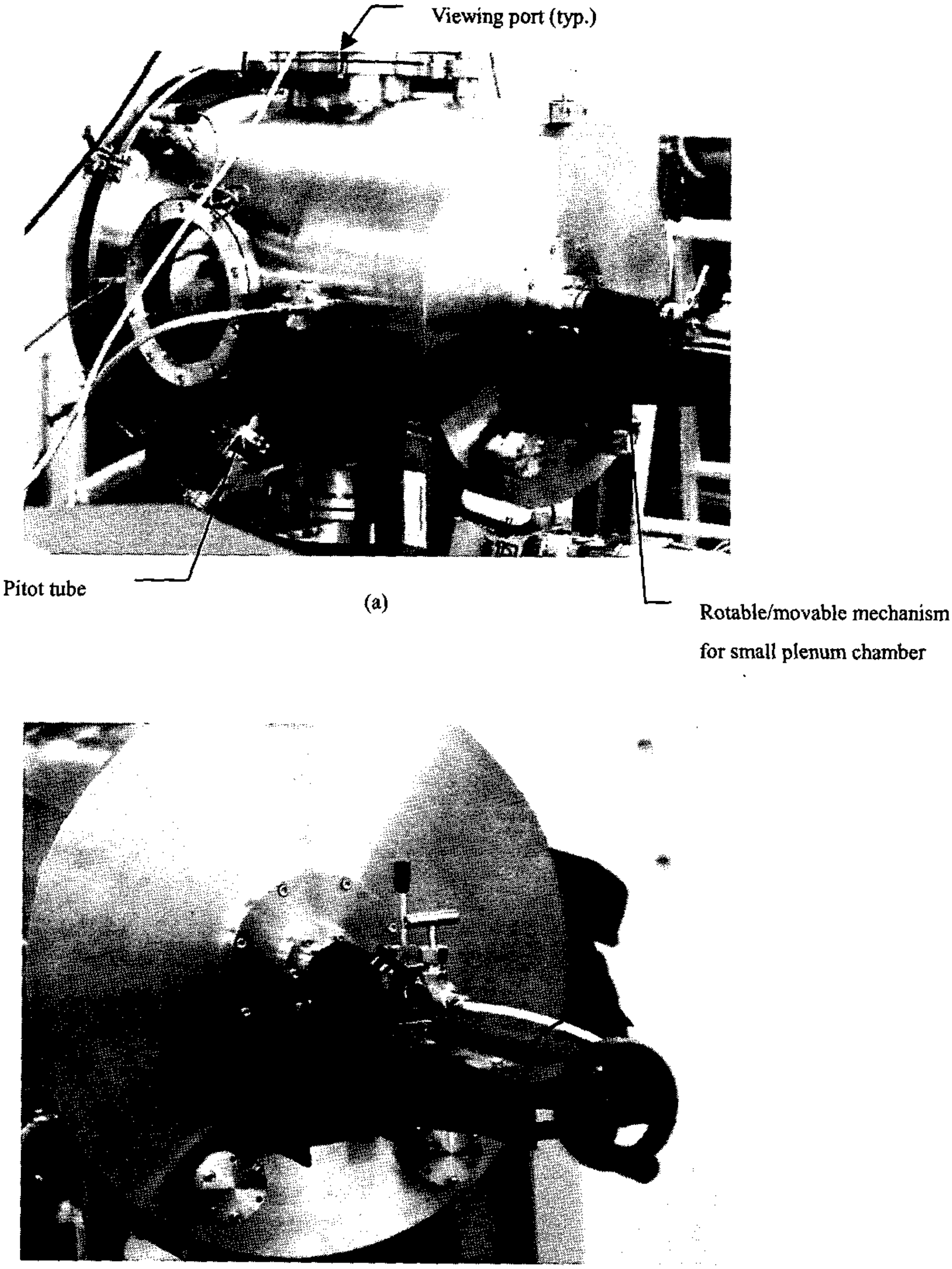

(a)

(b)

Fig. 11. Pictures of vacuum chamber:(a) Birdeye's view; (b) rotable/movable mechanism for small plenum chamber.

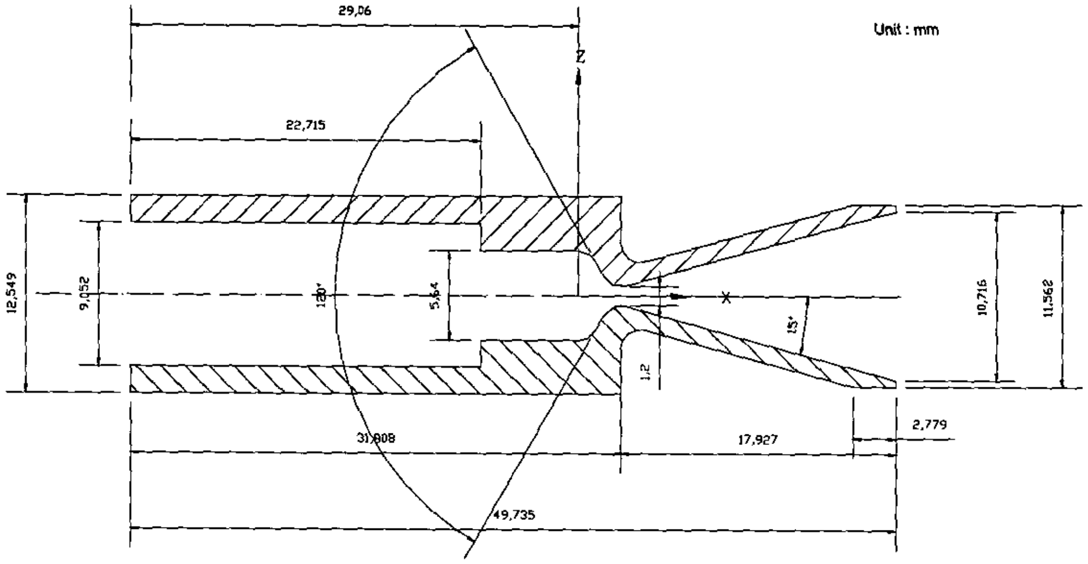

Fig 12. Detailed diagram of a C-D nozzle used in producing jet plume (1.41 × the size of thruster on ROCSAT-1)

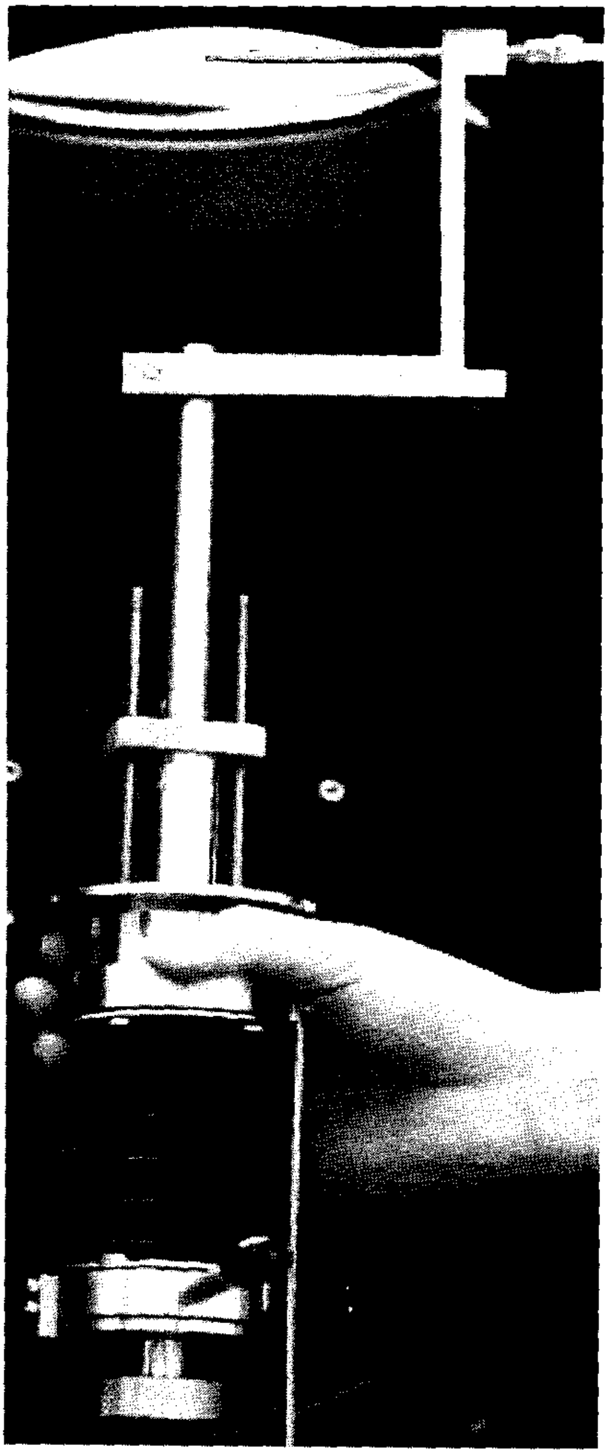

Fig. 13. Pitot tube for total pressure measurement.

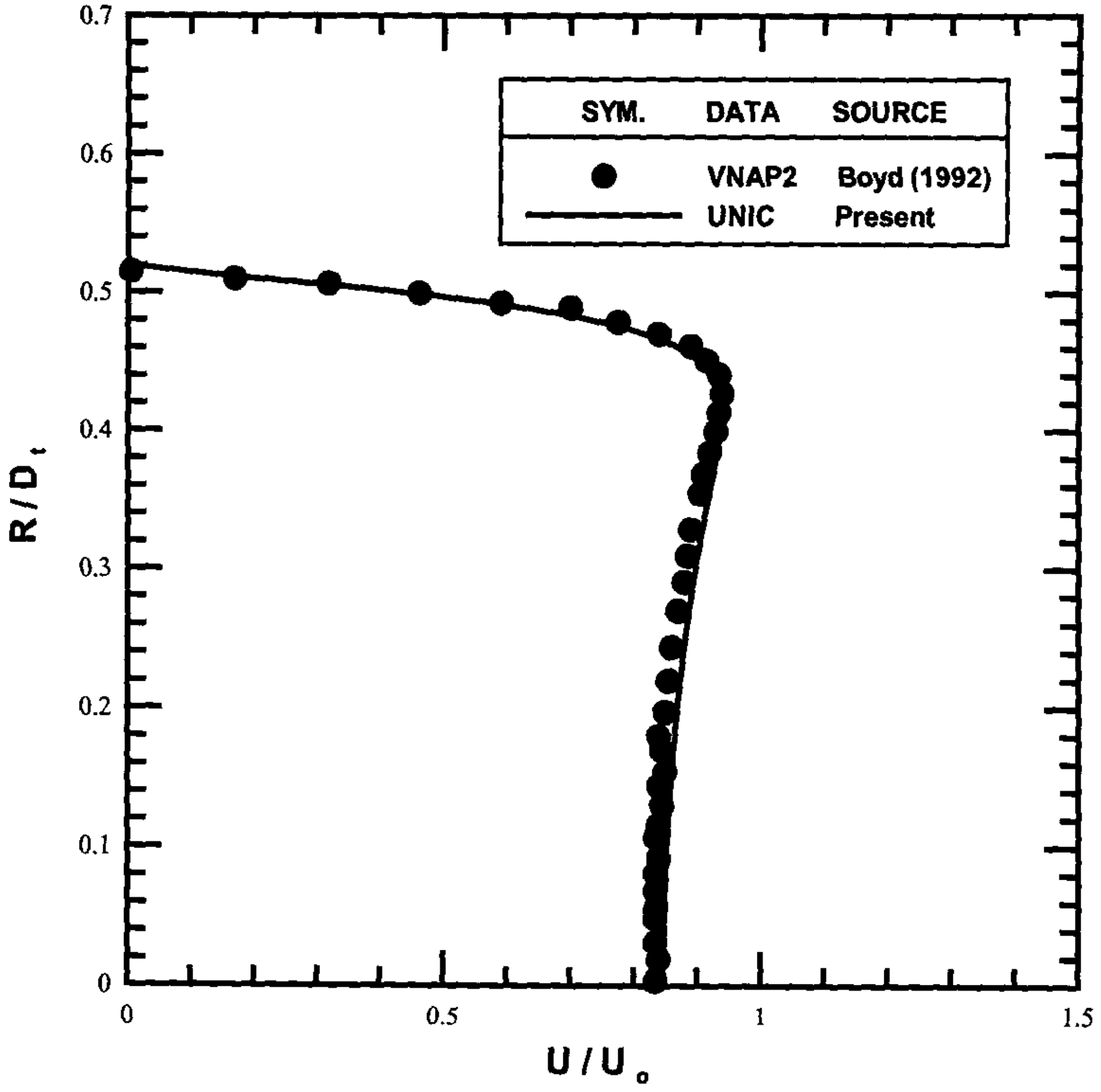

Fig. 14. Normalized inlet velocity for DSMC

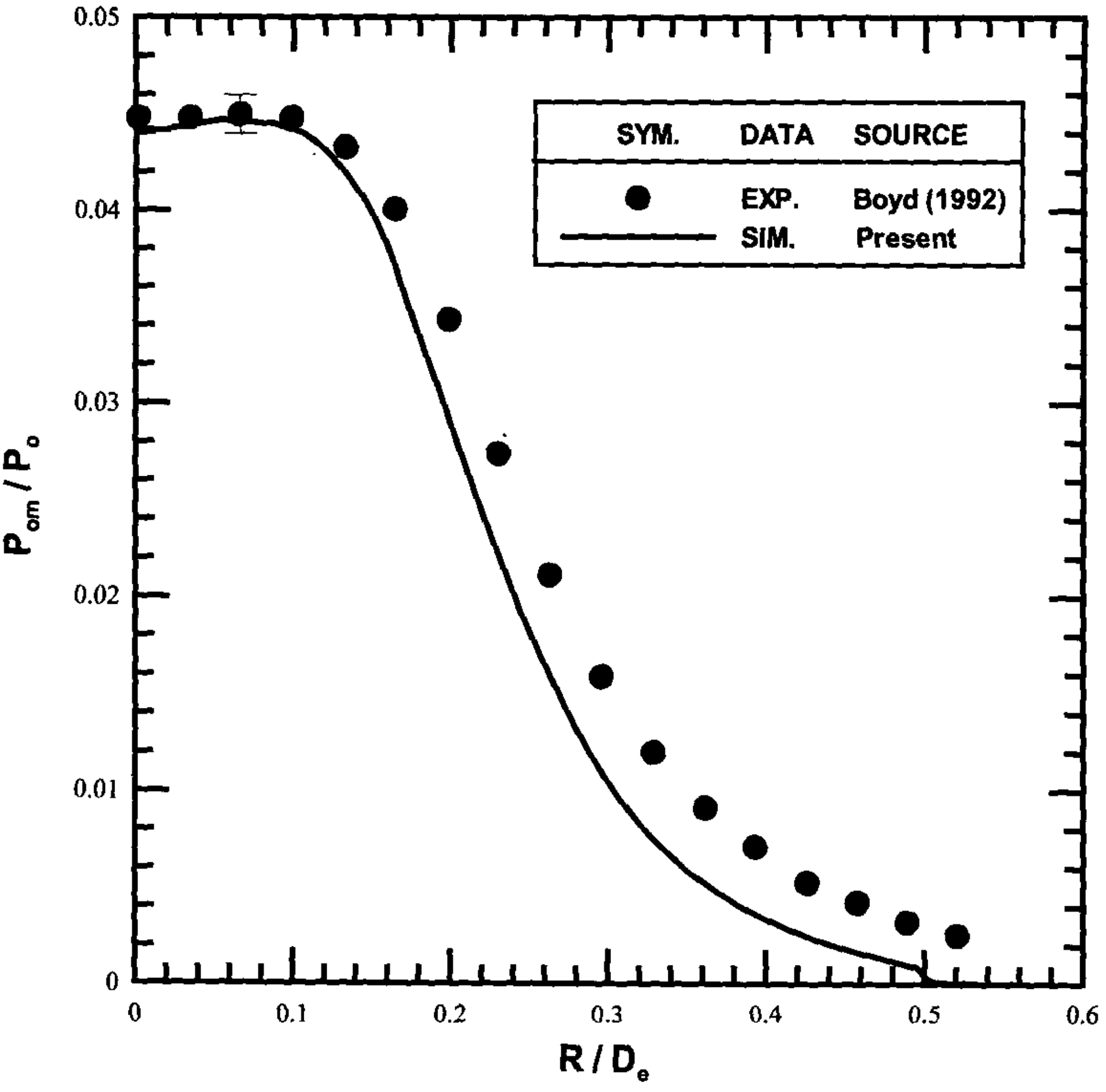

Fig. 15. Comparison computed and measured pitot pressure profile at nozzle exit plane (Z = 0 mm)

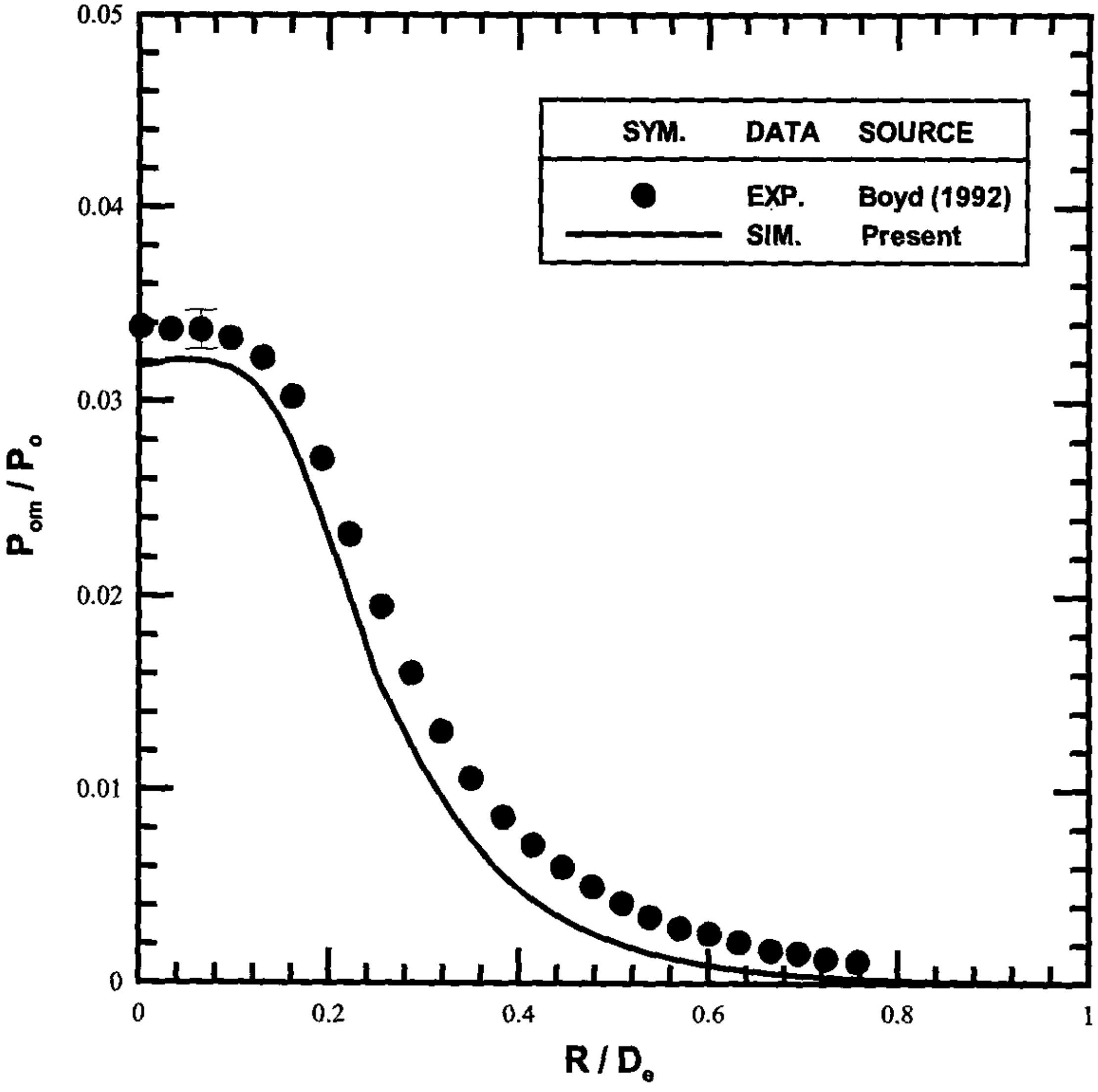

Fig. 16. Comparison computed and measured pitot pressure profile at Z = 12 mm

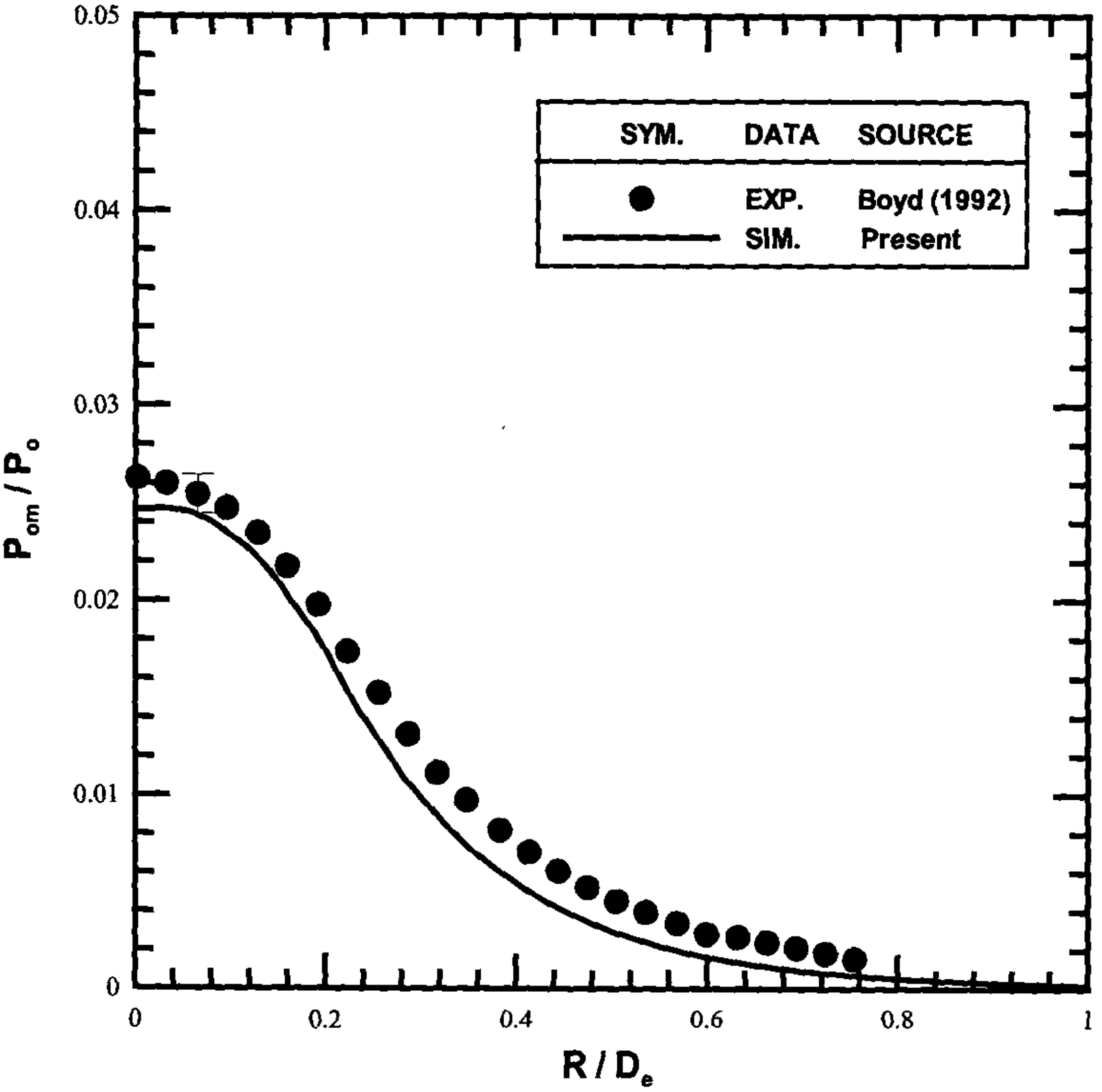

Fig. 17. Comparison computed and measured pitot pressure profile at Z = 24 mm

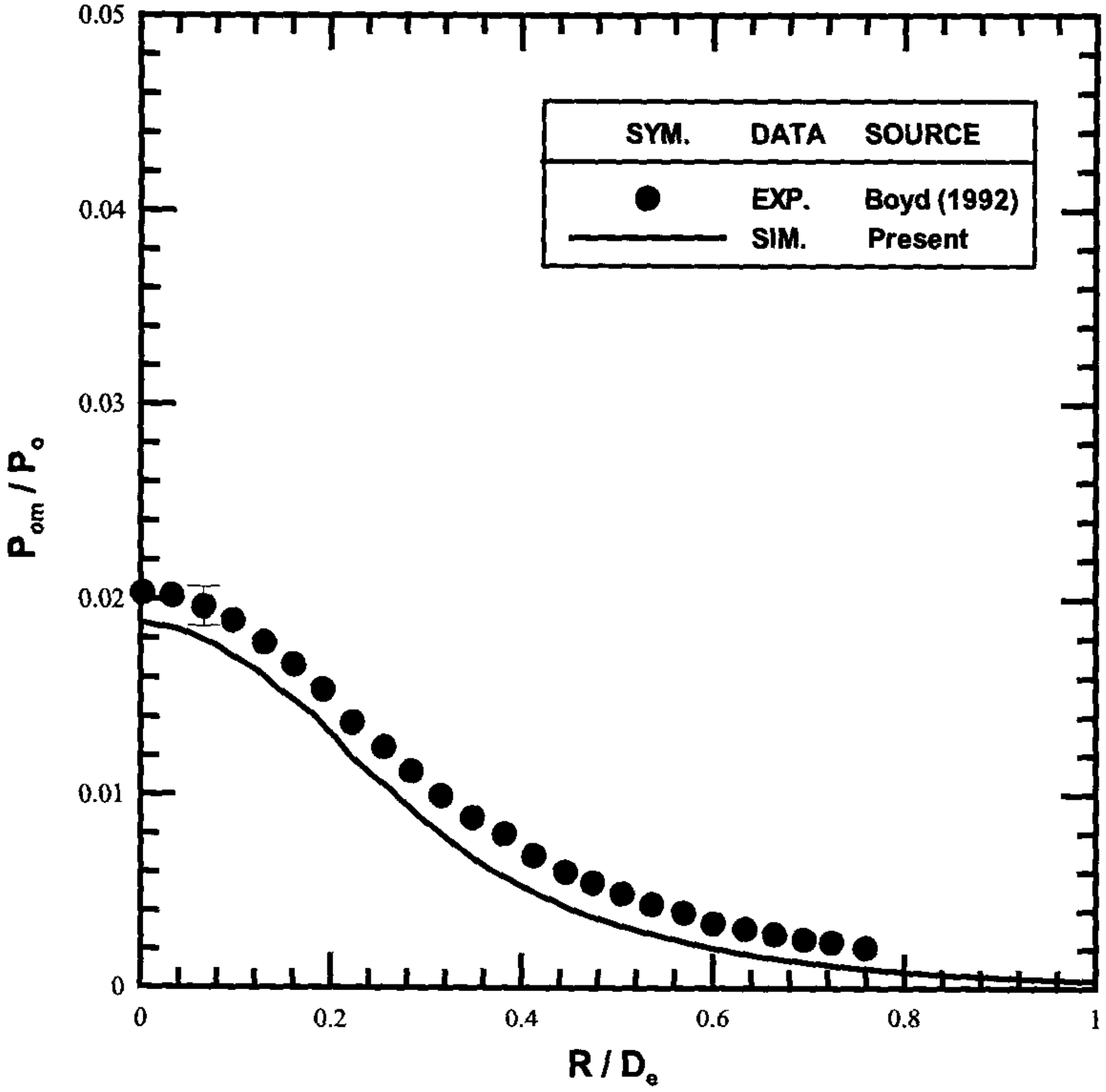

Fig. 18. Comparison computed and measured pitot pressure profile at Z = 36 mm

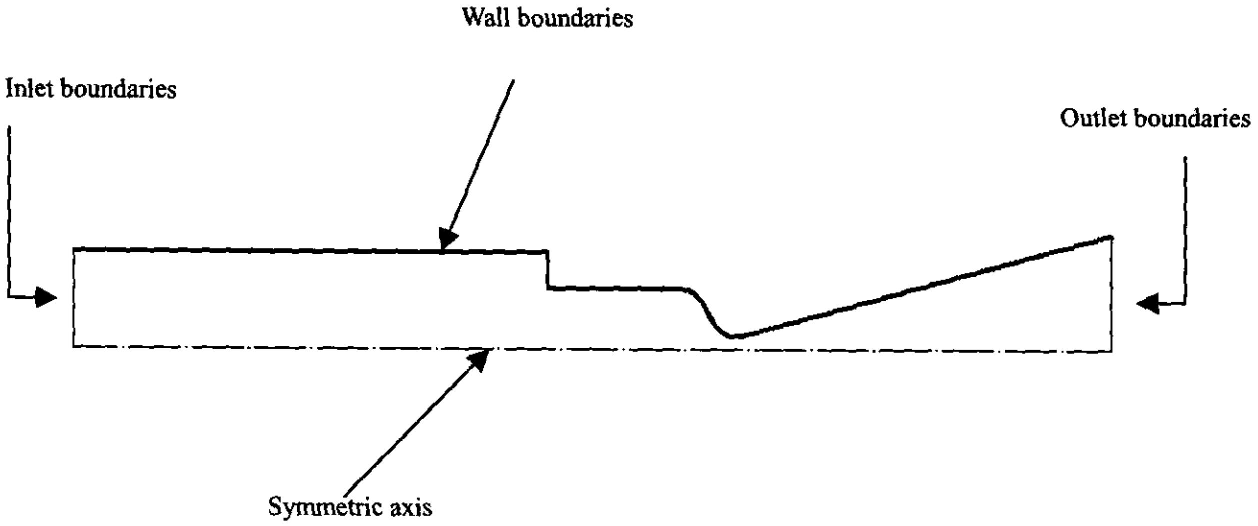

Fig.19. Sketch of boundary conditions for CFD solver, UNIC [18].

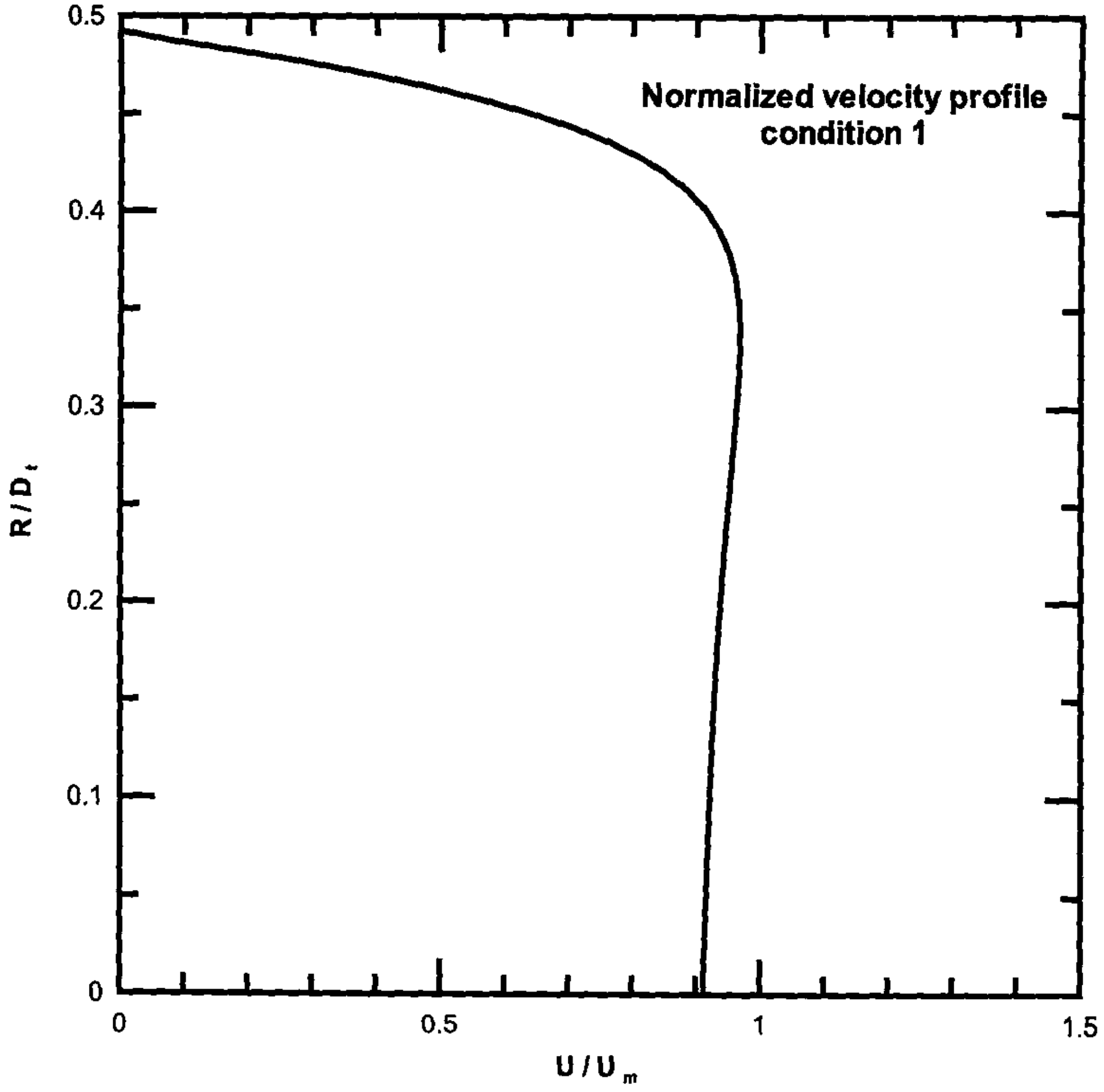

Fig. 20. Normalized axial velocity profiles at nozzle throat for DSMC simulation (condition 1).

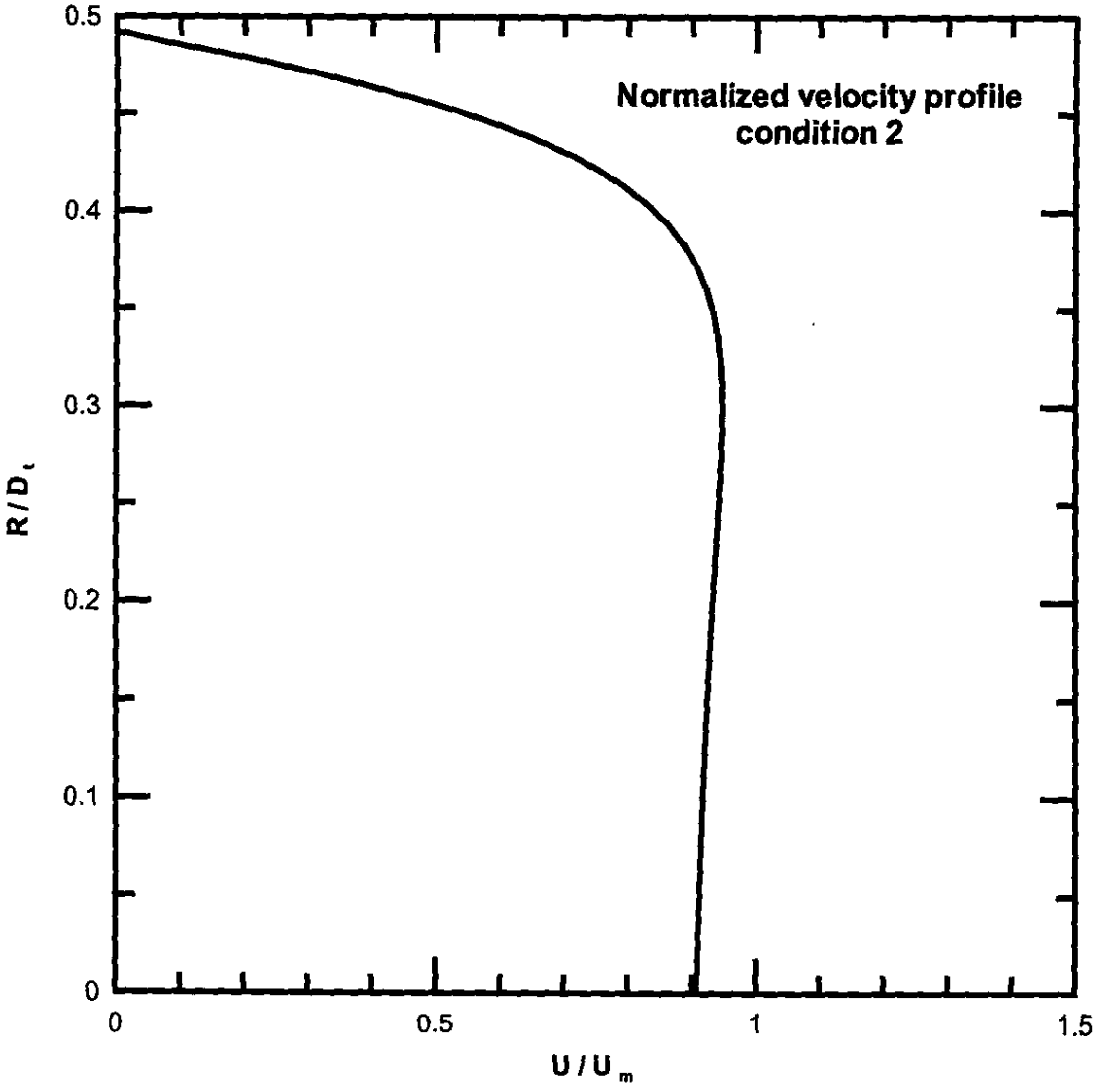

Fig. 21. Normalized axial velocity profiles at nozzle throat for DSMC simulation (condition 2).

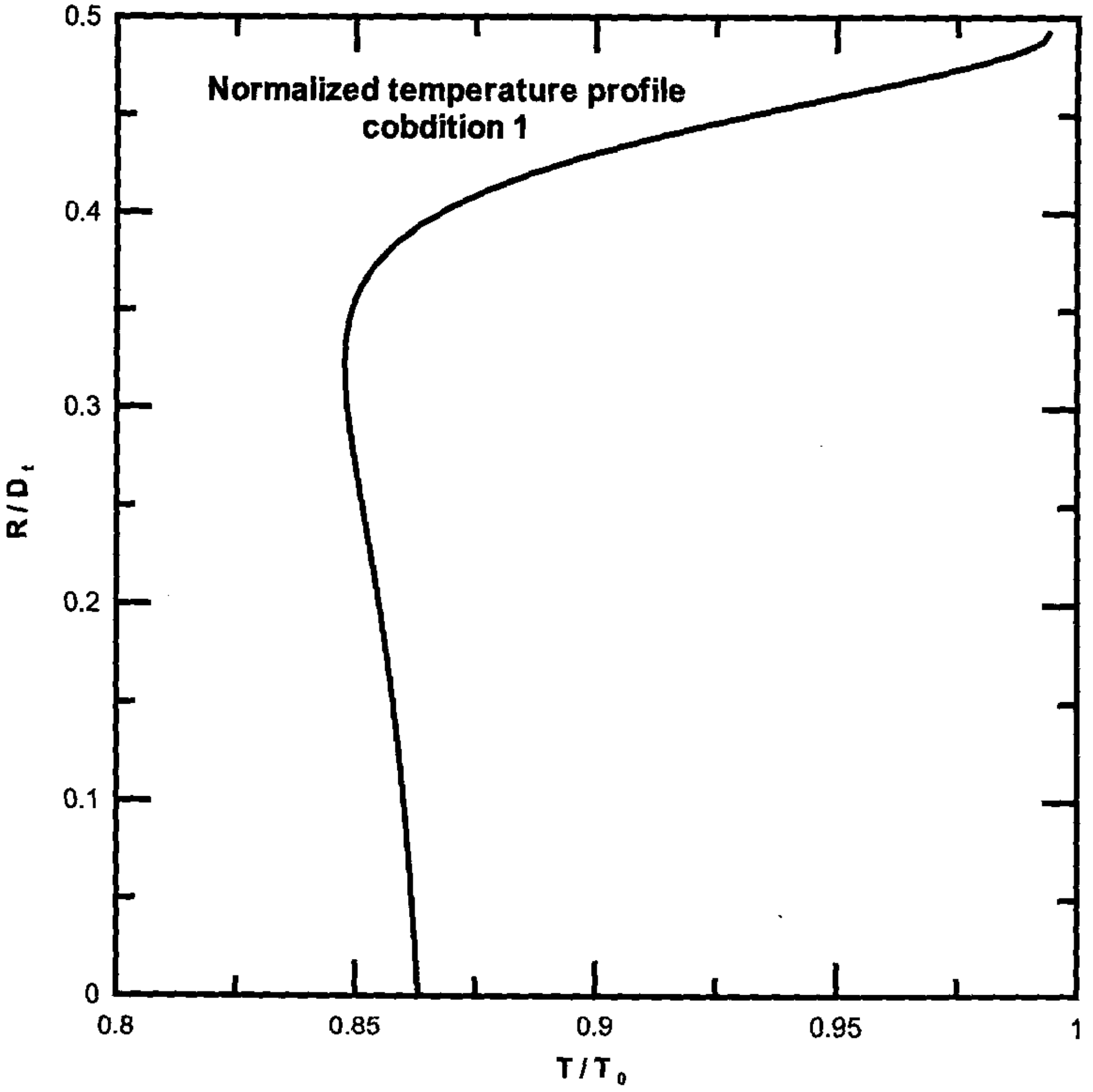

Fig. 22. Normalized temperature profiles at nozzle throat for DSMC simulation (condition 1).

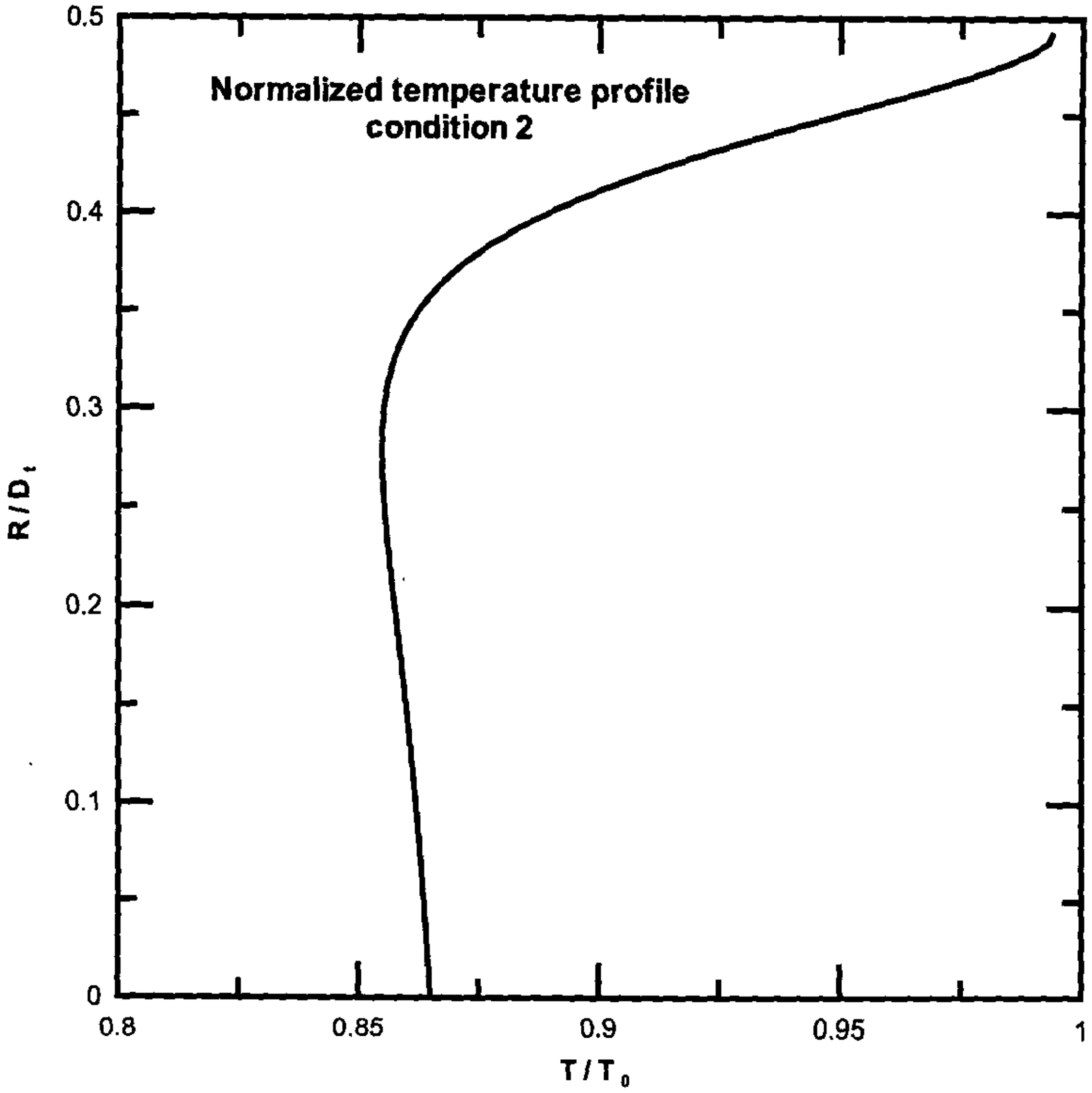

Fig. 23. Normalized temperature profiles at nozzle throat for DSMC simulation (condition 2).

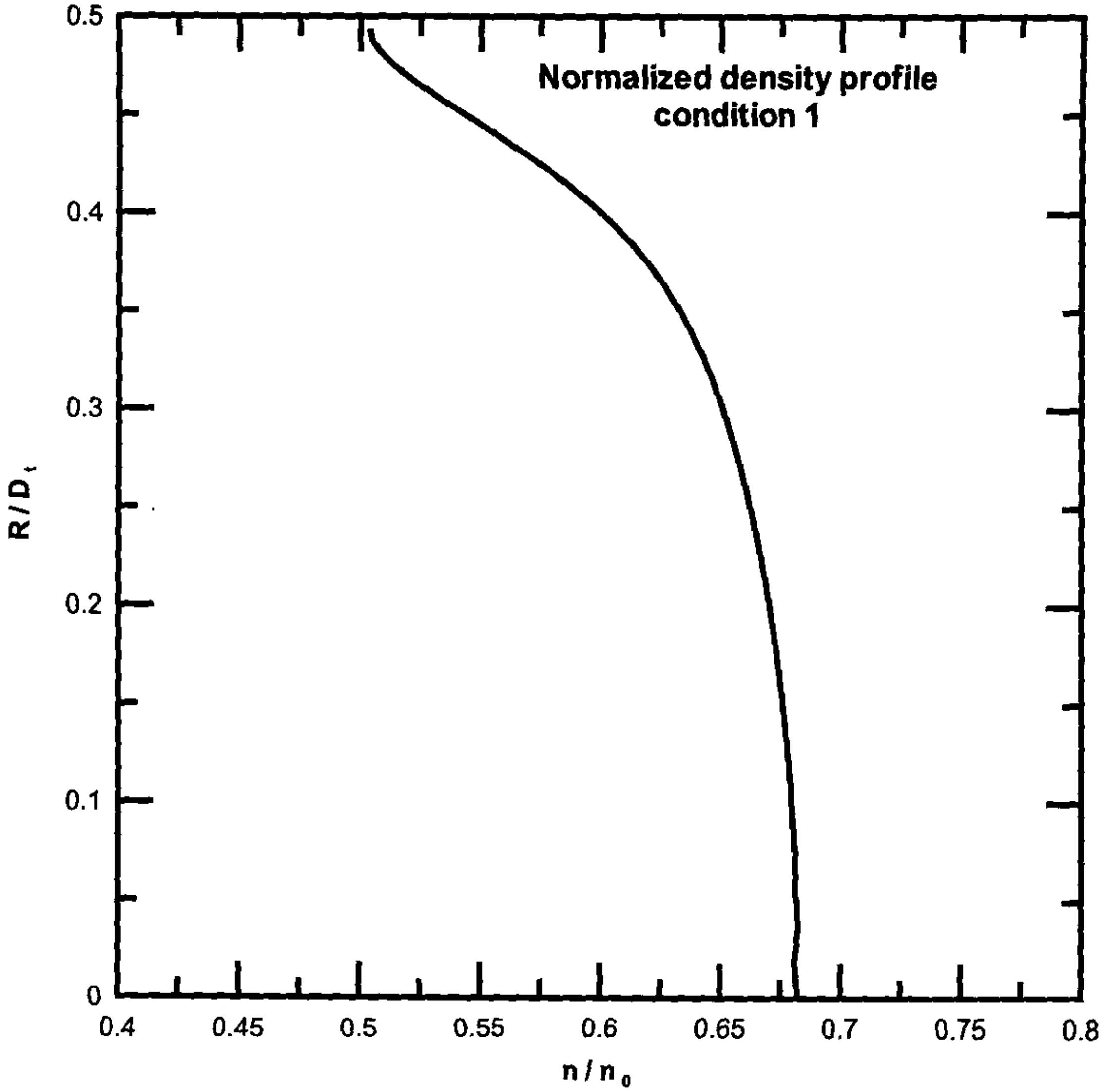

Fig. 24. Normalized density profiles at nozzle throat for DSMC simulation (condition 1).

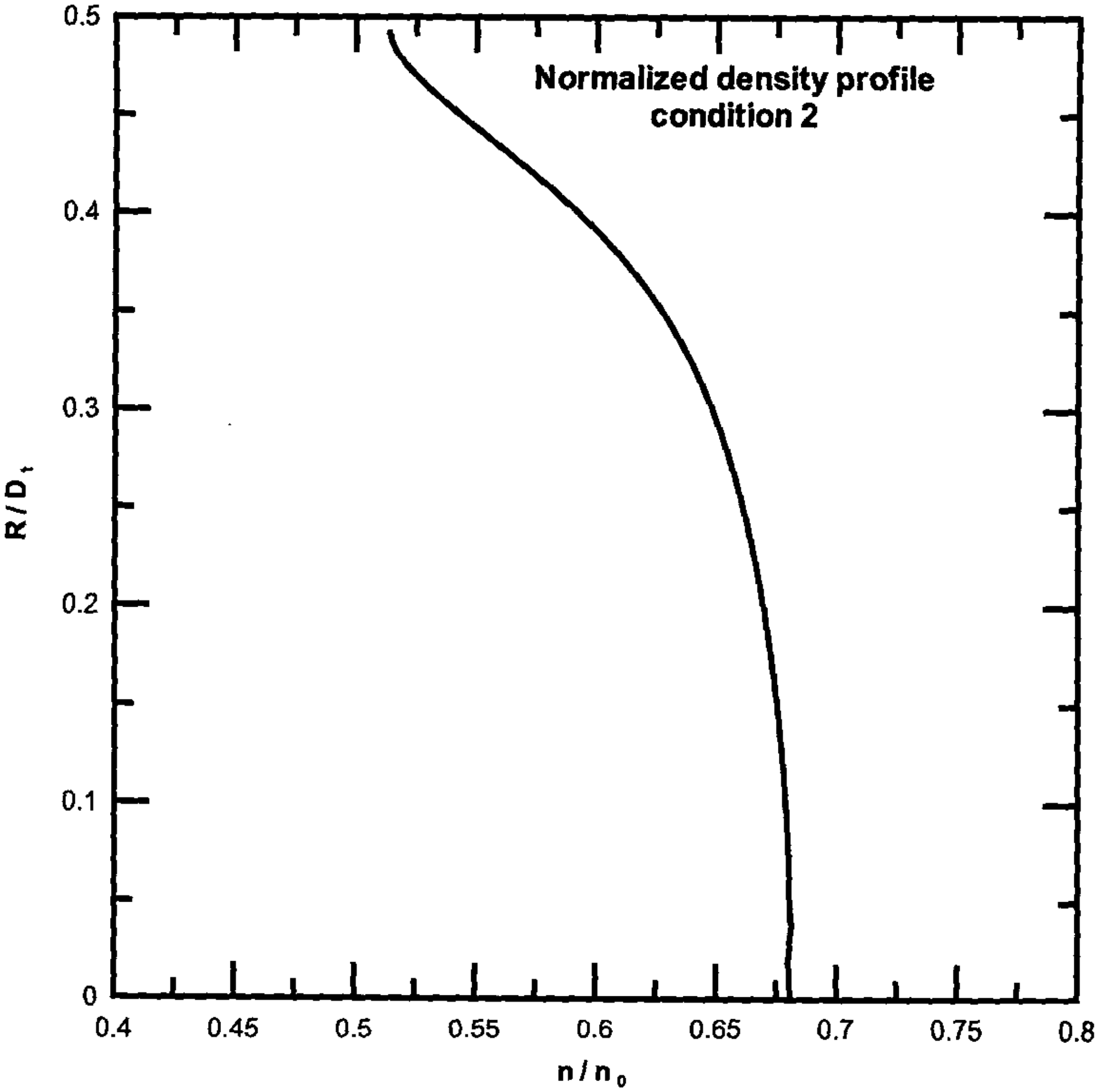

Fig. 25. Normalized density profiles at nozzle throat for DSMC simulation (condition 2).

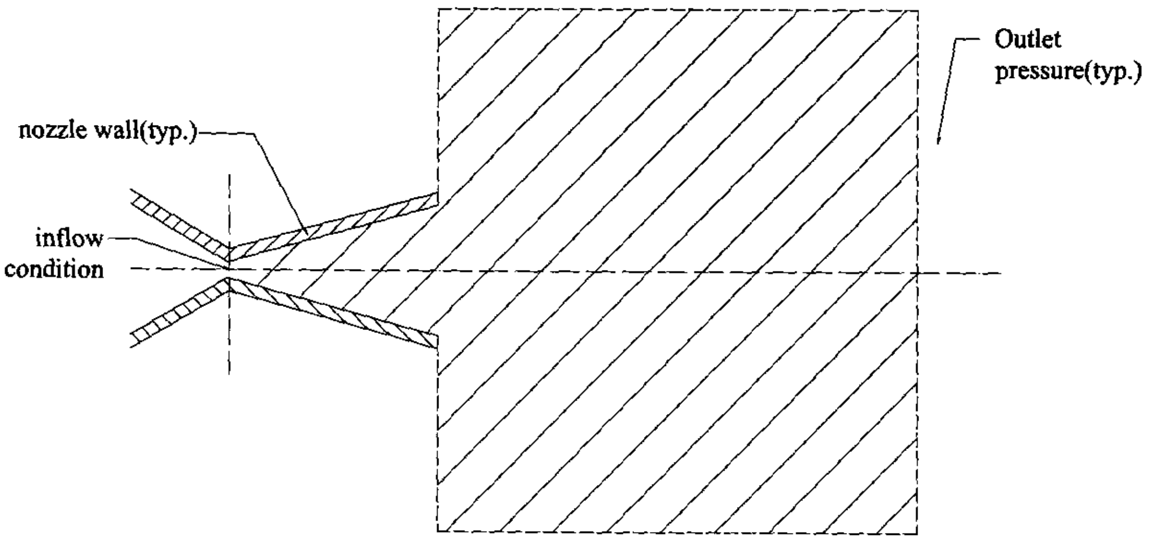

Fig. 26. Sketch of boundary conditions for DSMC simulation

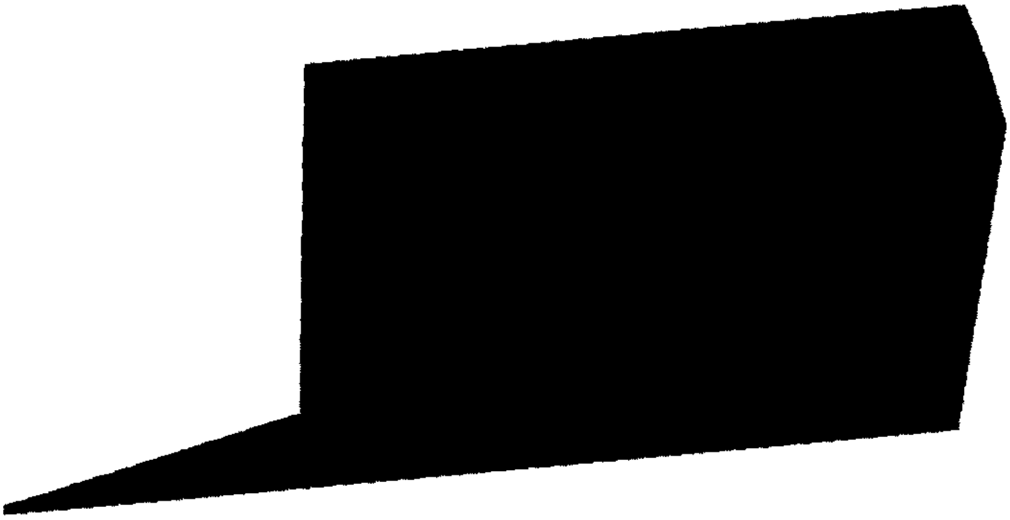

Fig. 27. Mesh for DSMC simulation

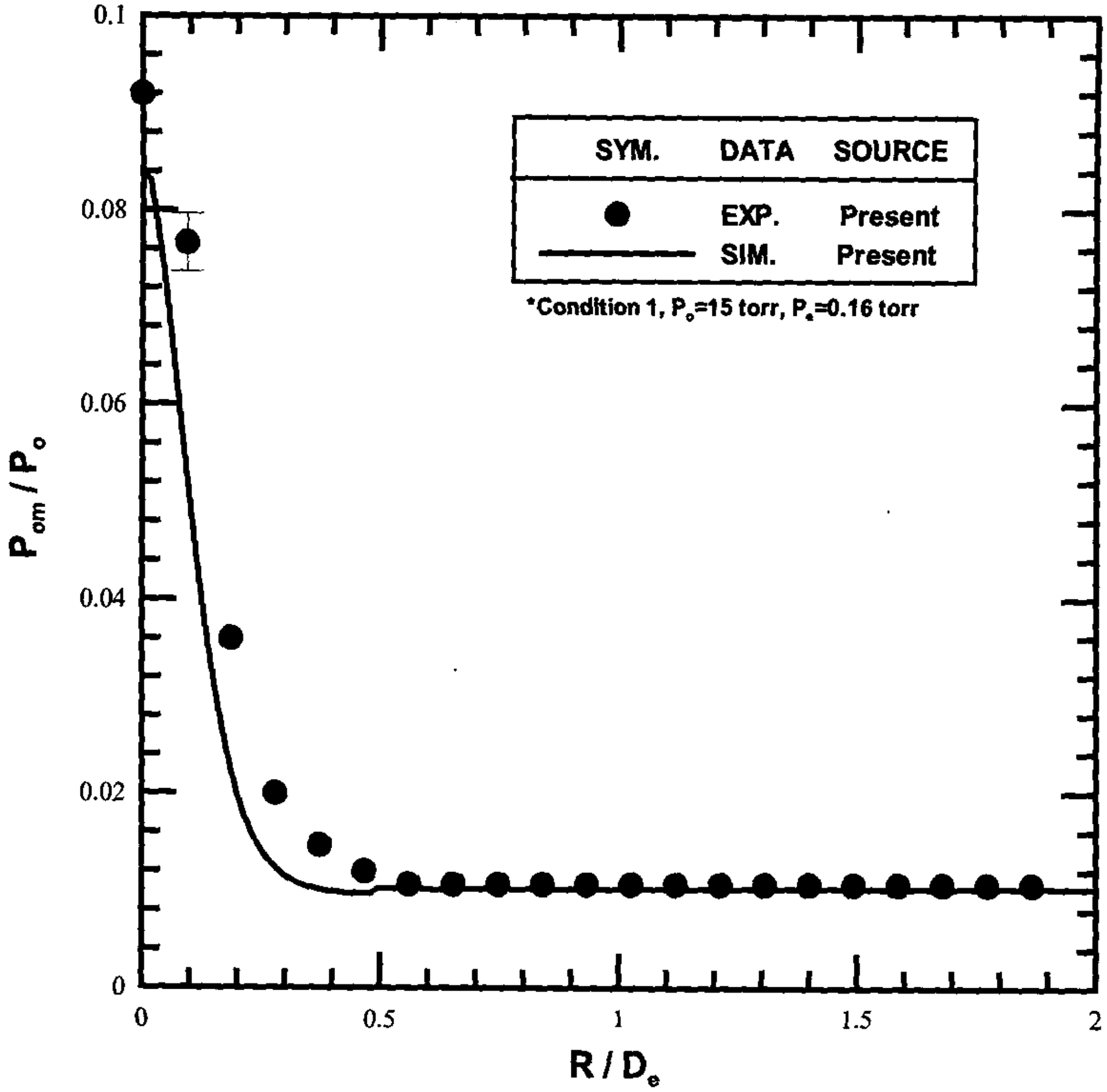

Fig. 28. Comparison of computed and measured pitot pressure profiles at nozzle exit plane (Z=0 mm).

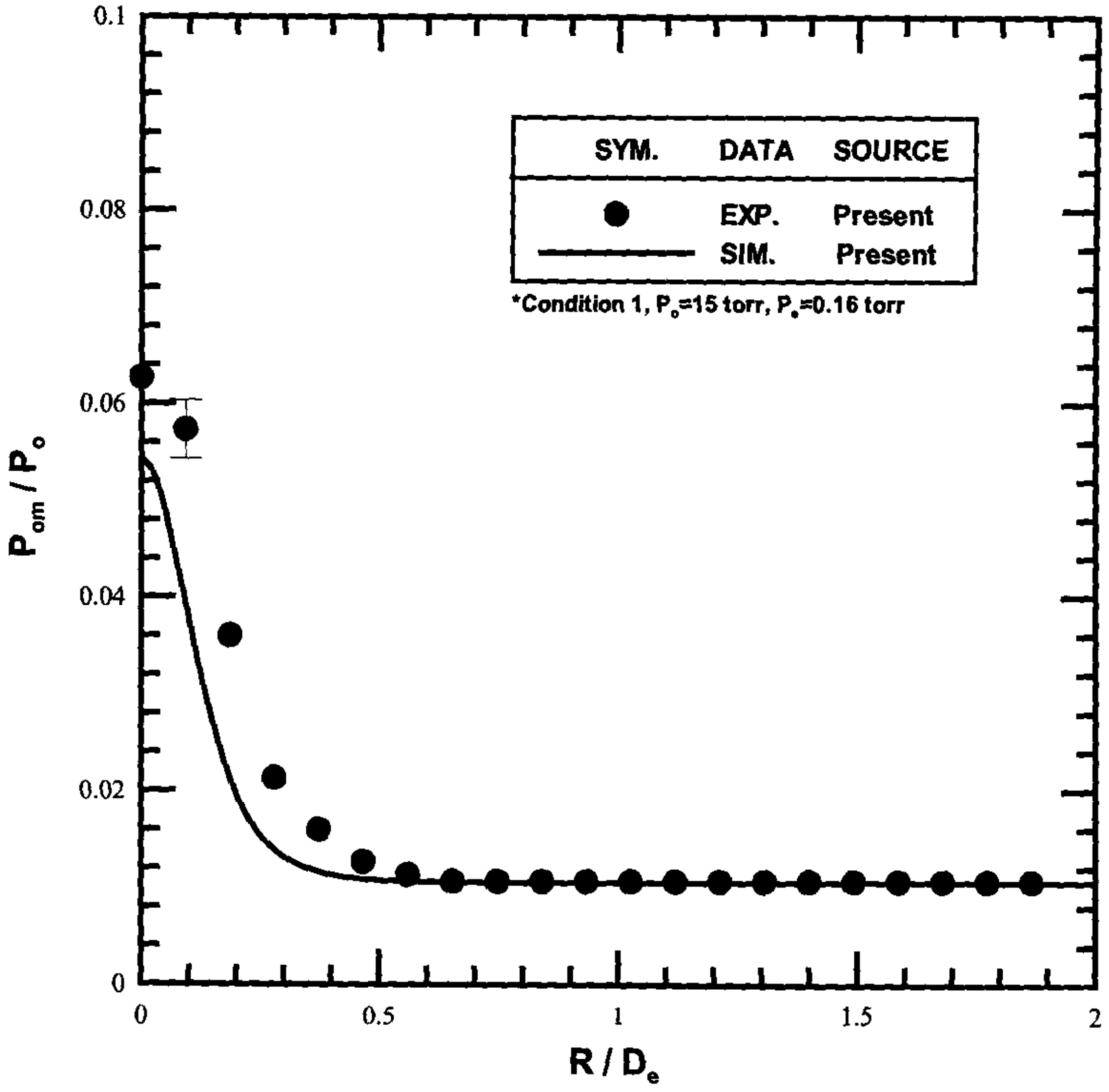

Fig. 29. Comparison of computed and measured pitot pressure profiles at Z = 5 mm.

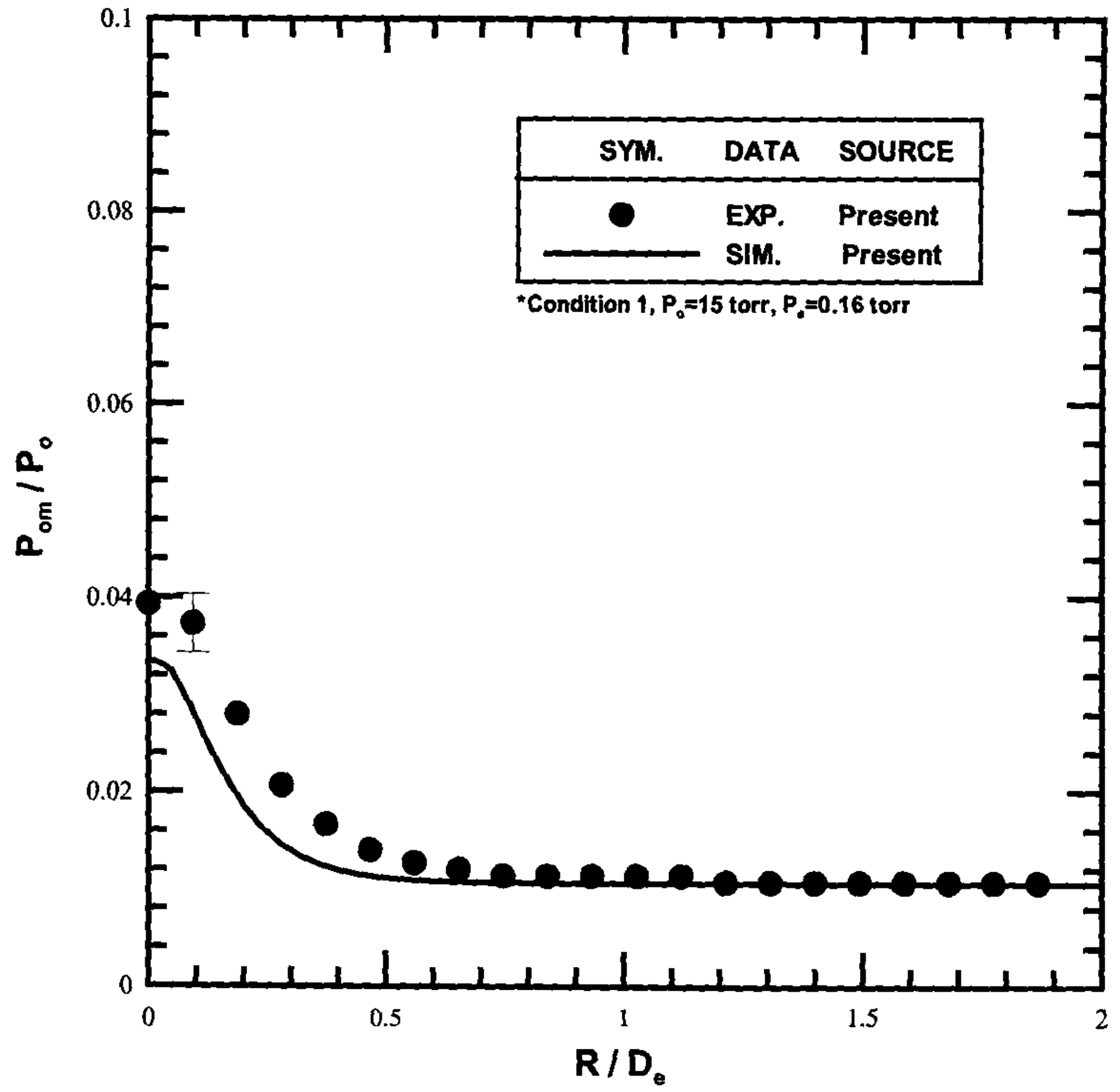

Fig. 30. Comparison of computed and measured pitot pressure profiles at Z = 10 mm.

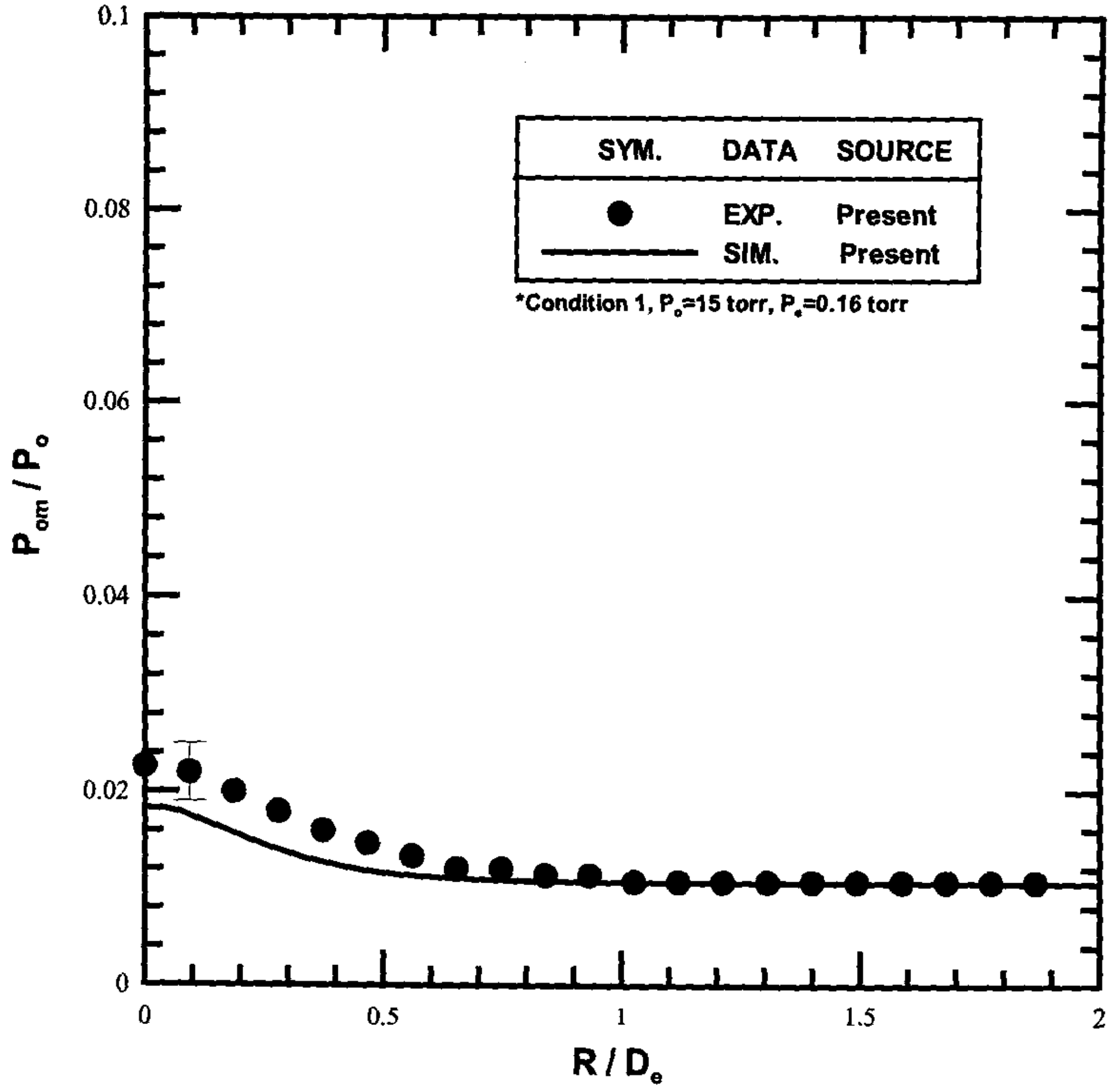

Fig. 31. Comparison of computed and measured pitot pressure profiles at Z = 20 mm.

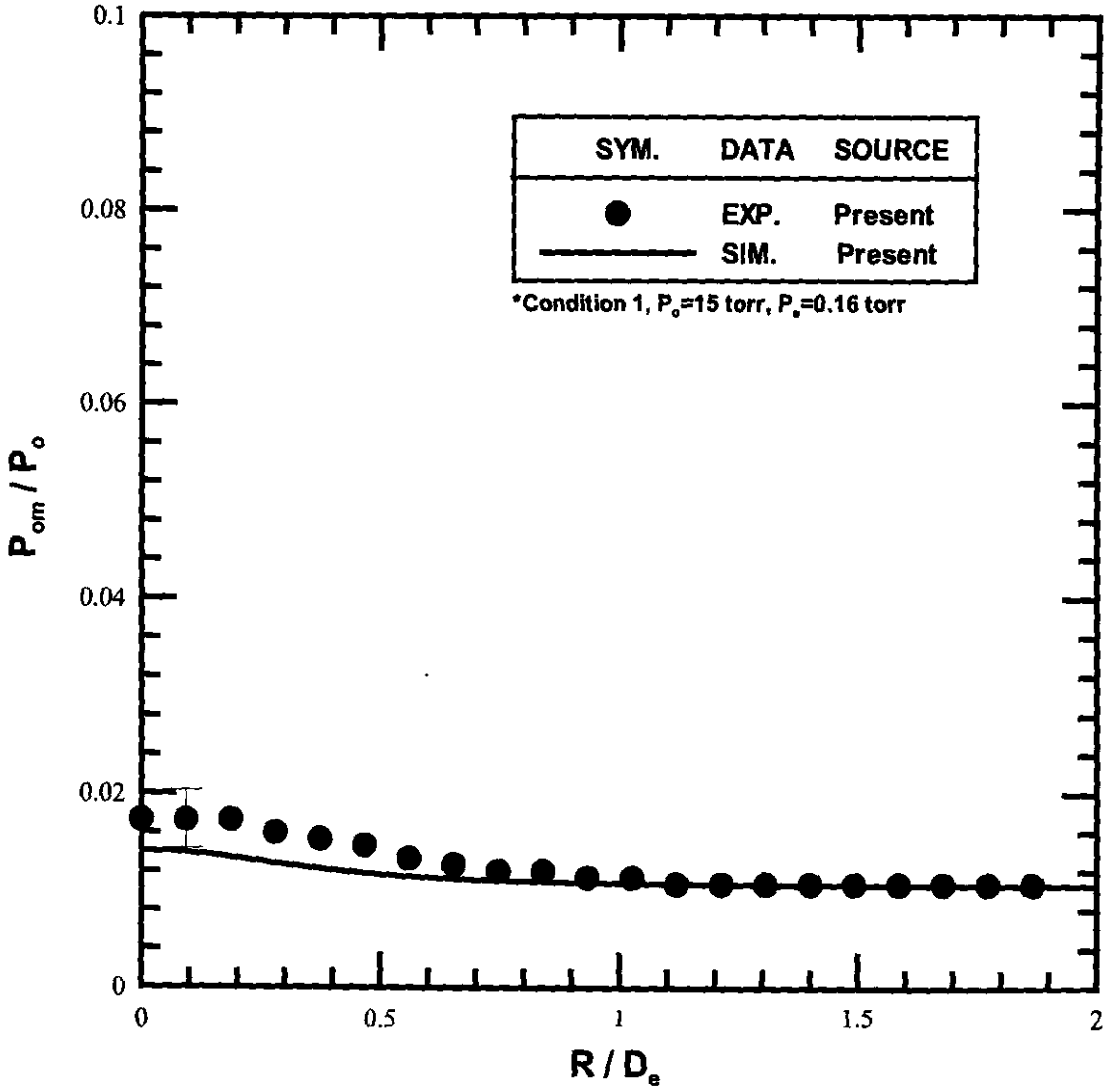

Fig. 32. Comparison of computed and measured pitot pressure profiles at Z = 30 mm.

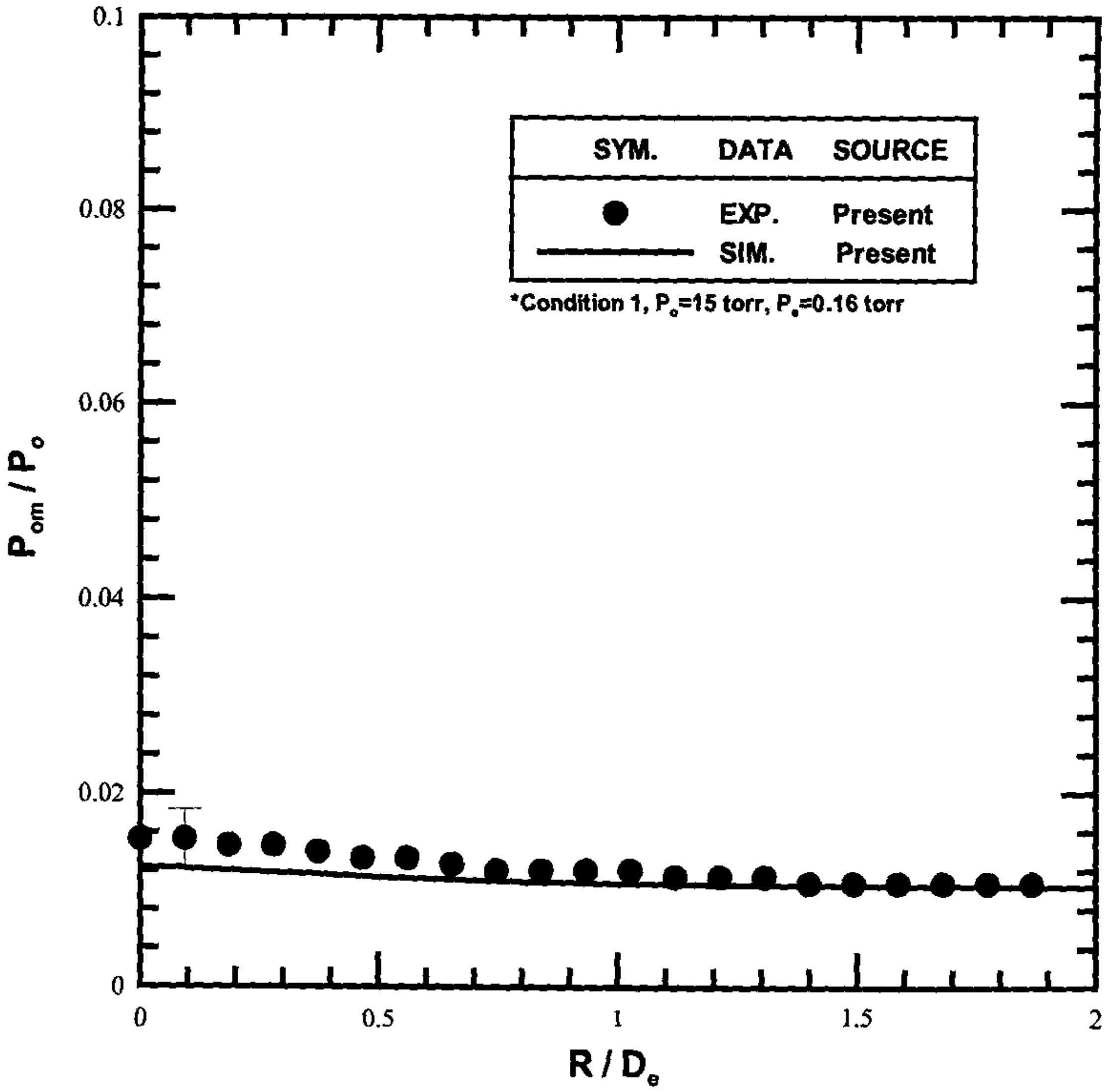

Fig. 33. Comparison of computed and measured pitot pressure profiles at Z = 40 mm.

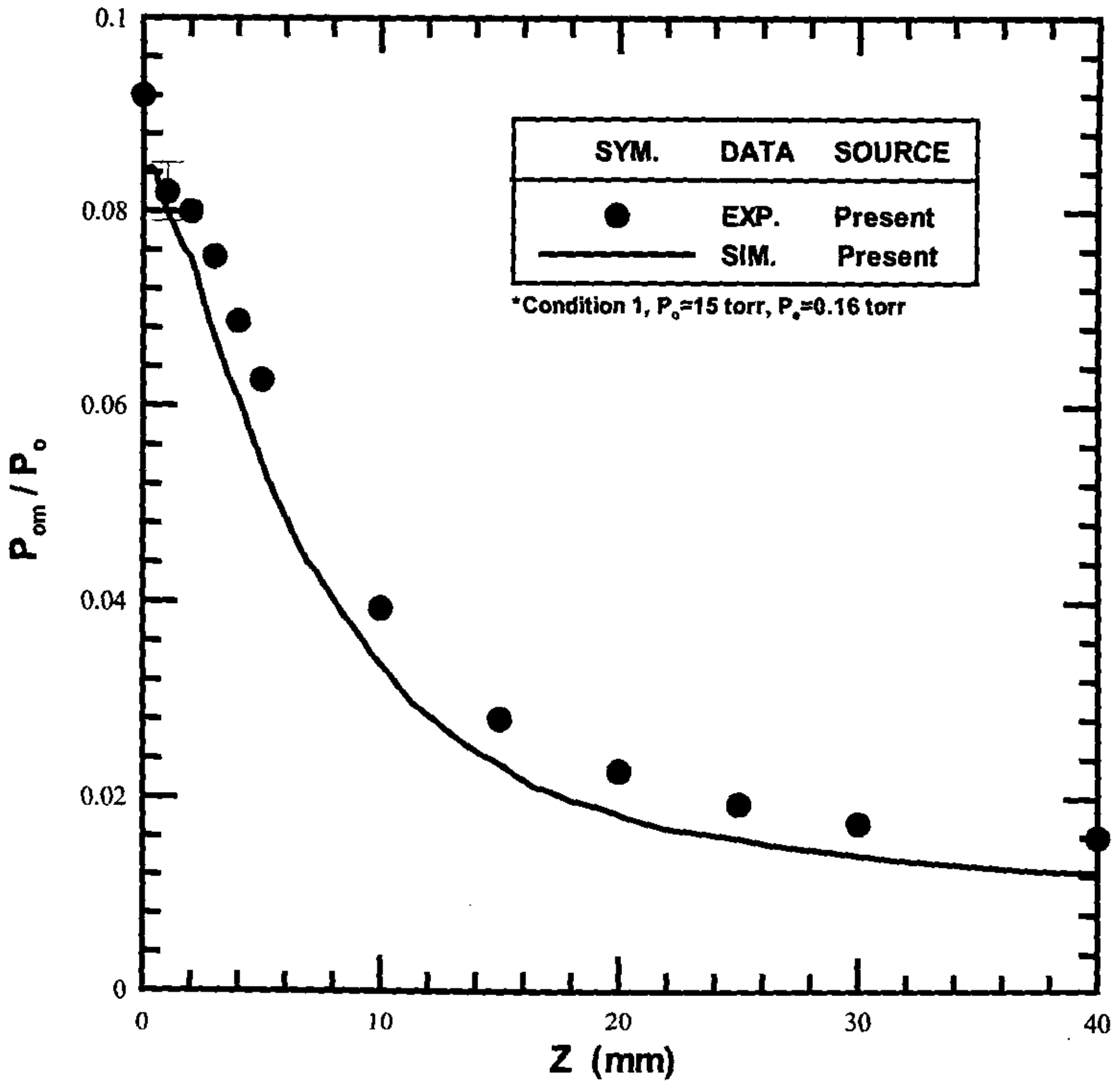

Fig. 34. Comparison of computed and measured pitot pressure profiles on the central line of nozzle (R=0 mm).

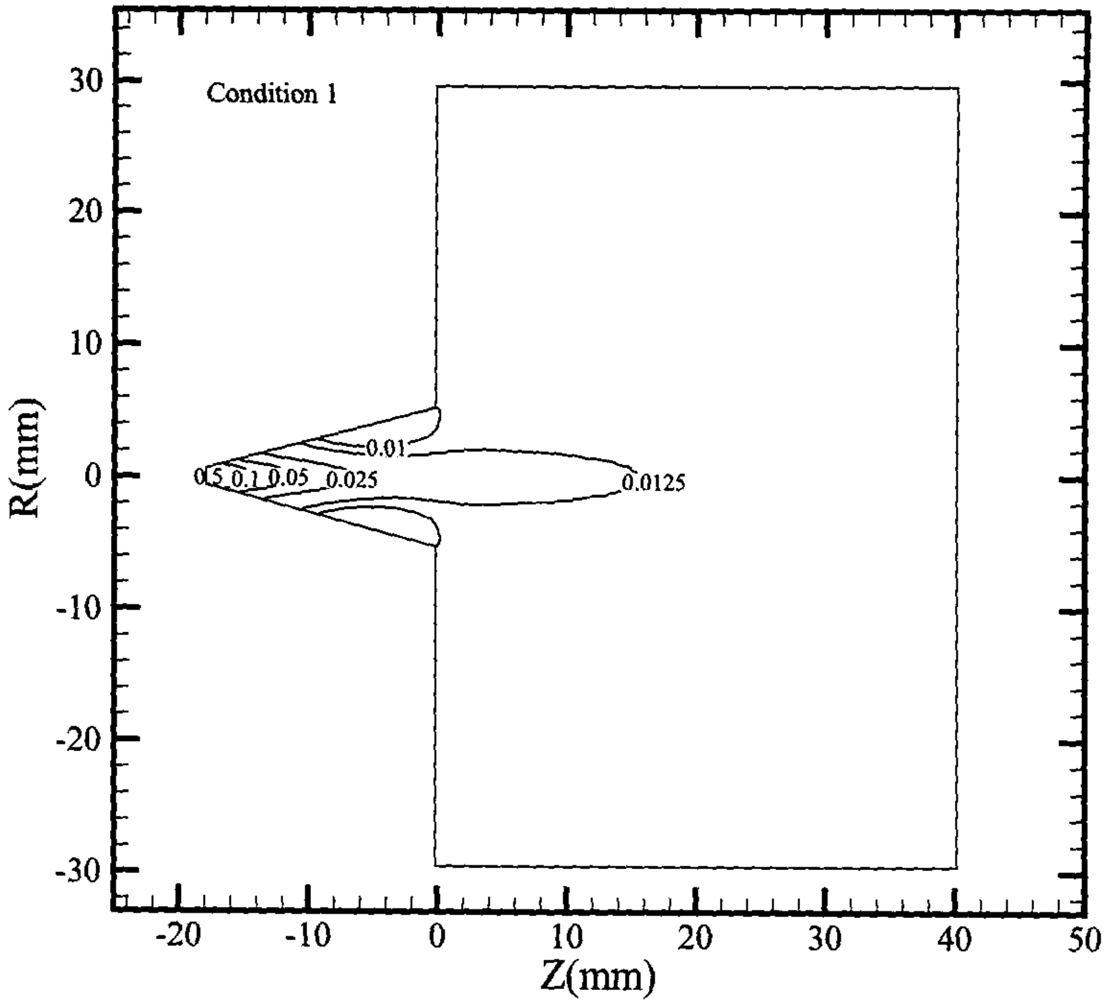

Fig. 35. Normalized density contours computed with DSMC (condition 1).

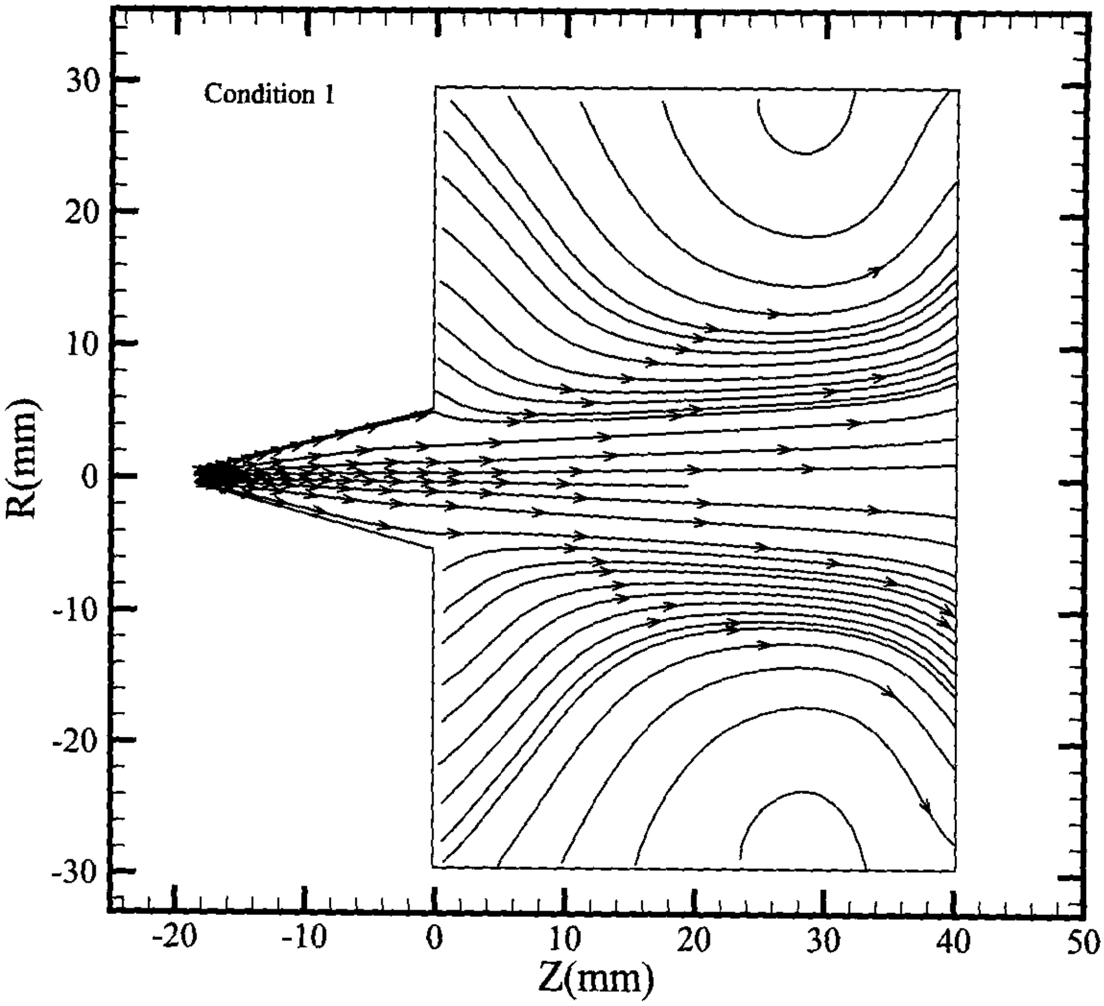

Fig. 36. Streamlines of nozzle jet plume (condition 1)

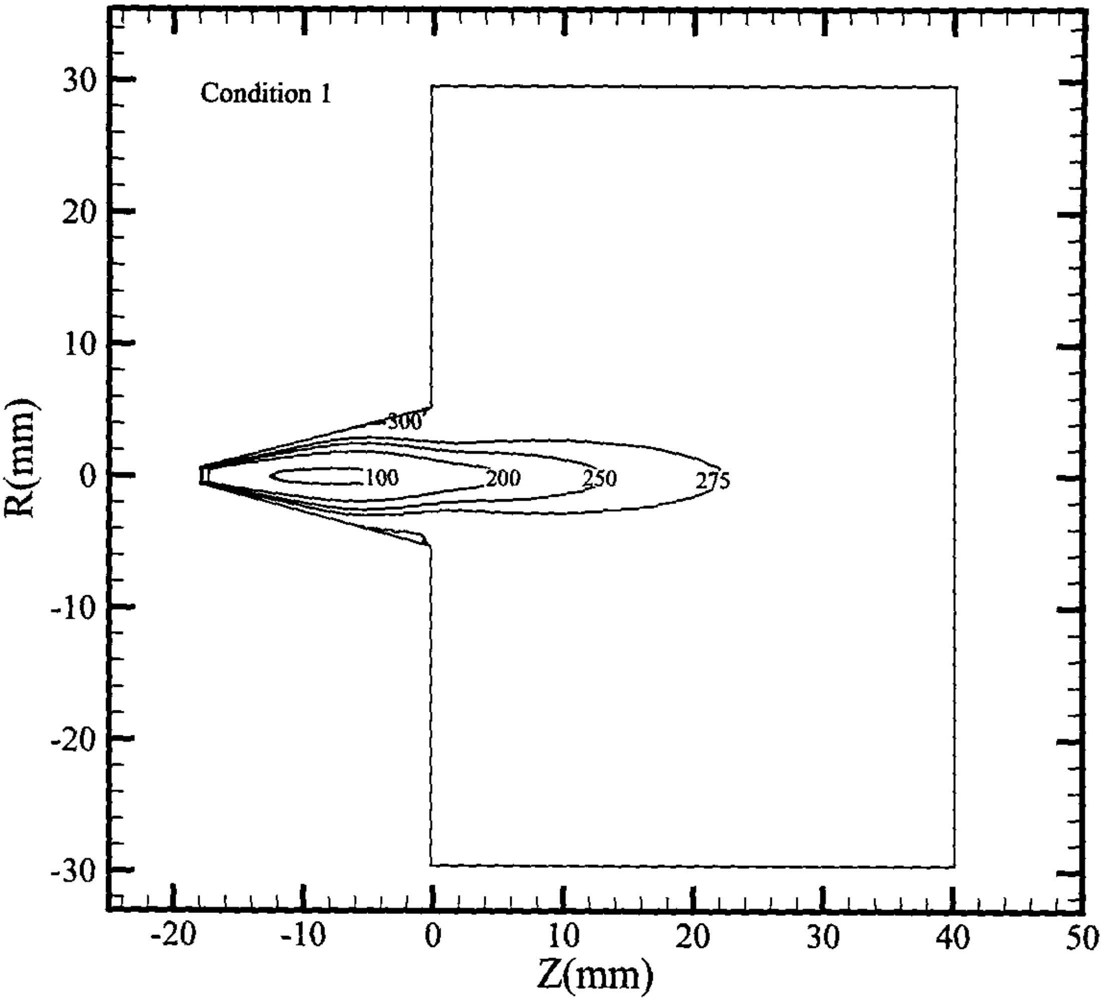

Fig. 37. Temperature contours computed with DSMC (condition 1).

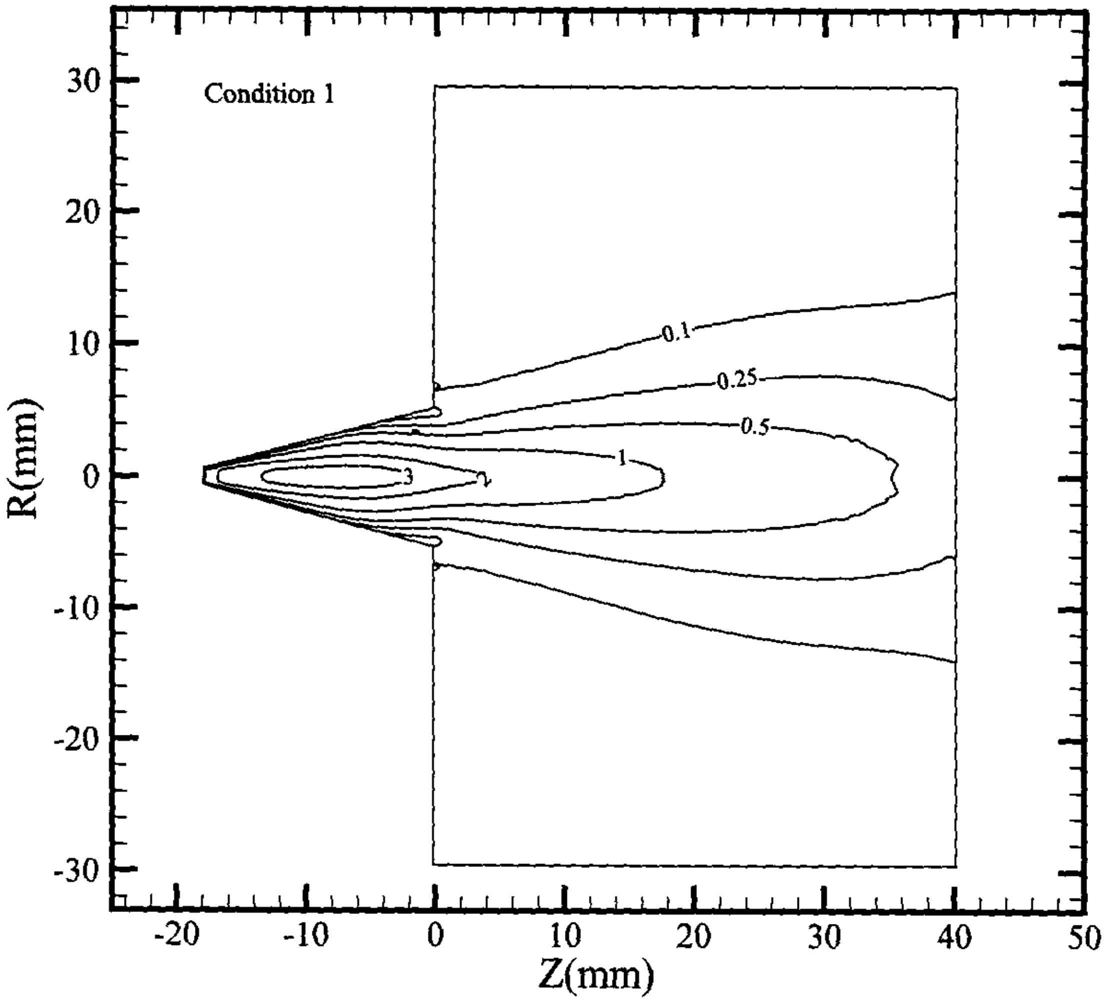

Fig. 38. Mach number contours computed with DSMC (condition 1).

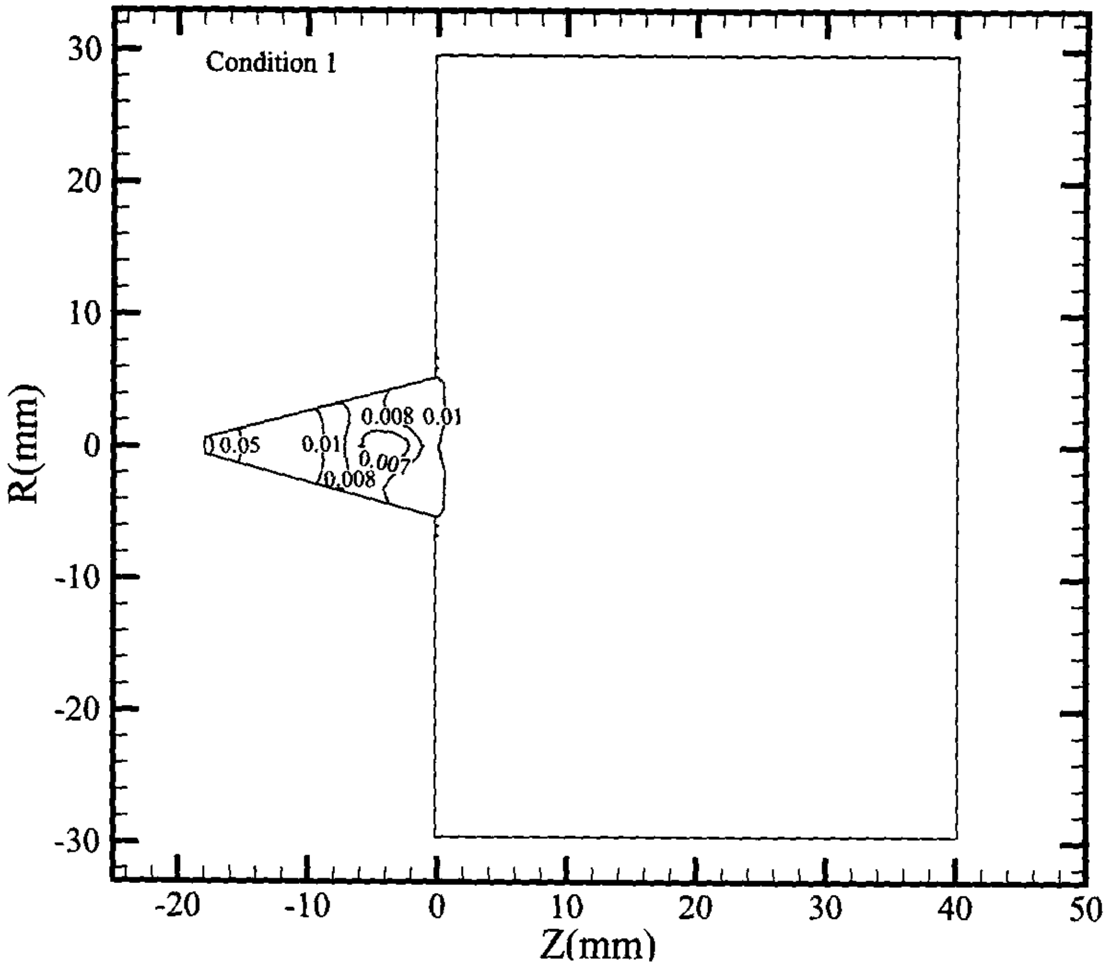

Fig. 39. Normalized pressure contours computed with DSMC (condition 1).

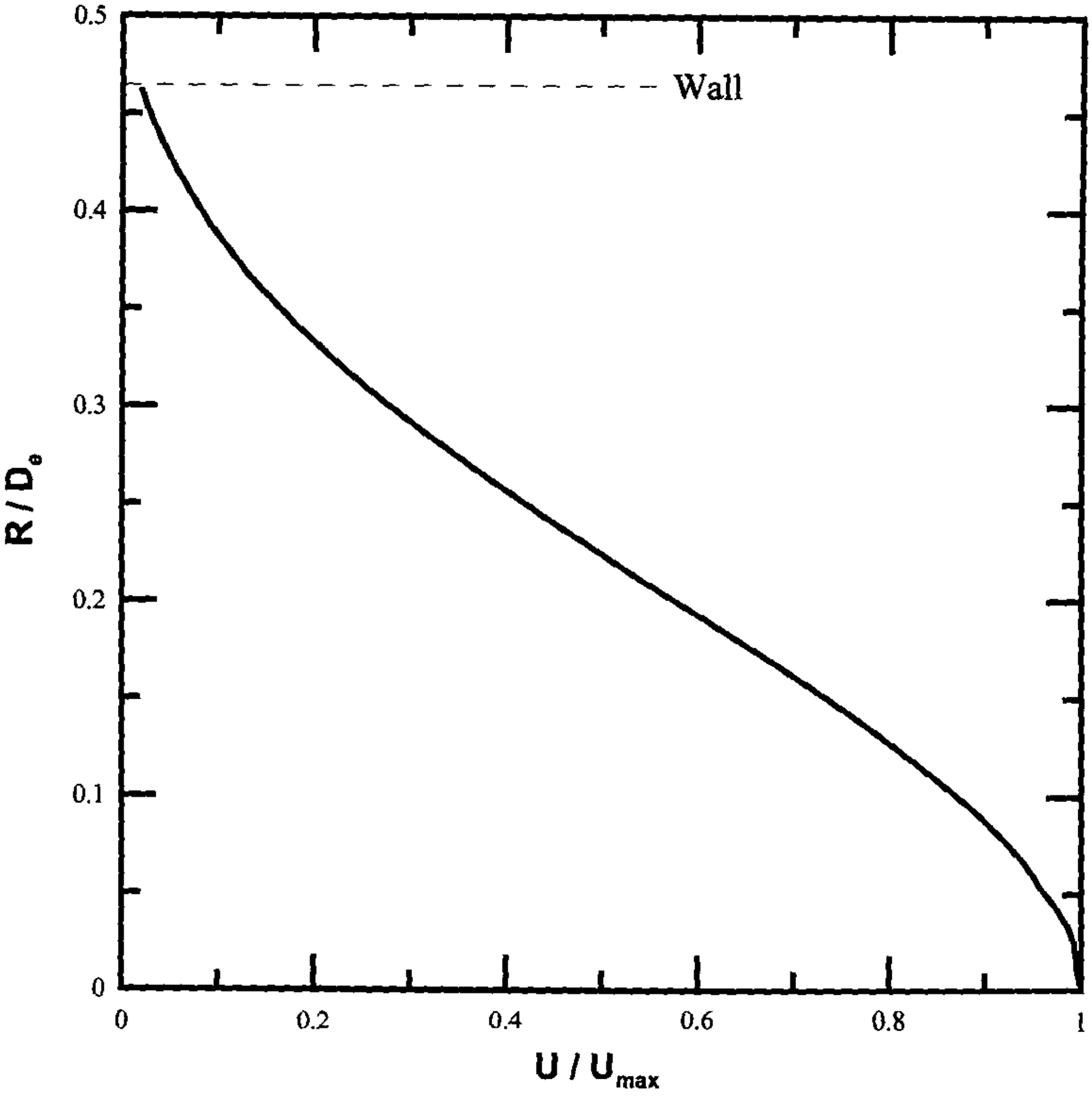

Fig. 40. Normalized axial velocity profiles computed with DSMC at Z = -1 plane (condition 1).

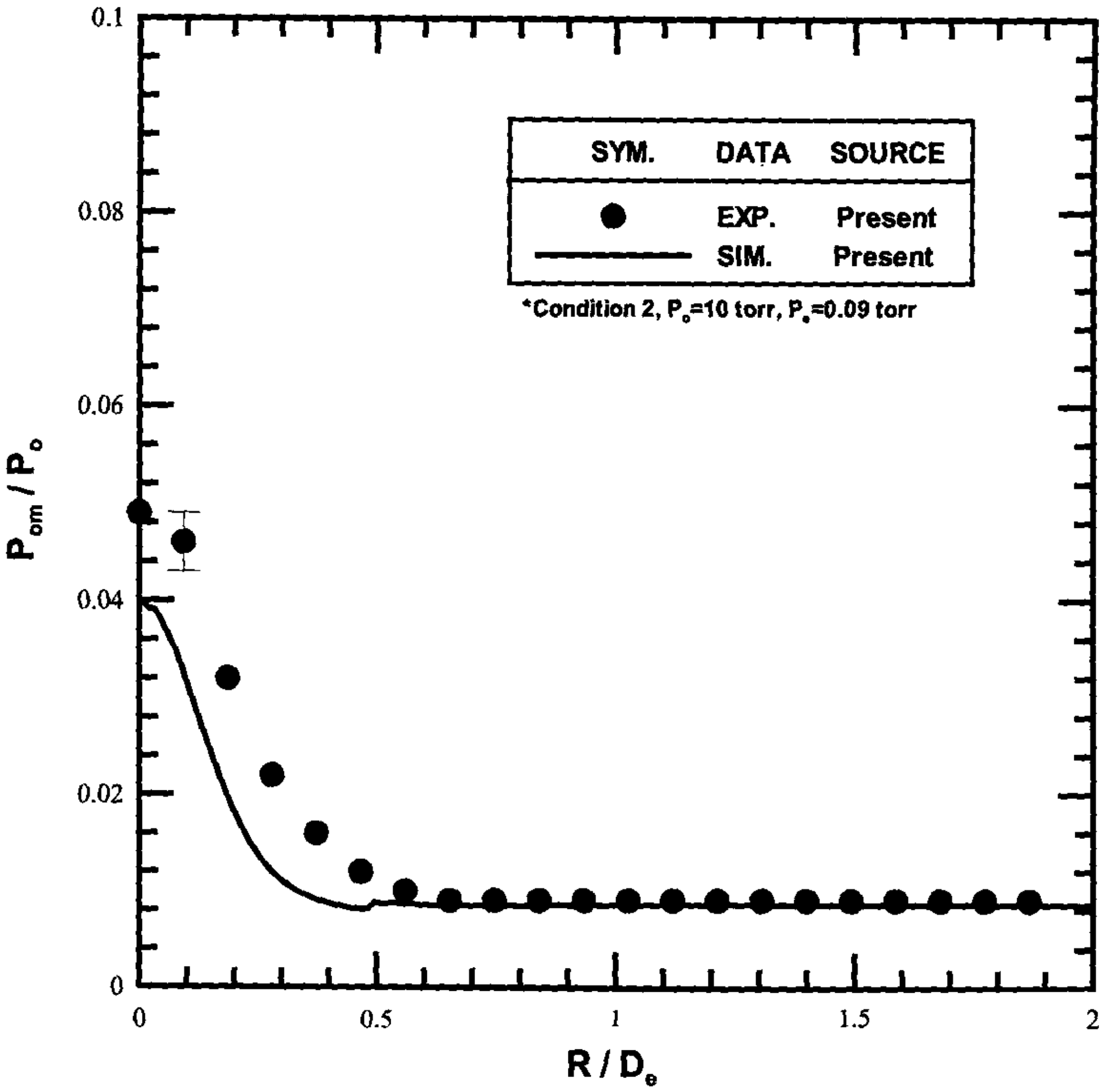

Fig. 41. Comparison computed and measured pitot pressure profile at nozzle exit plane (Z=0 mm)

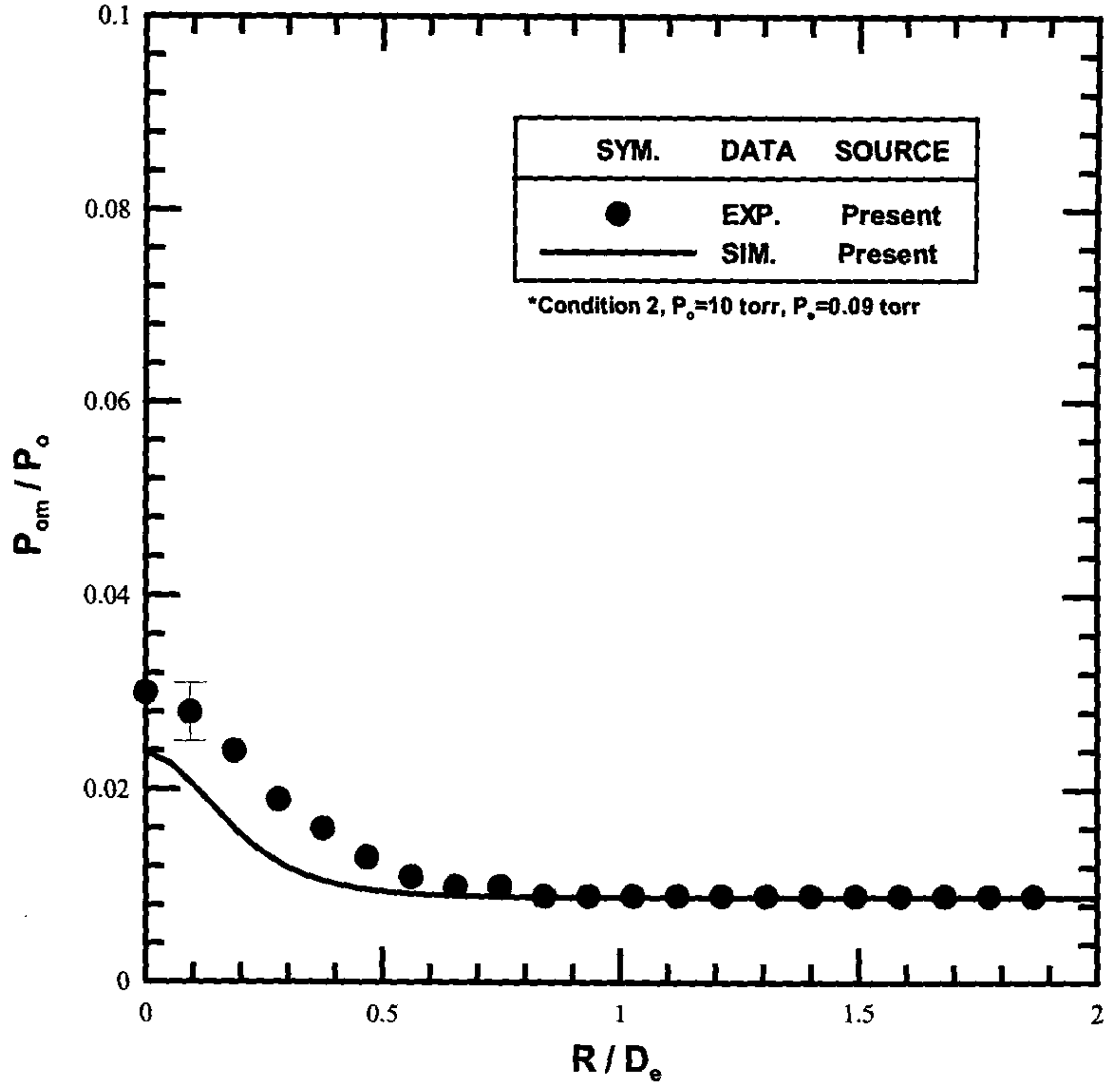

Fig. 42. Comparison computed and measured pitot pressure profile at Z = 5 mm

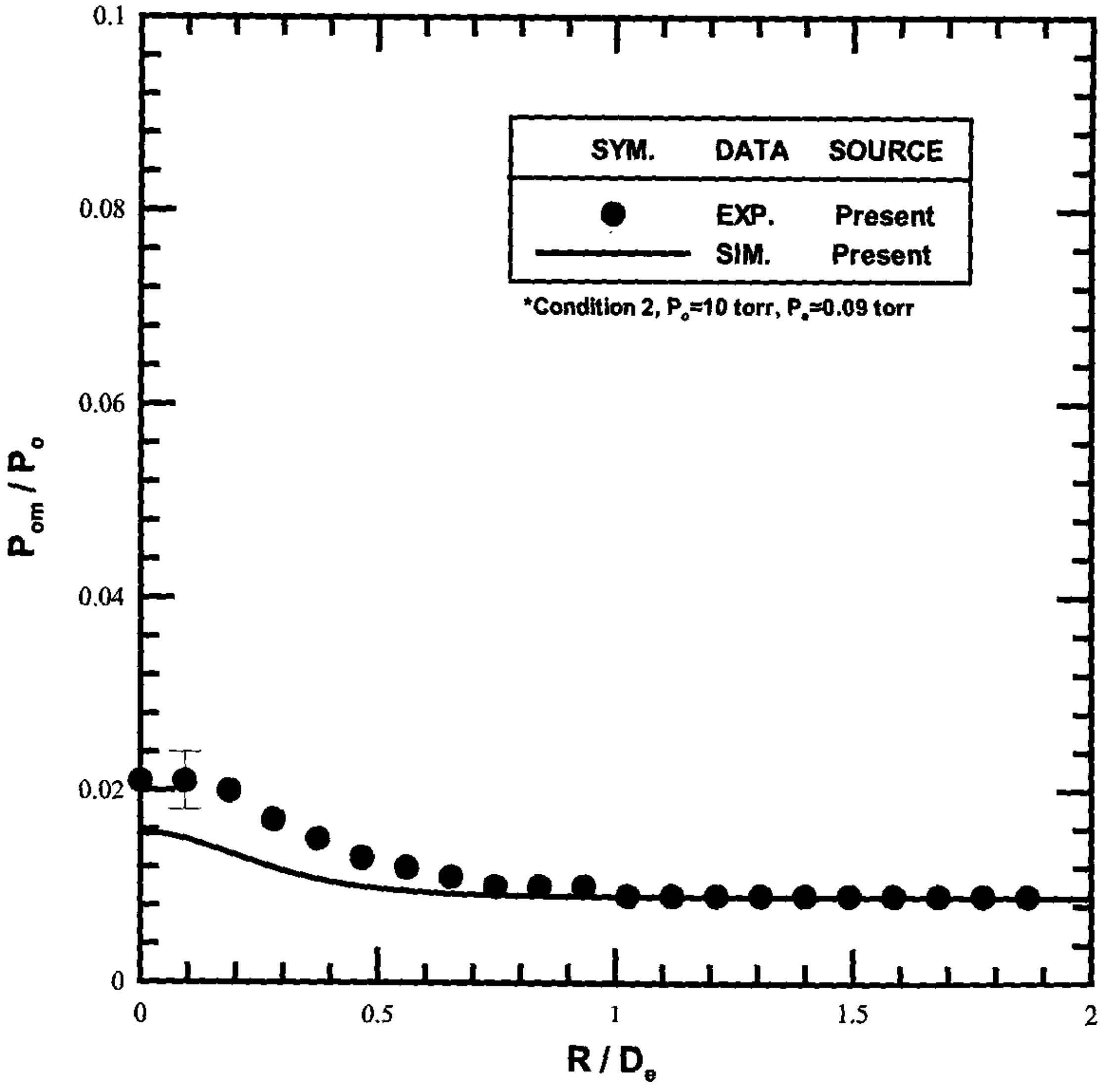

Fig. 43. Comparison computed and measured pitot pressure profile at Z = 10 mm

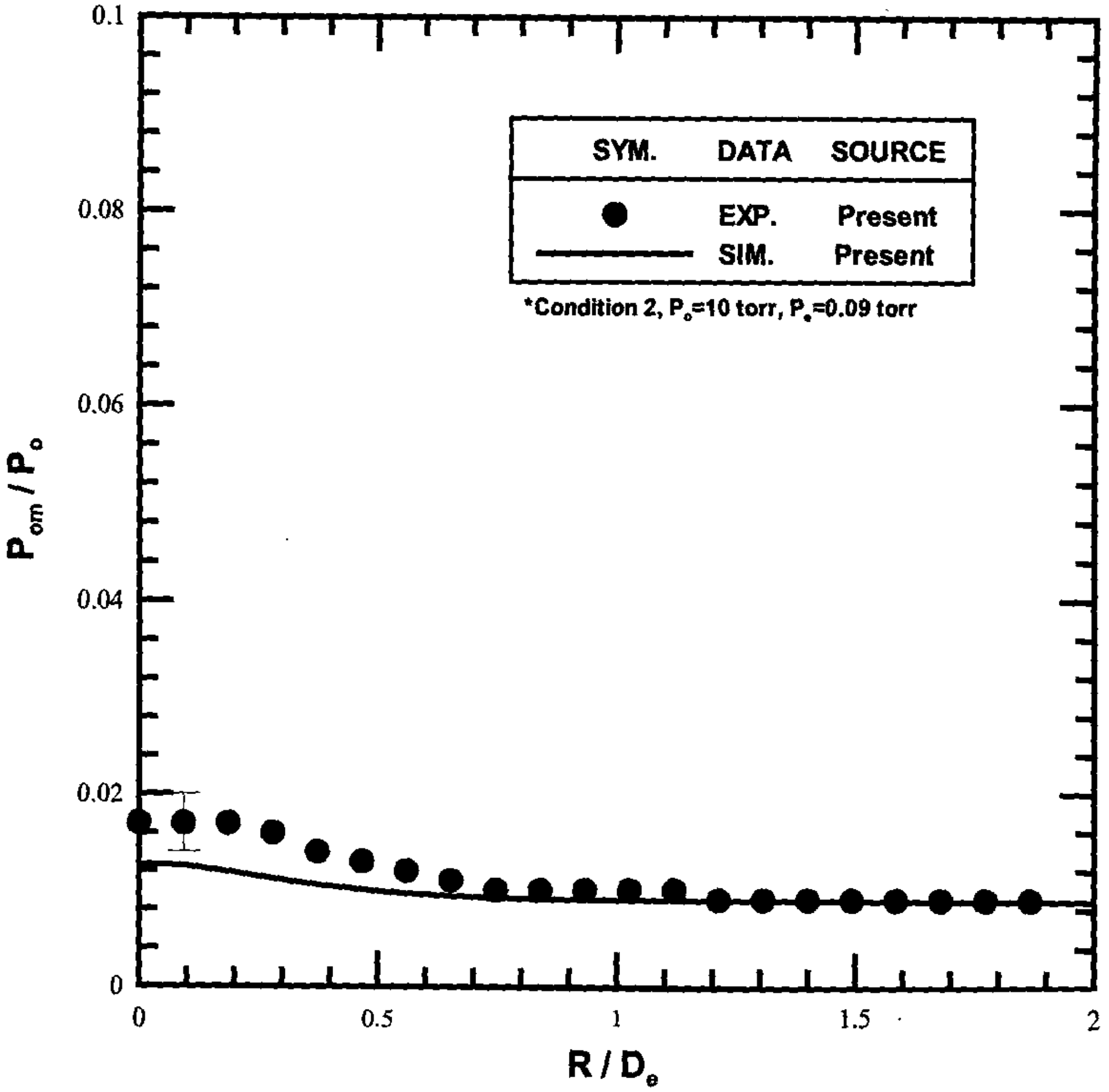

Fig. 44. Comparison computed and measured pitot pressure profile at Z = 15 mm

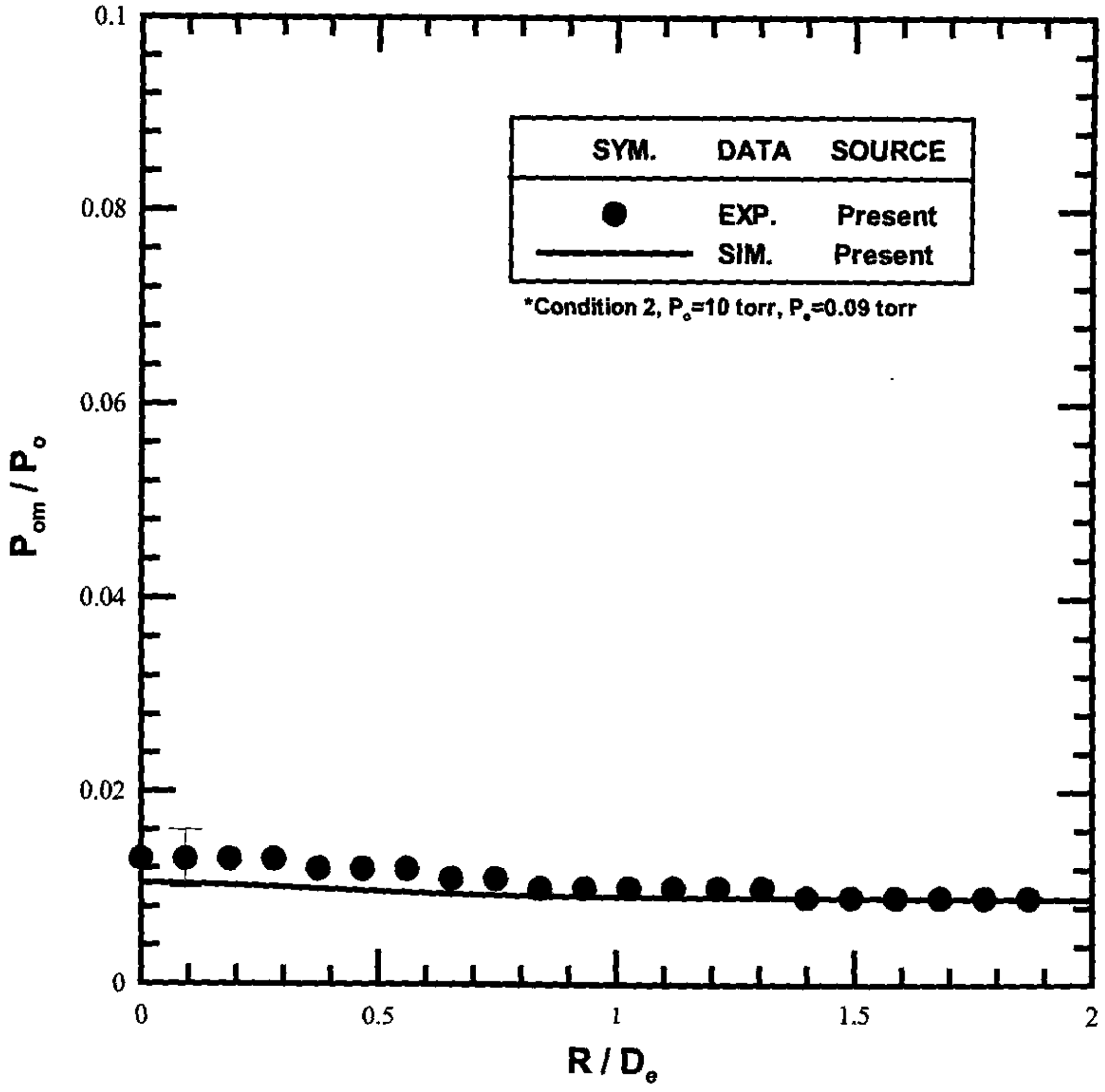

Fig. 45. Comparison computed and measured pitot pressure profile at Z = 25 mm

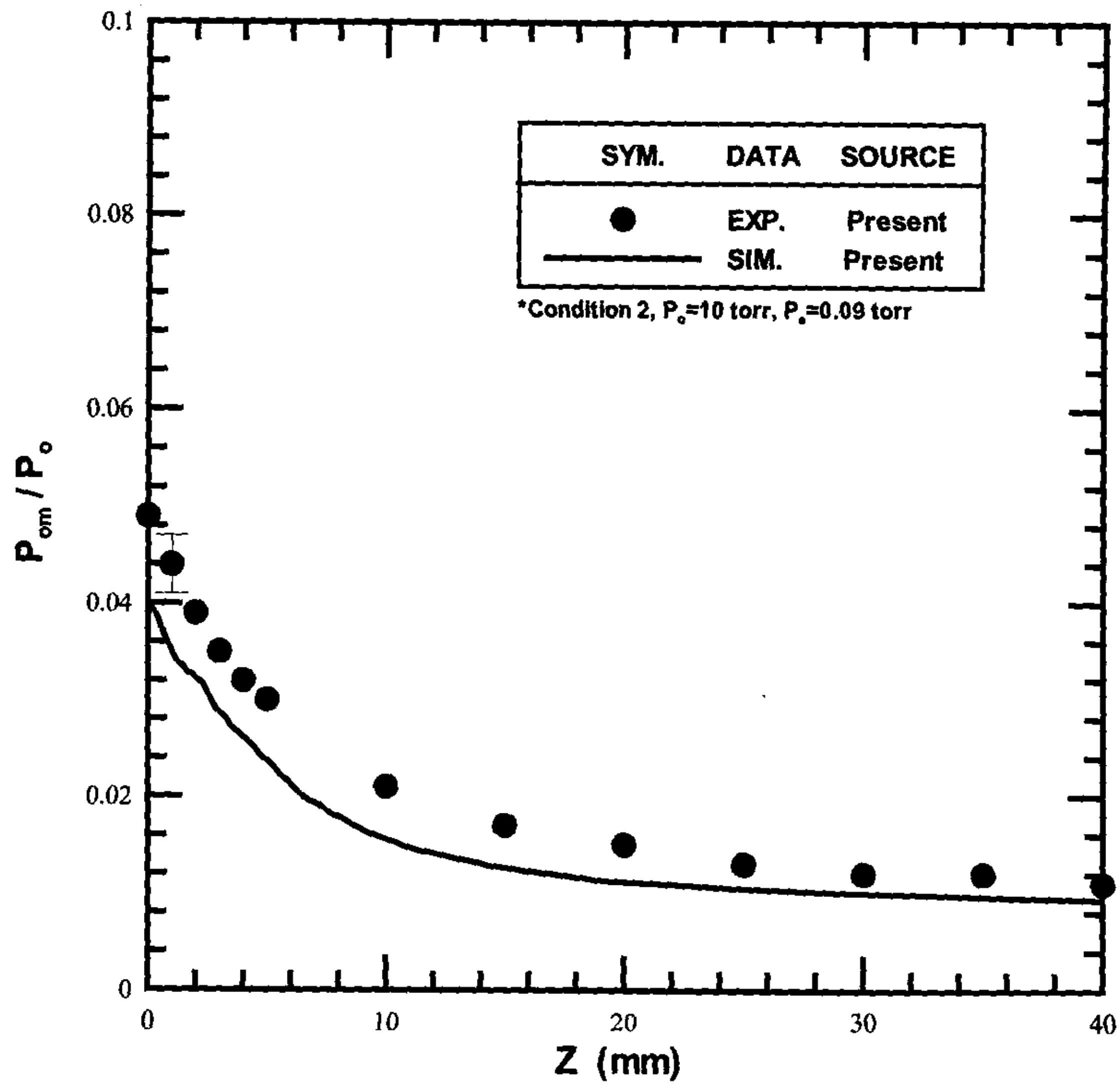

Fig. 46. Comparison of computed and measured pitot pressure profiles on the central line of nozzle (R=0 mm).

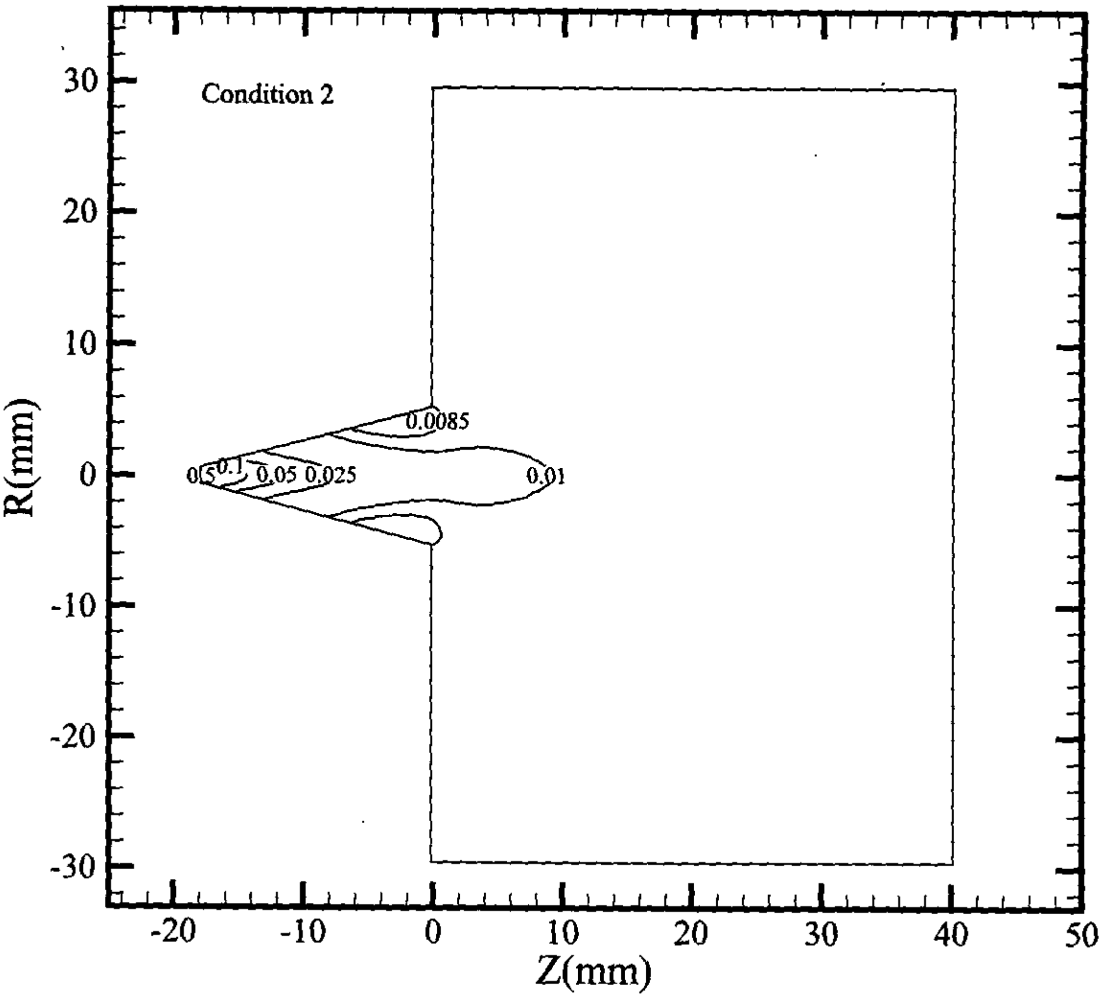

Fig. 47. Normalized density contours computed with DSMC (condition 2).

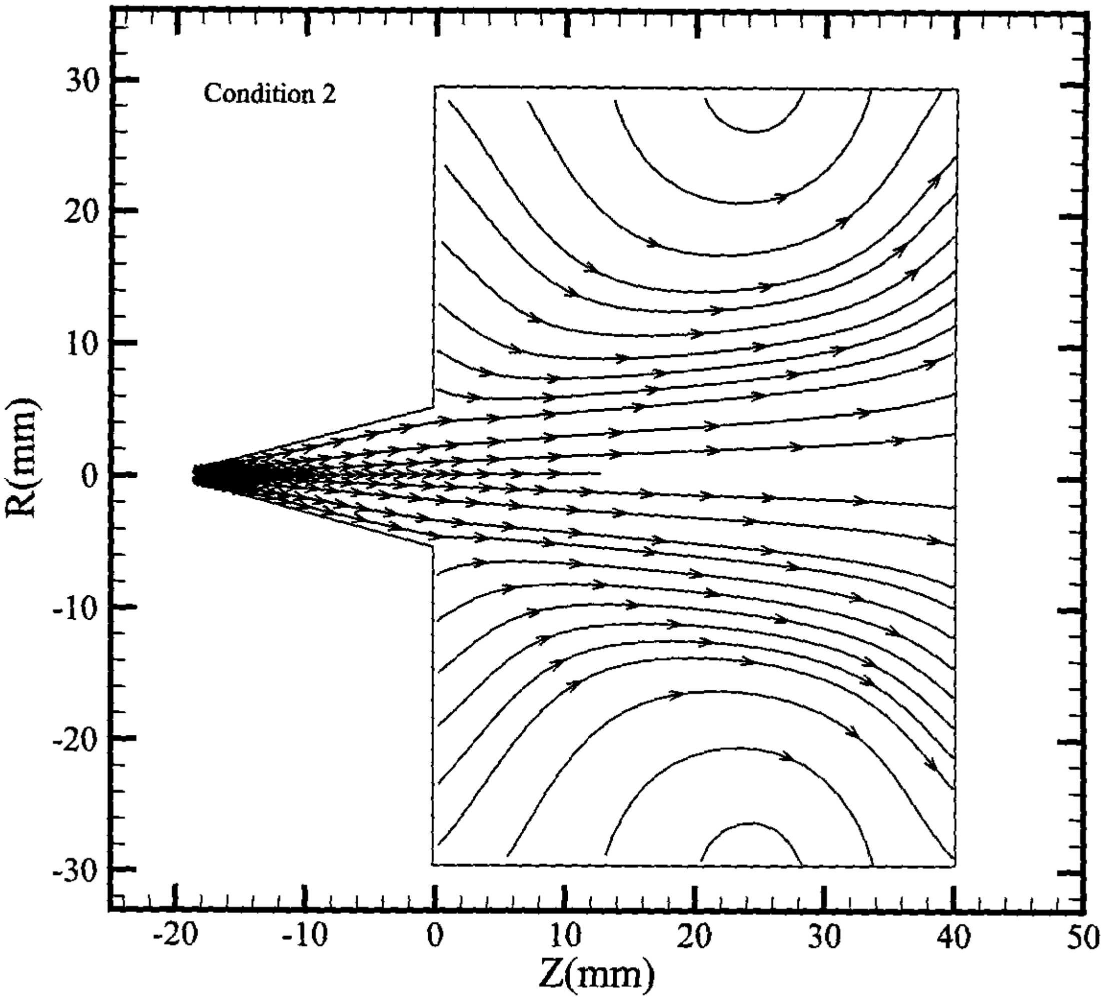

Fig. 48. Streamlines of nozzle jet plume (condition 2)

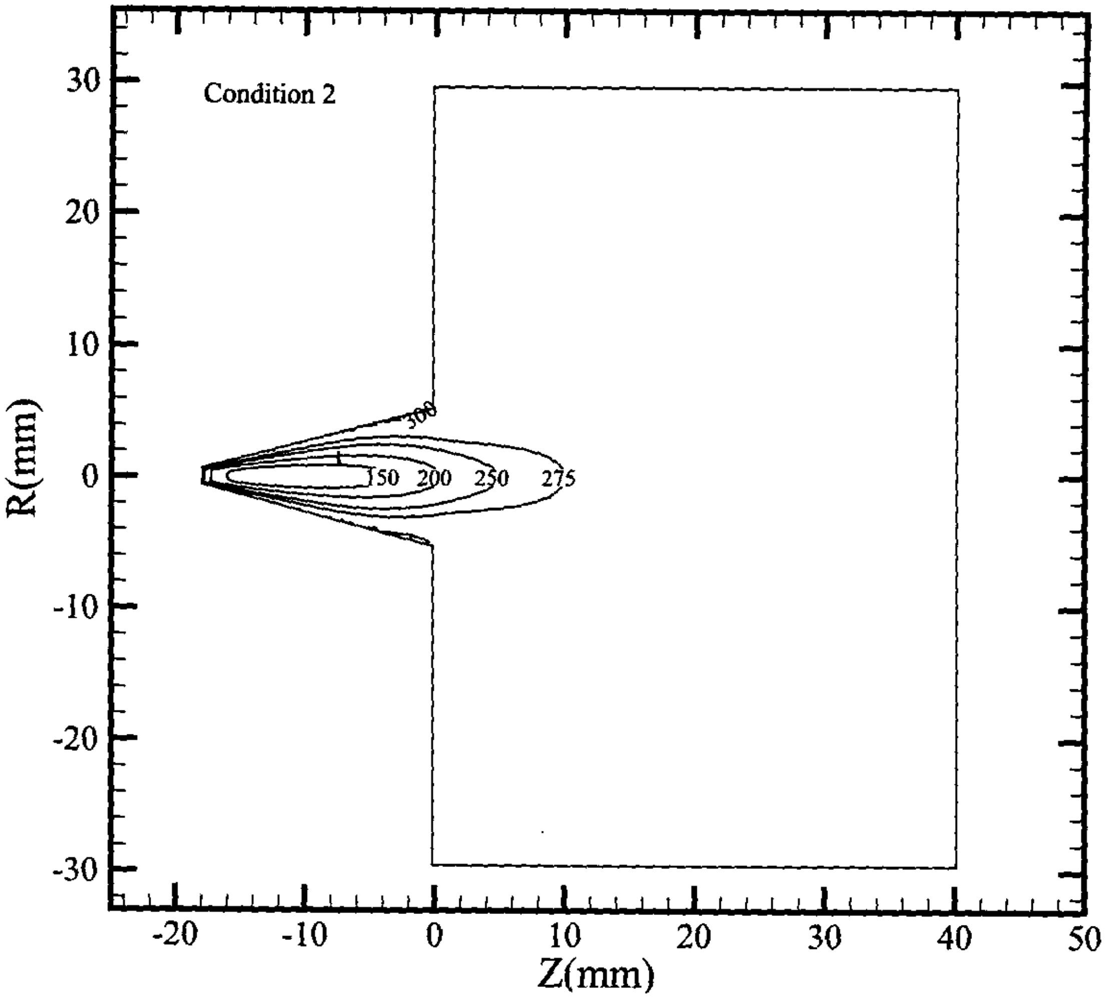

Fig. 49. Temperature contours computed with DSMC (condition 2).

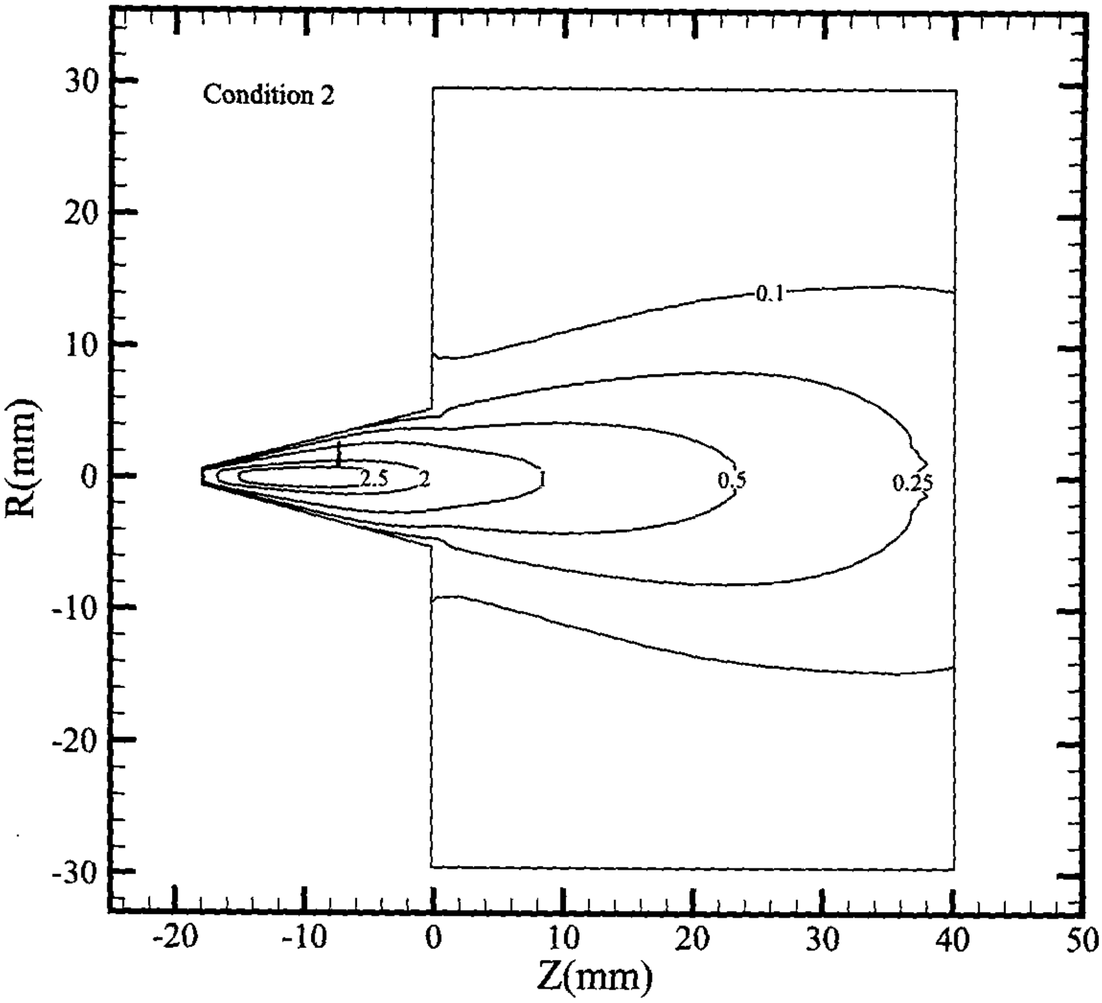

Fig. 50. Mach number contours computed with DSMC (condition 2).

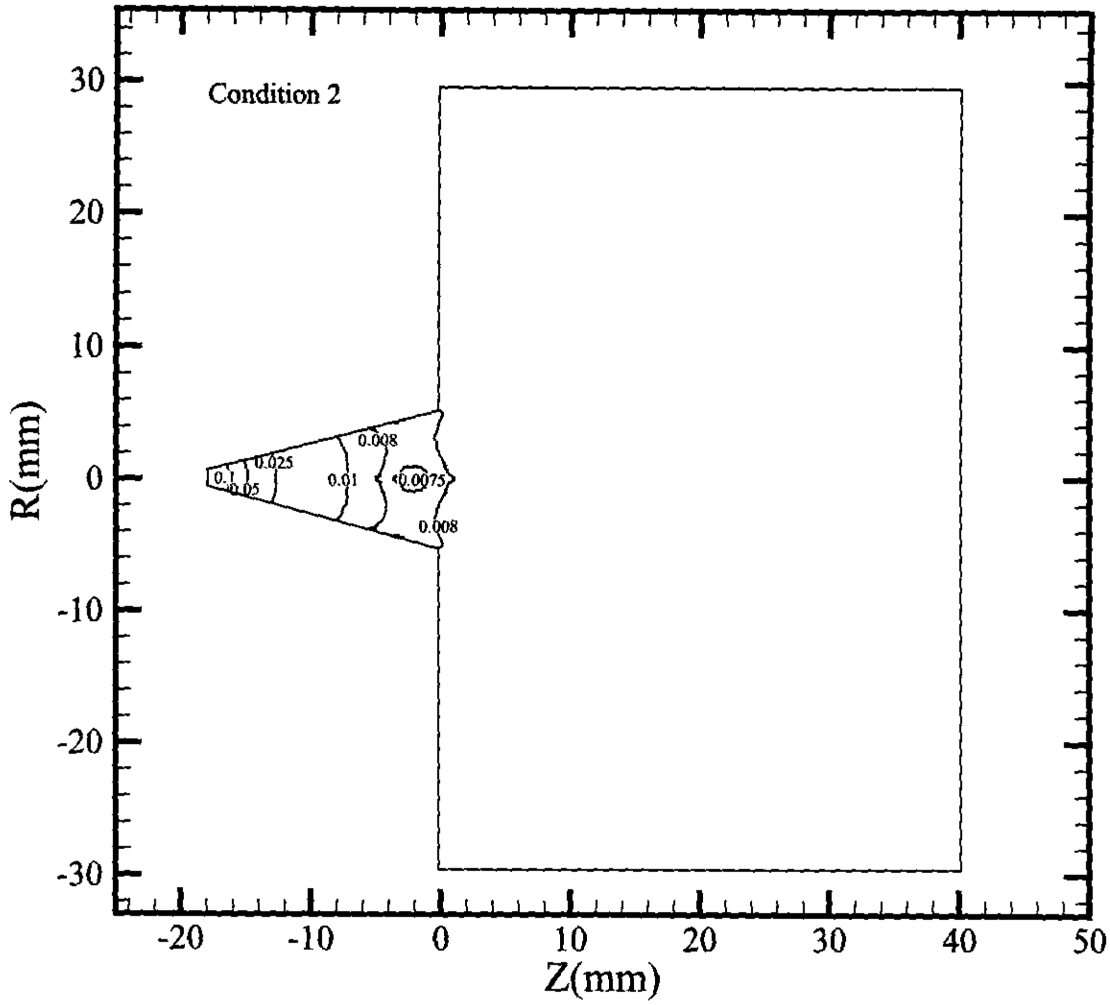

Fig. 51. Normalized pressure contours computed with DSMC (condition 2).

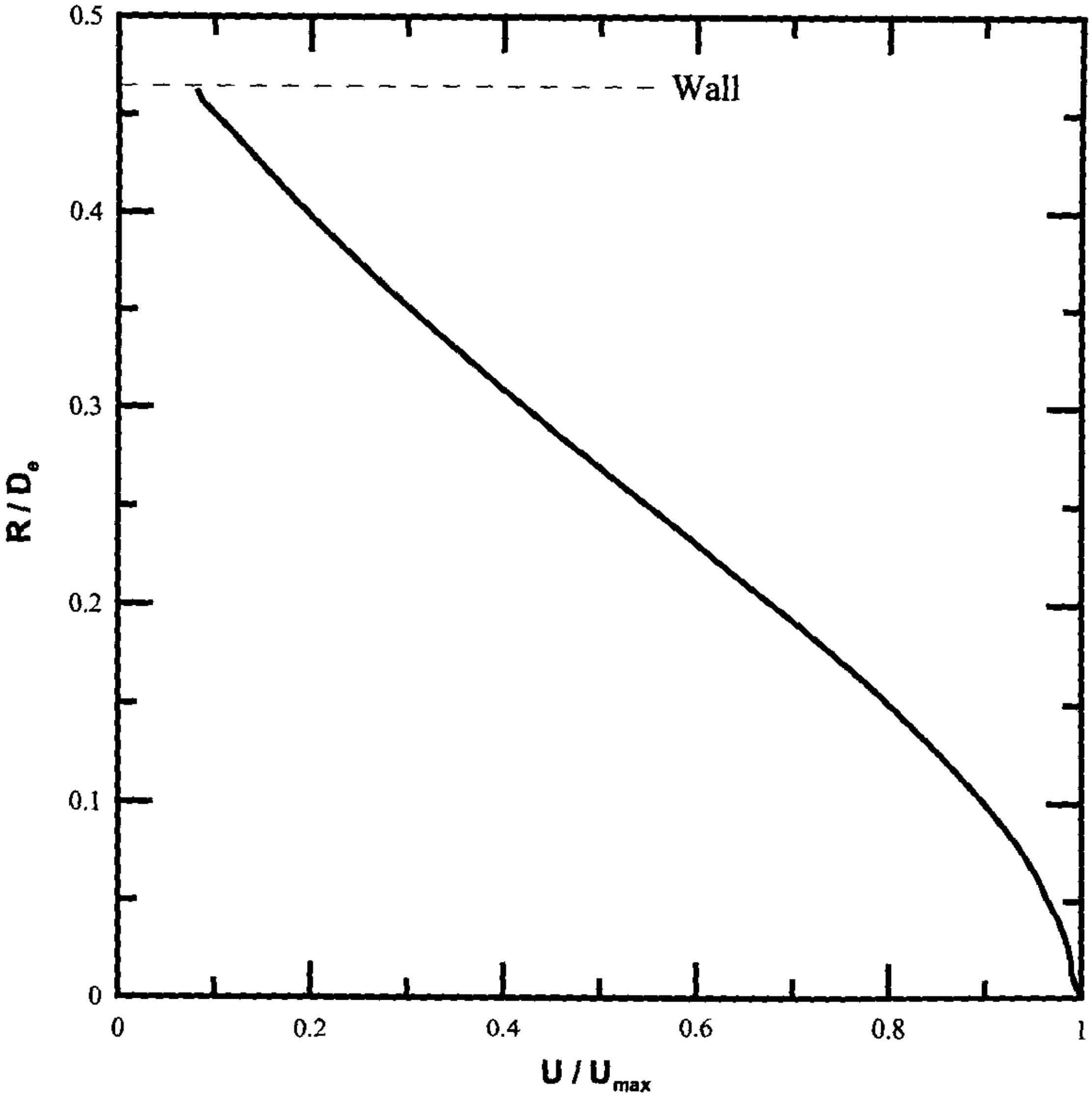

Fig. 52. Normalized axial velocity profiles computed with DSMC at Z = -1 plane (condition 2).

APPENDIX

EXPERIMENTAL UNCERTAINTY:

To provide a valid experimental result and reliability, experimental uncertainties analysis is necessary. The uncertainty analysis procedure of Kline [27] was applied to estimate experimental uncertainties. Consider a variable, Z, which ia a function several other measured variables, z_1, as follow:

$$Z=Z(z_1,z_2,z_3,\ldots\ldots,z_n) \tag{A.1}$$

$$\partial Z=[\sum_{i=1}^{n}(\frac{\partial Z}{\partial z_i}\Delta z_i)^2]^{1/2} \tag{A.2}$$

$$\frac{\partial Z}{Z}=[\sum_{i=1}^{n}\{(\frac{\partial \ln Z}{\partial \ln z_i})(\frac{\Delta z_i}{z_i})\}^2]^{1/2} \tag{A.3}$$

If $Z=z_1^{a_1}\cdot z_2^{a_2}\cdot z_3^{a_3}\cdot\ldots\ldots$, then eq(A.3) can be transform into eq(A.4)

$$\frac{\partial Z}{Z}=[\sum_{i=1}^{n}\{a_i(\frac{\Delta z_i}{z_i})\}^2]^{1/2} \tag{A.4}$$

In current study, pitot pressure was measured by a capacitance-manometer transducer (MKS 627B 100torr), the smallest pressure unit is 0.01 torr. And the lowest measured pitot pressure are 0.16 (condition 1) and 0.09 (condition 2). The relative positions of pitot tube and nozzle ware controlled by movement-mechanisms, its smallest length unit is 0.5 mm. The distance between two measure points are 1 mm in radial direction(R) and 5 mm in axial direction(Z).

According eq(A.4), pitot pressure uncertainty can present as follow:

$$\frac{\partial \mathrm{P_{0m}}}{\mathrm{P_{0m}}}=\left[\left(\frac{\Delta R}{R}\right)^2+\left(\frac{\Delta Z}{Z}\right)^2+\left(\frac{\Delta P}{P}\right)^2\right]^{1/2} \tag{A.5}$$

1.Pitot pressure uncertainties analysis of condition 1

$$\frac{\partial \mathrm{P_{0m}}}{\mathrm{P_{0m}}}=\left[\left(\frac{0.25}{1}\right)^2+\left(\frac{0.25}{5}\right)^2+\left(\frac{\Delta 0.005}{0.16}\right)^2\right]^{1/2}=25.68\%$$

2.Pitot pressure uncertainties analysis of condition 2

$$\frac{\partial \mathrm{P_{0m}}}{\mathrm{P_{0m}}}=\left[\left(\frac{0.25}{1}\right)^2+\left(\frac{0.25}{5}\right)^2+\left(\frac{\Delta 0.005}{0.09}\right)^2\right]^{1/2}=26.09\%$$